CYCLIC INJECTION, STORAGE, AND WITHDRAWAL OF HEATED WATER IN A SANDSTONE AQUIFER AT ST. PAUL, MINNESOTA: Analysis of thermal data and nonisothermal modeling of short-term test cycles

U.S. Geological Survey
Open-File Report 93-435

Prepared in cooperation with the
University of Minnesota
and the Minnesota Geological Survey

CYCLIC INJECTION, STORAGE, AND WITHDRAWAL OF HEATED WATER IN A SANDSTONE AQUIFER AT ST. PAUL, MINNESOTA: Analysis of thermal data and nonisothermal modeling of short-term test cycles

By R.T. Miller and G.N. Delin

U.S. Geological Survey
Open-File Report 93-435

Prepared in cooperation with the
University of Minnesota
and the Minnesota Geological Survey

Mounds View, Minnesota
1994

U.S. DEPARTMENT OF THE INTERIOR

Bruce Babbitt, Secretary

U.S. GEOLOGICAL SURVEY

Gordon P. Eaton, Director

For additional information write to:

District Chief
U.S. Geological Survey
2280 Woodale Drive
Mounds View, MN 55112

Copies of this report can be purchased from:

U.S. Geological Survey
Earth Science Information Center
Open-File Reports Section
Box 25286, MS 517
Denver Federal Center
Denver, CO 80225

Contents

Illustrations

Illustrations--Continued

Illustrations--Continued

Tables

Conversion Factors and Abbreviations

Multiply:	By:	To obtain:
meter (m)	3.281	foot
centimeter (cm)	.3937	inch (in.)
kilogram (kg)	2.205	pound avoirdupois
joule (J)	9.478×10^{-4}	British thermal unit
kilopascal (kPa)	0.1450	pound-force per square inch
liter per second (L/s)	15.85	gallon per minute
meter per day (m/d)	3.281	foot per day
square meter per day (m^2/d)	10.76	square foot per day
kilogram per cubic meter (kg/m^3)	6.243×10^{-2}	pound avoirdupois per cubic foot
watt per square meter (W/m^2)	8.804×10^{-5}	British thermal unit per square foot per second
watt per cubic meter (W/m^3)	2.684×10^{-5}	British thermal unit per cubic foot per second
joule per meter per day per degree [((J/m)/d)/° C]	1.605×10^{-4}	British thermal unit per foot Celsius per day per degree Fahrenheit
joule per cubic meter per degree Celsius [(J/m^3)/° C]	1.491×10^{-5}	British thermal unit per cubic foot per degree Fahrenheit
joule per kilogram per degree Celsius [(J/kg)/° C]	2.388×10^{-4}	British thermal unit per pound avoirdupois per degree Fahrenheit
	Temperature	
degree Celsius (°C)	°F = 1.8 °C + 32	degree Fahrenheit (°F)

Sea level: In this report sea level refers to the National Geodetic Vertical Datum of 1929 (NGVD of 1929)—a geodetic datum derived from a general adjustment of the first-order level nets of both the United States and Canada, formerly called Sea Level Datum of 1929.

CYCLIC INJECTION, STORAGE, AND WITHDRAWAL OF HEATED WATER IN A SANDSTONE AQUIFER AT ST. PAUL, MINNESOTA: Analysis of thermal data and nonisothermal modeling of short-term test cycles

By R.T. Miller and G.N. Delin

Abstract

In May 1980, the University of Minnesota began a project to evaluate the feasibility of storing heated water (150 degrees Celsius) in the Franconia-Ironton-Galesville aquifer (180 to 240 meters below land surface) and later recovering it for space heating. The University's steam-generation facilities supplied high-temperature water for injection. The Aquifer Thermal-Energy Storage system is a doublet-well design in which the injection-withdrawal wells are spaced approximately 250 meters apart. Water was pumped from one of the wells through a heat exchanger, where heat was added or removed. This water was then injected back into the aquifer through the other well.

Four short-term test cycles were completed. Each cycle consisted of approximately equal durations of injection and withdrawal ranging from 5.25 to 8.01 days. Equal rates of injection and withdrawal, ranging from 17.4 to 18.6 liters per second, were maintained for each short-term test cycle. Average injection temperatures ranged from 88.5 to 117.9 degrees Celsius.

Temperature graphs for selected depths at individual observation wells indicate that the Ironton and Galesville Sandstones received and stored more thermal energy than the upper part of the Franconia Formation. Clogging of the Ironton Sandstone was possibly due to precipitation of calcium carbonate or movement of fine-grain material or both. Vertical-profile plots indicate that the effects of buoyancy flow were small within the aquifer.

A three-dimensional, anisotropic, nonisothermal, ground-water-flow, and thermal-energy-transport model was constructed to simulate the four short-term test cycles. The model was used to simulate the entire short-term testing period of approximately 400 days. The only model properties varied during model calibration were longitudinal and transverse thermal dispersivities, which, for final calibration, were simulated as 3.3 and 0.33 meters, respectively. The model was calibrated by comparing model-computed results to (1) measured temperatures at selected altitudes in four observation wells, (2) measured temperatures at the production well, and (3) calculated thermal efficiencies of the aquifer. Model-computed withdrawal-water temperatures were within an average of about 3 percent of measured values and model-computed aquifer-thermal efficiencies were within an average of about 5 percent of calculated values for the short-term test cycles. These data indicate that the model accurately simulated thermal-energy storage within the Franconia-Ironton-Galesville aquifer.

Introduction

During the past decade, the concept of Aquifer Thermal-Energy Storage (ATES) has received increasing attention regarding its potential to decrease energy consumption and environmental contamination. Kazmann (1971), Meyer and Todd (1973), Hausz (1974), and Meyer and others (1976) were among the first to discuss the ATES concept. Most of these discussions, however, were restricted to economic and institutional concerns. Injection of heated or cooled fluids into aquifers had been practiced for many years (Leggette and Brashears, 1938; Guyton, 1946), but field experiments designed to evaluate the feasibility of ATES for long-term, large-scale energy storage were not conducted until 1975 (Werner and Kley, 1977), and the first demonstration project in the United States did not begin until 1976 (Molz and others, 1978). Many other contributions to understanding and evaluating ATES are described or summarized in Mercer and others (1980), Tsang (1979), and Lawrence Berkeley Laboratory (1978).

The University of Minnesota started a project in May 1980 to evaluate aquifer thermal-energy storage in a confined, sedimentary bedrock about 180 m beneath the St. Paul campus. The project was funded by the U.S. Department of Energy through Battelle Pacific Northwest Laboratories. Other participants in the project include the

Minnesota Geological Survey, the Minnesota Energy Agency, Orr-Schelen-Mayeron and Associates, National Biocentrics, Inc., and the U.S. Geological Survey. The project was designed to evaluate the feasibility and effects of storing high-temperature (150°C) water in the Franconia-Ironton-Galesville aquifer beneath the St. Paul campus and later recovering the heat for water and space heating.

The specific objectives of the U.S. Geological Survey in this investigation were to (1) develop an understanding of the ground-water-flow system near the site, (2) identify the hydraulic properties of the ground-water-flow system that are most important with respect to thermal-energy storage and identify data-collection needs for monitoring and evaluating the aquifer-system performance, (3) develop a method to evaluate flow and thermal-energy transport for various cyclic injection and withdrawal schemes to aid in selection of an efficient well-system design, and (4) assist in the collection of hydraulic and thermal data during injection-withdrawal tests and design a data-processing system to facilitate entry of the data into computer storage. Miller (1984; 1985) describes the anisotropy of the Franconia-Ironton-Galesville aquifer and preliminary modeling at the ATES site. Miller and Voss (1986) describe design of the finite-difference grid at the ATES site. Miller and Delin (1993) describe (1) analysis of field observations for aquifer characterization and observation-network design, (2) preliminary model analyses to determine model sensitivity to hydraulic and thermal characteristics and to facilitate final model design, and (3) model simulations of the aquifer's thermal efficiency.

Purpose and Scope

This report describes the analysis of thermal data and nonisothermal modeling for four short-term test cycles of heated-water injection, storage, and withdrawal. This report is one in a series that describes the potential for thermal-energy storage within the Franconia-Ironton-Galesville aquifer beneath the St. Paul campus of the University of Minnesota.

Hydrogeologic Setting

The St. Paul Metropolitan Area is underlain by a stratified sequence of Proterozoic and early Paleozoic sedimentary formations consisting of porous sandstone and fractured dolomite which can by grouped into four major regional aquifers. The aquifers generally are separated by semipermeable sandstone, siltstone, and shale formations. The major aquifers are the St. Peter, Prairie du Chien-Jordan, Franconia-Ironton-Galesville, and Mount Simon-Hinckley-Fond du Lac (fig. 1).

The St. Peter aquifer consists of the St. Peter sandstone, which is composed of a light-yellow or white, massive, quartzose, fine- to medium-grained, well-sorted, and friable sandstone. Thin beds of siltstone and shale near the base of the St. Peter Sandstone form a lower confining layer. The upper confining layer, consisting of the Platteville and Glenwood Formations, overlies the St. Peter Sandstone and is in contact with glacial drift. At the test site the St. Peter aquifer is approximately 57 m below land surface and is 50 m thick. Transmissivity ranges from 220 to 280 m^2/d and the storage coefficient ranges from 9.0×10^{-5} to 9.75×10^{-3}. Porosity ranges from 0.28 to 0.30. The hydraulic gradient was estimated to be 0.006 and the pore velocity was estimated to be 0.18 m/d Norvitch and others (1973).

The Prairie du Chien-Jordan aquifer consists of the Prairie du Chien Group and the Jordan Sandstone (fig. 1). The Prairie du Chien Group is predominantly a light brownish-gray or buff, sandy, thin- to thick-bedded dolomite that is vuggy and fractured and contains some thin layers of interbedded grayish-green shale. The underlying Jordan Sandstone is a white to yellow, quartzose, fine- to coarse-grained sandstone that is massive or thick to thin bedded and varies from friable to well cemented. Despite the differing lithologies, the Prairie du Chien Group and Jordan Sandstone function as one aquifer because there is no regional confining bed between them. At the test site the aquifer is approximately 107 m below land surface and is 69 m thick. The average transmissivity is approximately 1,235 m^2/d, with a porosity of 0.3. The hydraulic gradient was estimated to be approximately 0.005 and the pore velocity was estimated to be 0.3 m/d by Norvitch and Walton (1979).

The St. Lawrence Formation is 176 m below land surface and is approximately 8 m thick at the test site. It is a gray and greenish-gray, laminated, thin-bedded, dolomitic siltstone, silty dolomite, and shale. The porosity ranges from 0.15 to 0.20 and transmissivities range from 1 to 10 m^2/d.

The Franconia-Ironton-Galesville aquifer consists of the Franconia Formation, and the Ironton and Galesville Sandstones. The Franconia Formation is divided into four members: Reno, Mazomanie, Tomah, and Birkmose (Walton and others, 1991). The Reno Member in the upper part of the Franconia is a fine- to very-fine-grained, quartz, and glauconitic sandstone. The Reno is divided into two sections and is located approximately between 180 and 183 m and between 193 and 206 m below land surface. The Mazomanie Member in the upper part of the Franconia is located between the depths of 174 and 184 m below land surface. The Mazomanie also is a fine- to very-fine-grained, quartz sandstone but has minor

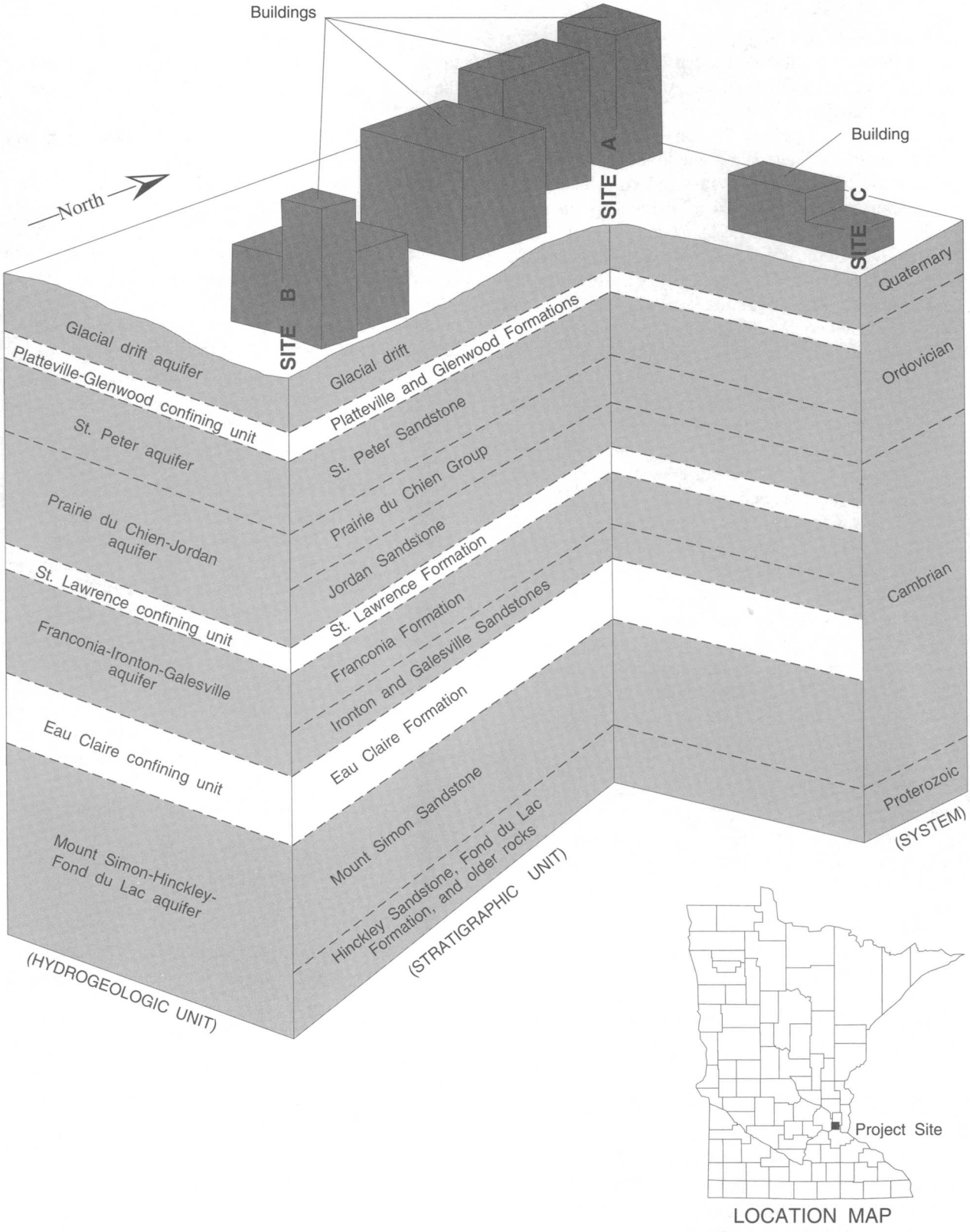

Figure 1.--Location and generalized schematic of hydrogeology at the Aquifer Thermal-Energy Storage (ATES) site.

glauconite content. The Tomah Member in the lower part of the Franconia is an interbedded sequence of fine- to very-fine-grained, silty sandstone with interbedded siltstone or shale. The Tomah is located between 206 and 219 m below land surface. The Birkmose Member in the lower part of the Franconia is a dolomitic siltstone with some shale and fine- to very-fine-grained glauconitic sandstone interbedded. Based on laboratory permeability tests (Walton and others, 1991), the horizontal hydraulic conductivity of the upper part of the Franconia is about 158 times the hydraulic conductivity of the lower part of the Franconia. Natural gamma logs indicate a thick shale layer in the lower part of the Franconia Formation corresponding to the lower Reno, Tomah, and Birkmose Members (Walton and others, 1991). Analysis of results of packer tests indicate two hydraulic zones within the Franconia Formation (Miller and Delin, 1993). Based on the distinct differences in grain size, geophysical logs, and hydraulic properties between the upper and lower parts of the Franconia Formation, the upper 14 m of the Franconia was considered an aquifer and the lower 25 m of the Franconia was considered a confining unit. The Ironton Sandstone is white, medium-grained, moderately well-sorted quartz arenite that contains some silt-sized material. The Galesville Sandstone consists of a white to light-gray slightly glauconitic, well- to moderately well-sorted, mostly medium-grained quartzose sandstone. The approximate depth and thickness of the Franconia-Ironton-Galesville aquifer beneath the site are 183 m and 62 m, respectively. The total transmissivity is 97.5 m^2/d and the storage coefficient is 2.75×10^{-5}. Transmissivity of the Franconia-Ironton-Galesville aquifer is anisotropic, with the principal axis of transmissivity oriented about 30 degrees east of north. Average porosity ranges from 0.25 to 0.31 with a hydraulic gradient of 0.002 and an estimated pore velocity of 0.05 m/d.

The Eau Claire Formation consists of interbedded siltstone, shale, and fine silty sandstone with a few thin layers of dolomite. The approximate depth and thickness of the formation beneath the site are 241 m and 30 m, respectively. Transmissivity ranges from 0.5 to 5 m^2/d and porosity ranges from 0.28 to 0.35 (Norvitch and others, 1973)

The Mount Simon-Hinckley-Fond du Lac aquifer consists of the Mount Simon and Hinckley Sandstones and the Fond du Lac Formation. The Mount Simon Sandstone is fine to coarse grained, contains very thin beds of shale, and commonly is gray, white, or pink. The Hinckley Sandstone is fine to coarse grained and pale red to light pink. The Fond du Lac Formation contains lenticular beds of fine to medium grained arkosic sandstone interbedded with mudstone and is dark red to pink. The top of the aquifer is approximately 274 m below land surface and the aquifer is approximately 60 m thick. The transmissivity is approximately 250 m^2/d and the storage coefficient is about 6×10^{-5} (Norvitch and others, 1973). The porosity averages 0.25, the hydraulic gradient is 0.0025, and the pore velocity is approximately 0.03 m/d (Norvitch and others, 1973).

Aquifer Selection

The selection of an aquifer for heat-storage testing was based on the following criteria: (1) minimal use of water from the aquifer in the Twin Cities area, (2) ability of the confining units above and below the aquifer to contain the injected heated water, and (3) the hydrogeologic properties and natural gradients within the aquifer and their effect on the transfer of heat.

Description of Test Facility

The University of Minnesota test facility was a doublet-well system in which the wells were spaced approximately 250 m apart (fig. 2). Production wells A and B were screened from about 180 to 195 m (upper part of the Franconia Formation) and from 225 to 240 m (Ironton and Galesville Sandstones) below land surface, respectively (Miller and Delin, 1993). The land surface is 287 m above sea level. Initial testing of the ATES system was with a series of short-term cycles of heated-water injection, storage, and withdrawal. Each cycle was planned to be approximately 24 days long; the injection, storage, and withdrawal steps for each cycle were to be approximately 8 days in duration. Conversely, the duration of the long-term test cycles was planned to be 180 days long; with injection, storage, and withdrawal steps of 60 days each. During injection, water was pumped from the Franconia-Ironton-Galesville aquifer from production well B at site B (fig. 1), transported through a heat exchanger (fig. 3) where it was heated, and then injected back into the aquifer through production well A at site A. During withdrawal, water was pumped from the Franconia-Ironton-Galesville aquifer from production well A, transported through the radiator, where it was cooled, and then injected back into the aquifer through production well B. The doublet-well system and sites A and B at the ATES site are shown diagrammatically in figure 3.

Temperature measurements within the observation wells (fig. 4) were made by use of type-T (copper-constantan) thermocouples. As described in detail by Miller and Delin (1993), as many as 12 thermocouples were installed in 1 or 2 manufactured strings (one containing 8 thermocouples and one containing 4) in a protective 5.1-cm-diameter steel casing within the observation wells at the altitudes shown in figure 4.

Individual thermocouples were coated with Teflon[1] for resistance to heat, and each four- or eight-thermocouple string was covered with a stainless-steel overbraid to add rigidity and to protect each string as it was lowered into the steel casing. The overbraid tended to twist and kink, however, and created excessive wear to the thermocouple wire where the kinks rubbed on the side of the well casing. Several thermocouples failed because of electrical shorts in thermocouple wires at these points of excessive wear. Temperatures measured at the thermocouples probably were slightly less than the actual temperatures in the aquifer because of conductive heat losses to the well casing; however, these temperature losses are minimal and measured temperatures are considered representative of temperatures in the aquifer.

Submersible pressure transducers were used to measure pressures in the observation wells. Pressures from 0 to 1,724 kPa could be measured in a temperature range of 10 to 121°C. Measurement accuracy was ±2 percent of the full-scale output over the compensated temperature range, or a maximum of ±34 kPa at 121°C.

All temperature and pressure-transducer data were transmitted through buried cables to a central data logger with which data were recorded on electrostatic paper and nine-track computer tape. The operation of the data logger and the computer programs written to reduce the stored data are described in detail by Czarnecki (1983).

Individual data-collection points will be referred to in this report by their observation-well location with respect to production well A and by their vertical position within each observation well as referenced to sea level. Reference to sea level is justified because the formations are flat lying and of uniform thickness across the area. The locations of observation wells AM1, AM2, AM3, and AS1 with respect to production well A are shown in figure 3. The altitudes of individual measurement points for the observation wells are shown in figure 4.

Downhole gyroscopic surveys were conducted in several observation wells (Miller and Delin, 1993) to determine deviations of each well bore with respect to land surface. The bottoms of some wells deviate from their land-surface locations by as much as 8 m horizontally (fig. 5). These horizontal deviations were considered during interpretation of temperature data.

[1] Use of brand names in this report is for identification purposes only and does not constitute endorsement by the U.S. Geological Survey.

Preliminary Injection of Heated Water

Prior to conducting the short-term test cycles, a preliminary heat-injection phase was completed to test equipment at the ATES site and finalize plans for the actual tests. For this pilot phase of the study, water at ambient temperature was pumped from production well B and injected in production well A at 18.6 L/s for approximately 2 days in May 1982. The temperature of the injection water then was increased to 82°C, and injection continued for approximately 2 more days. As a result of the temperature increase, calcium carbonate precipitated within the above-ground piping and within the well bore of production well A and caused pressures in the above-ground piping and well bore to increase (fig. 6). Injection of heated water was stopped after pressures in production well A increased beyond the maximum pressures measured during an 8-day injection test with ambient-temperature water done earlier in the month. The initial pressure drop observed during injection of the heated water was related to decreases in the viscosity and density of the heated water as it mixed with ambient-temperature water.

Indications of clogging of the well bore at production well A also were apparent from pressure changes in the upper part of the Franconia Formation and the Ironton and Galesville Sandstones at observation well AM2 (fig. 6). During ambient-temperature injection, pressures in these formations measured at observation well AM2 were similar to pressures measured during the previous 8-day ambient-temperature injection test; pressures in the Ironton and Galesville Sandstones ranged from 100 to 110 kPa, greater than pressures in the upper part of the Franconia Formation. This trend continued until after about 1,250 minutes of heated-water injection. At that time, pressures in the Ironton and Galesville Sandstones started to decrease while pressures in the upper part of the Franconia Formation started to increase. Until the test was stopped, pressures in the upper part of the Franconia Formation increased while pressures in the Ironton and Galesville Sandstones decreased. These variations in recorded pressure probably are due to clogging of production well A in the interval screened opposite the Ironton and Galesville Sandstones. The Ironton and Galesville Sandstones are known to have a hydraulic conductivity at least twice that of the upper part of the Franconia Formation (Miller, 1984); therefore, it is likely that twice as much water per unit time can be injected into this part of the aquifer. Because more water can be injected into the Ironton and Galesville Sandstones, the potential for precipitation of calcium carbonate is greater in this part of the aquifer than in the upper part of the Franconia Formation. If the permeability near the well bore in the Ironton and Galesville Sandstones were

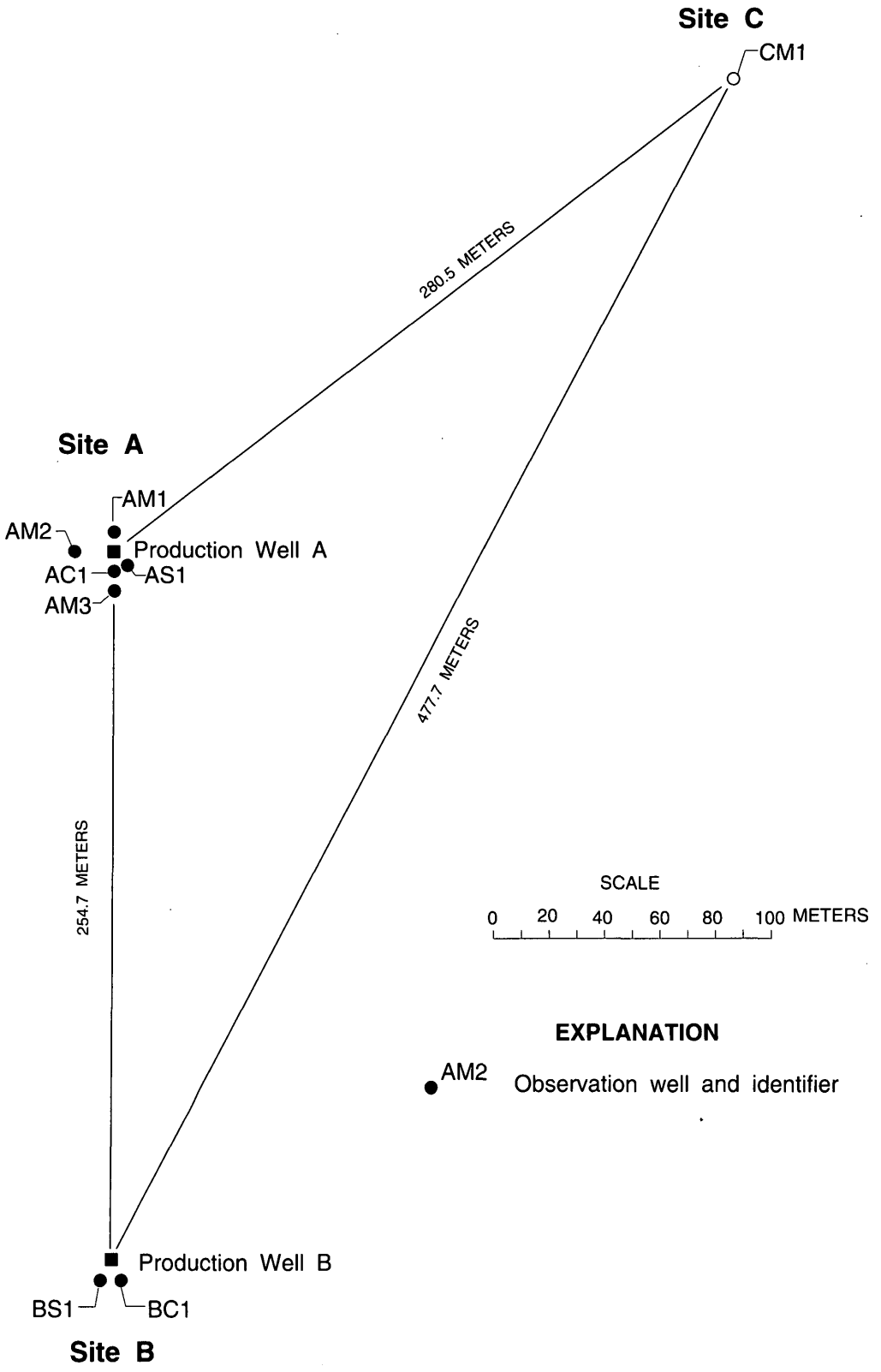

Figure 2.--Plan view of the Aquifer Thermal-Energy Storage (ATES) site.

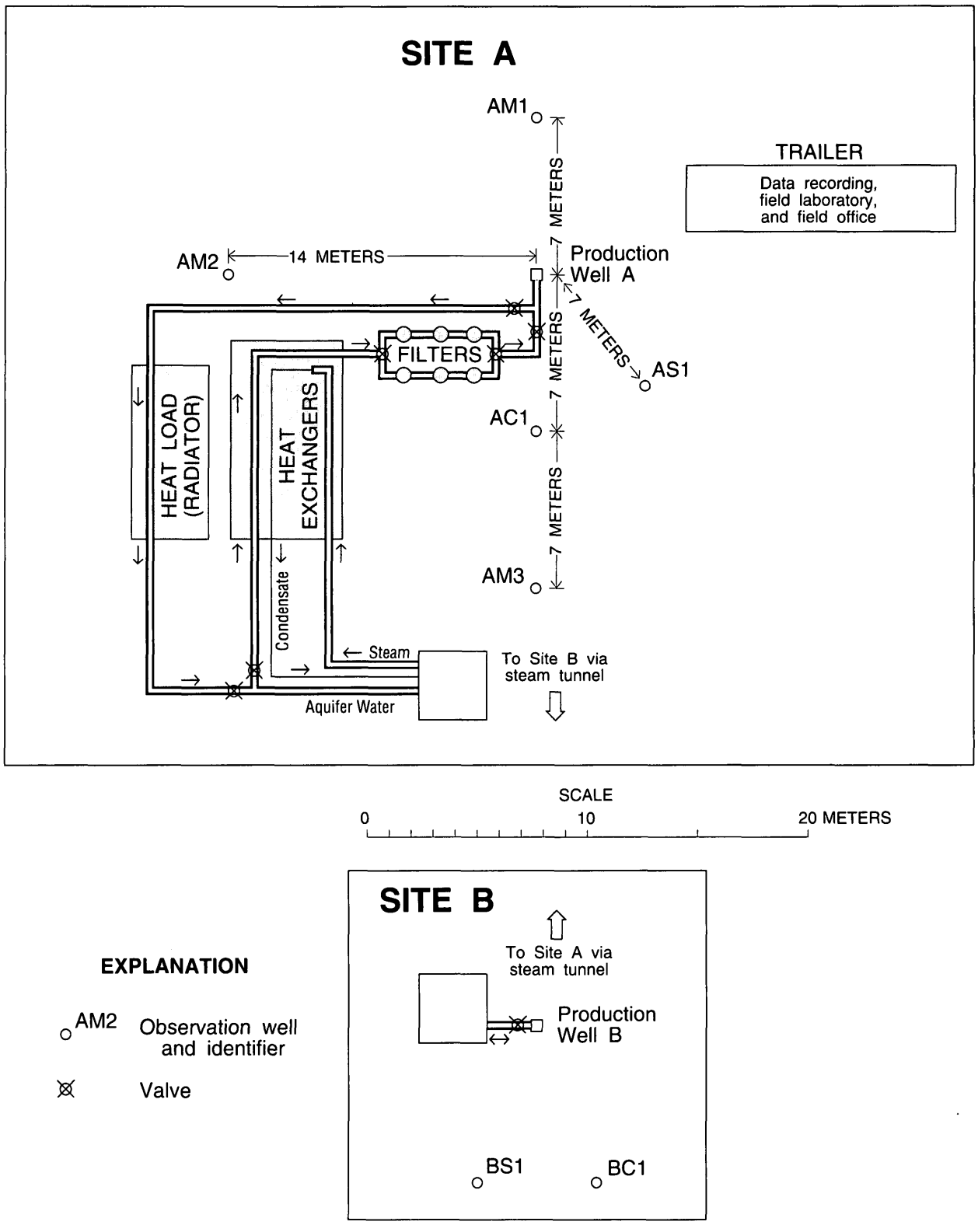

Figure 3.--Schematic diagram of sites A and B at the Aquifer Thermal-Energy Storage (ATES) site. (Modified from Walton and others, 1991).

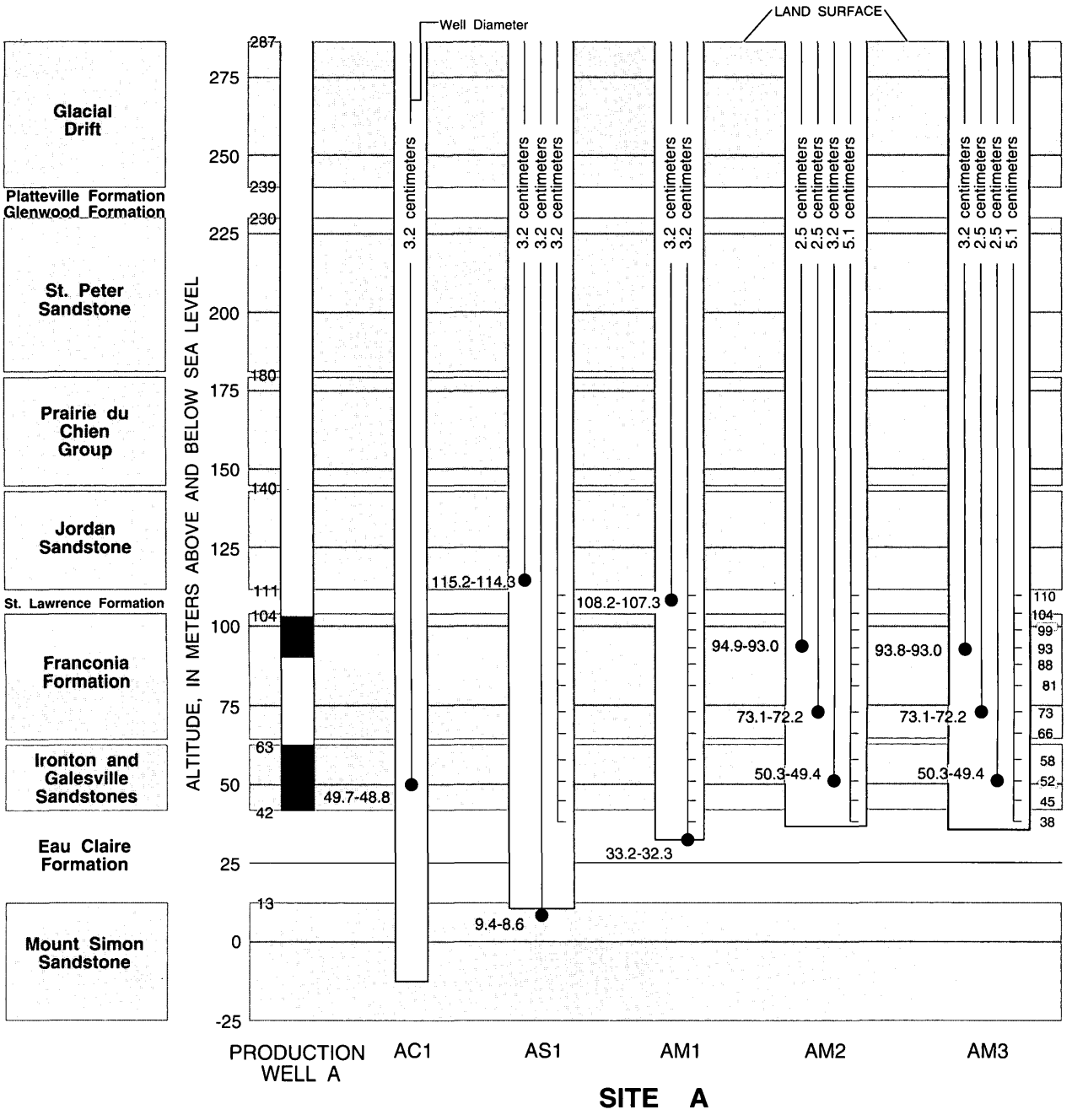

EXPLANATION

Screened interval in production well

49.7-48.8 Altitude range of screened interval, in meters.

110 Temperature measurement point and altitude, in meters. (refer to well AM3 for measurement altitudes).

Figure 4.--Depths of screened intervals of observation wells, Thermal-Energy Storage (ATES) site. (Horizontal

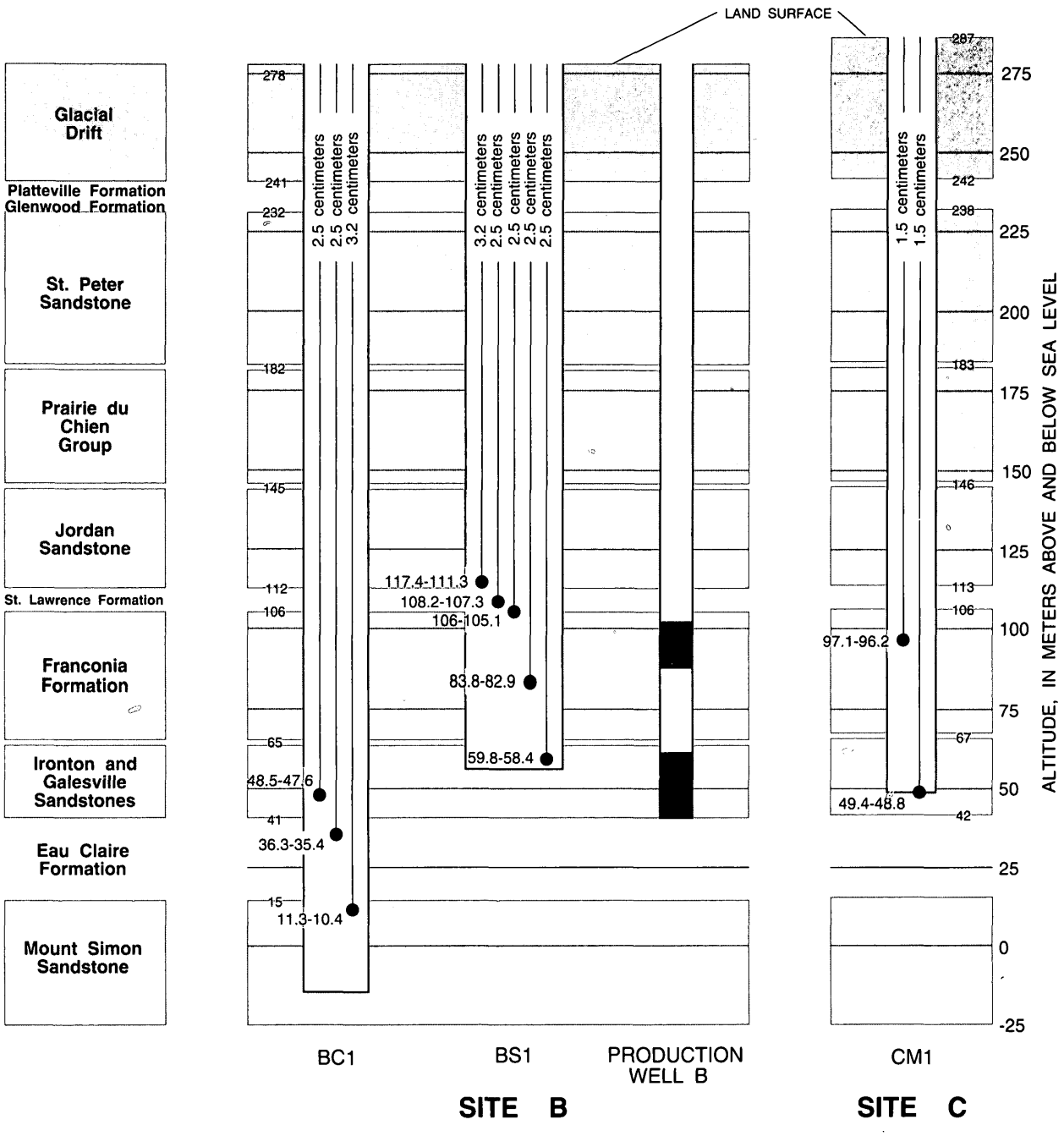

stratigraphy, and location of measurement points of the Aquifer arrangement of wells is arbitrary and not to scale.)

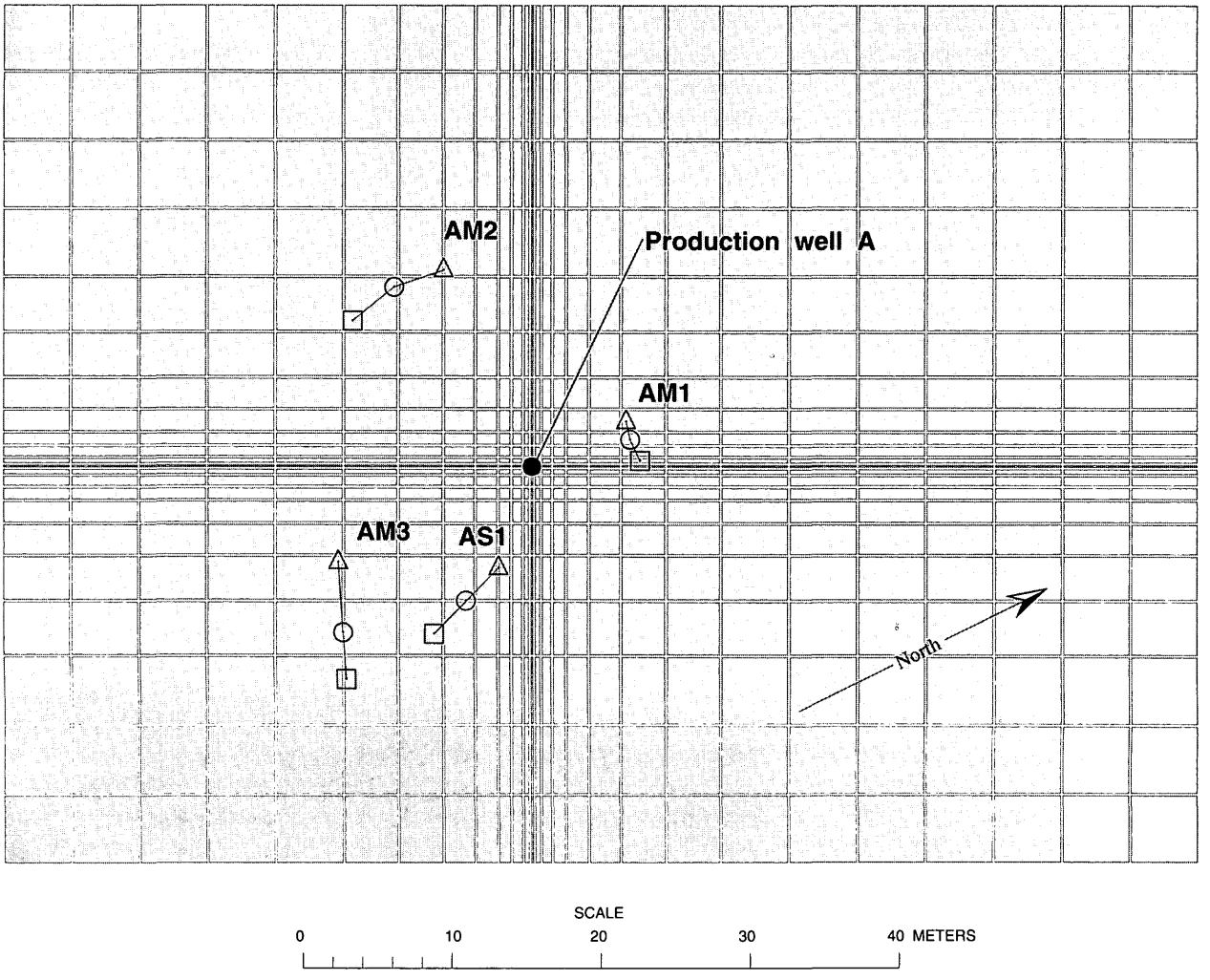

EXPLANATION

Position of observation well:

At land surface

In model-layer 1 (St. Lawrence Formation)

In model-layer 6 (Eau Claire Formation)

Figure 5.--Model grid and position of observation wells.

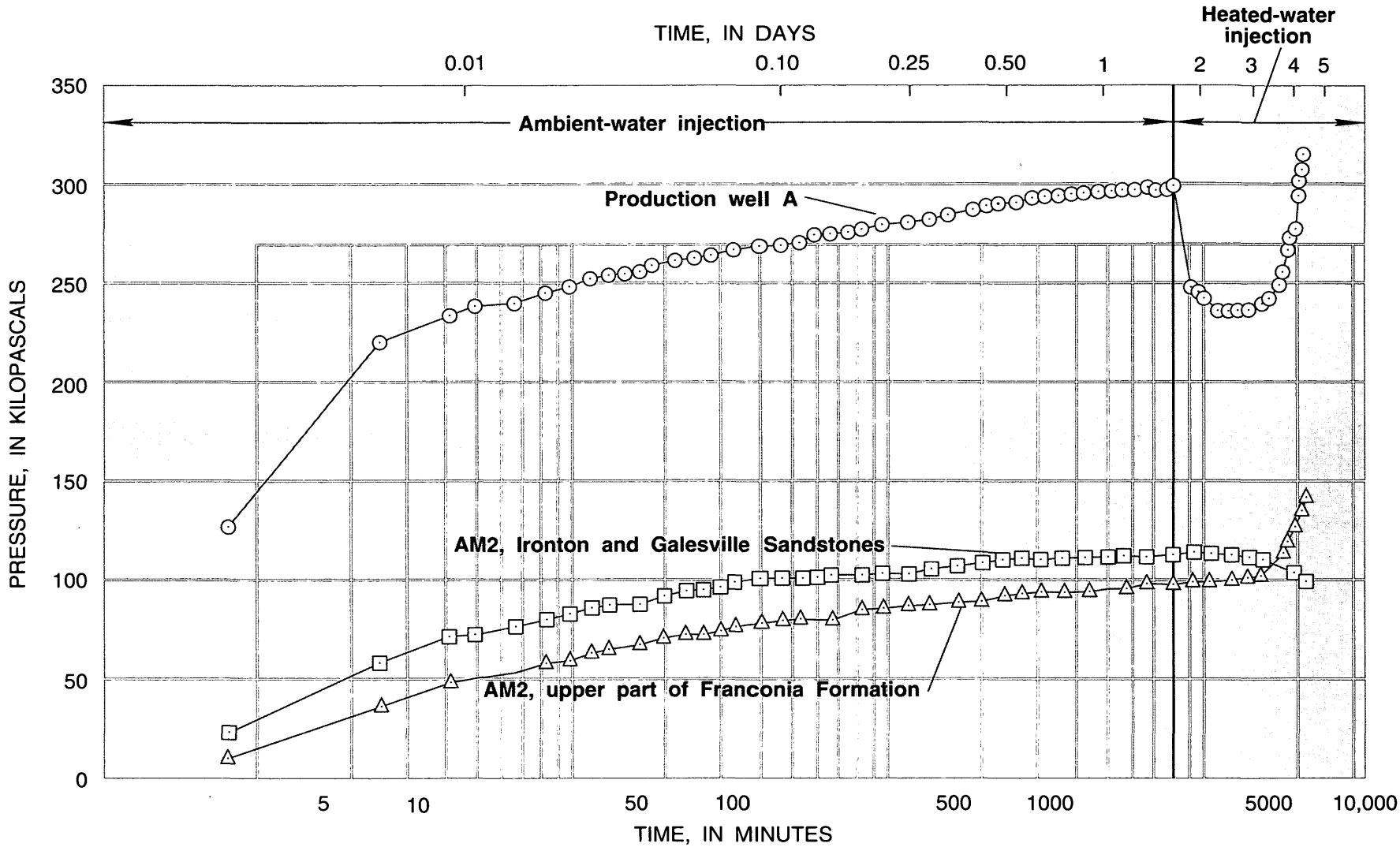

Figure 6.--Pressure changes in production well A and in observation well AM2 for about 2 days of injection of ambient water and about 2 days of injection of heated water (82 degrees Celsius) at 18.6 liters per second.

lowered because of the clogging, more water would be forced into the upper part of the Franconia Formation, and the pressure in the upper part of the Franconia would rise. Because less water would be injected into the Ironton and Galesville Sandstones than before, and because most of the head loss through the Ironton and Galesville Sandstones would take place near the well bore, the pressure measured in this formation at observation well AM2 would decrease.

Because additional water would be injected into the upper part of the Franconia Formation, and because the upper part of the Franconia would not clog at the same rate as the Ironton and Galesville Sandstones, pressures measured in upper part of the Franconia at observation well AM2 would increase. If aquifer clogging had increased, pressures in the upper part of the Franconia Formation and in the Ironton and Galesville Sandstones would likely have stabilized. Pressure stabilization was not observed in the field data; therefore, the well bore and aquifer probably were not completely clogged.

Production well A was treated with acid and then pumped at rates ranging from 18.9 to 27.0 L/s for several hours during September 1982. After redevelopment ended, the well was allowed to recover for approximately 16 hours. Water levels in production well A recovered to within 0.03 m of prepumping water levels. This recovery was considered sufficient to conduct a step-drawdown test on production well A.

The step-drawdown test done in September 1982 was similar to tests done on production wells A and B in October 1981 (Miller, 1984). The test included three pumping steps at rates of 20.8 L/s for 120 minutes, 23.0 L/s for 120 minutes, and 25.7 L/s for 160 minutes.

The water temperature measured at the wellhead in production well A increased during the test from 20.0°C to 28.3°C as residual stored heat from the aborted heat injection test was pumped out. Because pressures measured in the well will vary with water viscosity, a temperature-correction factor was applied to the recorded pressure data, as described by Wenzel (1942) and Sniegocki (1963). The correction factor adjusted the resulting drawdowns to a temperature of 10°C, the ambient temperature of the ground water, which enabled the analysis of the data to be directly comparable with the step-drawdown tests done in 1981.

The minimization technique described by Labadie and Helweg (1975) for calculation of the aquifer- and well-loss coefficients in the step-drawdown equation was used to analyze the test data. This method was used to analyze step-drawdown data from tests done on production wells A and B in 1981 and is described in Miller and Delin (1993).

Well-efficiency curves were constructed for production well A using the method of Rorabaugh (1953) just after initial well completion and after well redevelopment by acidization (fig. 7). The well efficiency of 83 percent, calculated for an 18.9-L/s pumping rate, indicates adequate redevelopment of production well A by acidization. The comparison of these two curves can be somewhat misleading, however, if variations in equipment efficiency are not considered. During removal of the pump in production well A on April 30, 1982, the pump-shaft spider-bearing holders were found to have been initially installed backwards. Because the bearing holders are designed to minimize the turbulence of pumped water flowing past them, reverse installation would probably increase turbulence. The increased turbulence could effectively increase the well-loss part of the step-drawdown equation and decrease the overall efficiency of the well. The increased well loss probably resulted in a low efficiency at high pumping rates computed for the step-drawdown test done in 1981. Thus, it is likely that the efficiencies calculated for the step-drawdown tests done in 1981 would have been higher if the pump-shaft spider-bearing holders had been installed correctly. In addition to reinstallation of the bearing holders, one pump bowl was removed from the pump shaft, and the lifting capability of the pump was decreased. Removal of the pump bowl resulted in a lower efficiency because the pump shaft was spinning at a greater rate than previously to maintain the injection rate.

Ambient-temperature water at 10°C was injected into production well A at 18.6 L/s for approximately 2.5 days in late September 1982 to obtain information on the feasibility of injecting water into production well A and to further assess the extent of well redevelopment with acid. Pressure changes in the well during the 8-day injection test in May 1982 (before heat injection) and during the 2.5-day injection test after well redevelopment are illustrated in figure 8. The effects of residual calcium-precipitate are reflected in the approximately 35-kPa increase in pressure in the well compared with pressures measured during the 8-day injection test. This increase in pressure was not considered significant and, after approximately 2 days, the rate of change of pressure with time was similar to the rates for the test before heat injection.

In October 1982, a precipitation filter was installed in the above-ground piping between the heat exchanger and production well A (fig. 3) to reduce precipitation of calcium carbonate on the well screen during future testing. The precipitation filter consisted of two sets of three tanks approximately 1.8 meters long and 0.36 meters in diameter connected in series and filled with a graded, high-purity limestone aggregate. Heated water

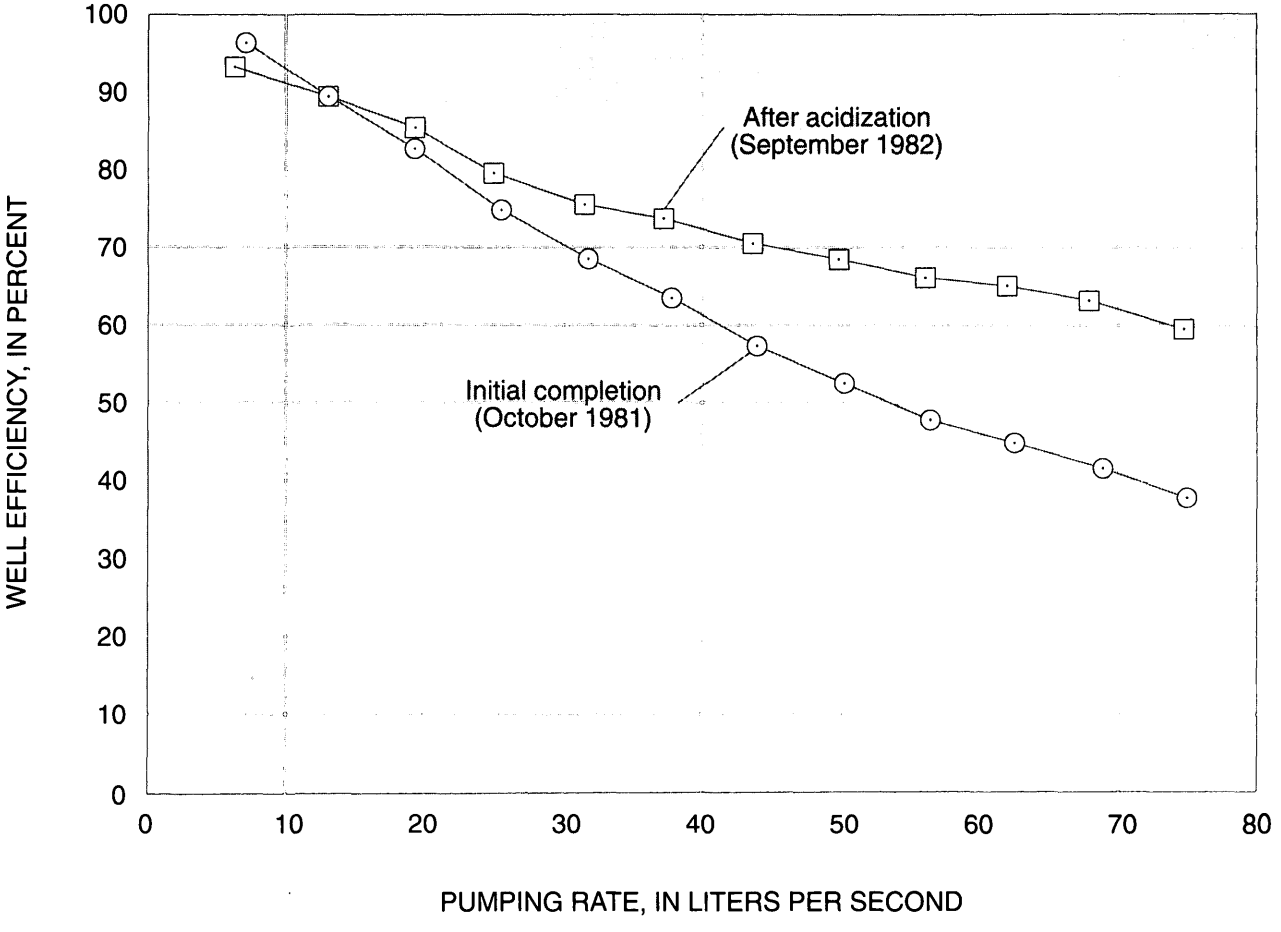

Figure 7.--Well efficiency for production well A after initial completion and after redevelopment by acidization.

was pumped through the tanks where calcium was allowed to precipitate out of solution onto the limestone.

The limestone filter effectively reduced the degree of calcium carbonate supersaturation and reduced the potential for calcium carbonate precipitation within the well bore; however, because water was pumped through the heat exchanger before it was filtered, calcium carbonate precipitation was not reduced within the heat exchanger. Precipitation of calcium carbonate within the heat exchanger resulted in increased pressures in the above-ground pipeline (fig. 3). Consequently, it was necessary to clean the heat exchanger with acid during subsequent tests after approximately every 40 hours of operation to remove all carbonate precipitate. The limestone filter material was replaced with new aggregate while the heat exchanger was cleaned. Maintenance of the filters and heat exchanger required 8 to 15 hours.

Short-Term Test Cycles I-IV

Four short-term test cycles of heat injection were conducted from November 1982 through December 1983. The duration, average rate of injection and withdrawal, and average temperature during injection for the four short-term test cycles are summarized in table 1. The time required for removing the carbonate precipitate from the heat exchanger and for changing the graded limestone material in the precipitation filters interrupted the injection period of each cycle; therefore, the total calendar time of the injection period for a particular cycle was longer than the total storage or total withdrawal periods, although the actual time of heated water injection was approximately equal to that of storage and withdrawal. Four maintenance periods were needed during each of the four test cycles; the result was five individual injection subperiods (termed heat 1 through

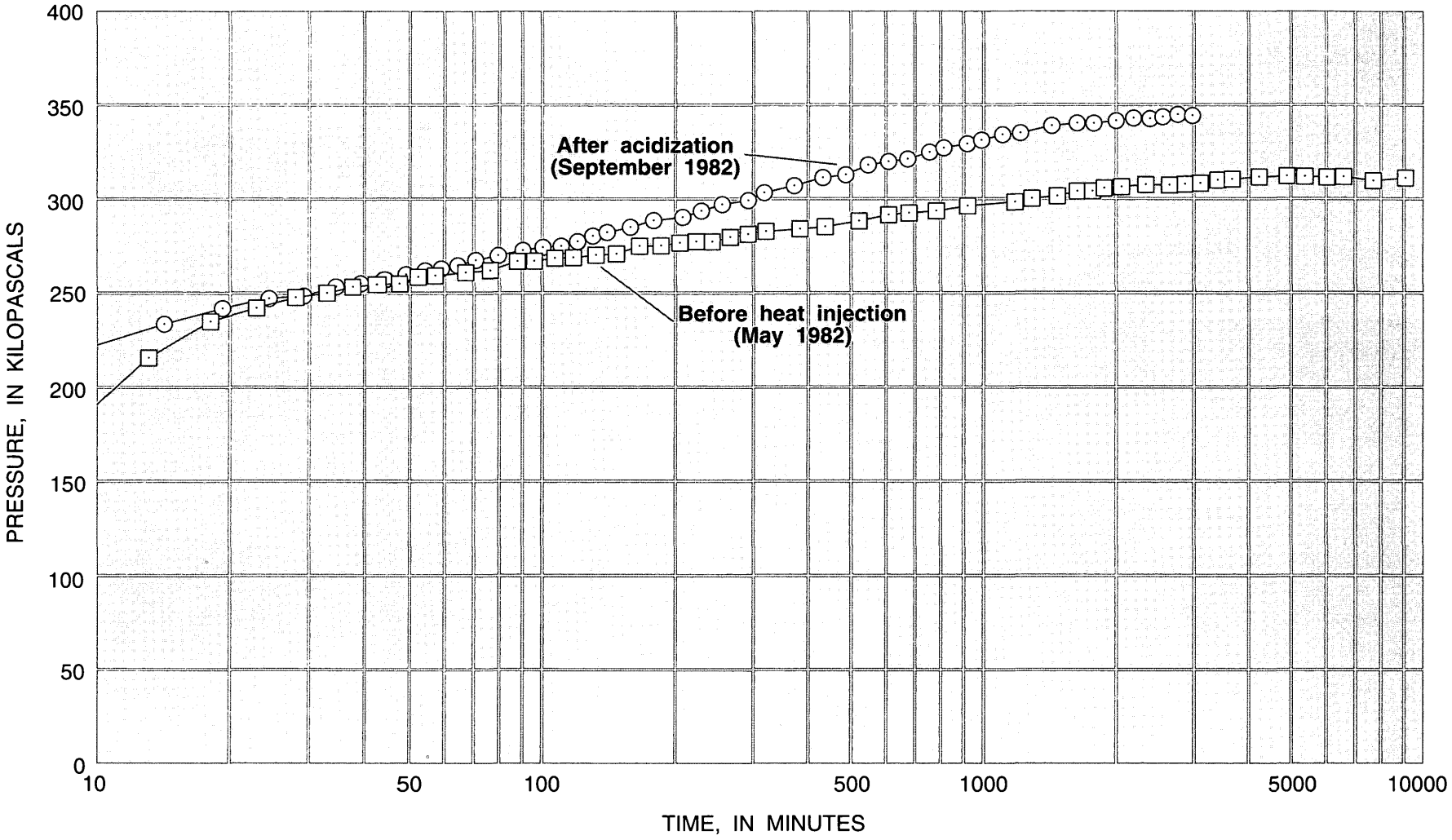

Figure 8.--Pressure changes in production well A during injection at 18.6 liters per second before heat injection and after redevelopment by acidization.

Table 1.--Summary of duration, average rate of injection and withdrawal, and average temperature of injection for four short-term test cycles
[--, not applicable]

Period	Subperiod (heat) number	Duration (days)	Average rate of injection and withdrawal (liters per second)	Average injection temperature (degrees Celsius)
		TEST CYCLE I		
Injection	1	1.26	17.9	88.5
	2	1.13	18.3	92.6
	3	0.94	18.3	90.0
	4	.96	18.3	91.9
	5	.96	19.3	91.7
Total duration of injection	1-5	5.25	18.4	90.9
Storage	--	13.03	--	--
Withdrawal	--	5.28	18.4	--
		TEST CYCLE II		
Injection	1	1.71	18.2	95.5
	2	1.63	17.7	96.3
	3	1.83	17.6	97.9
	4	1.64	17.5	98.0
	5	1.20	17.4	99.7
Total duration of injection	1-5	8.01	17.7	97.5
Storage	--	89.71	--	--
Withdrawal	--	8.00	17.7	--
		TEST CYCLE III		
Injection	1	1.70	18.6	104.4
	2	1.75	18.5	107.2
	3	1.49	18.2	105.6
	4	1.67	18.2	106.1
	5	1.09	18.0	105.0
Total duration of injection	1-5	7.70	18.3	105.7
Storage	--	9.62	--	--
Withdrawal	--	7.91	17.8	--
		TEST CYCLE IV		
Injection	1	1.83	18.4	111.9
	2	1.70	17.9	115.6
	3	1.71	17.5	117.9
	4	1.66	17.9	114.9
	5	.79	17.7	112.6
Total duration of injection	1-5	7.69	17.9	114.6
Storage	--	10.13	--	--
Withdrawal	--	7.71	17.8	--

heat 5 in this report) within each respective cycle (fig. 9). For example, the total duration of injection during test cycle I is equivalent to the sum of the five heats, or 5.25 days. This terminology will be used in the report to describe specific events during injection periods of individual test cycles.

The average injection rates in each test cycle were maintained below the scheduled 18.6 L/s to reduce the back pressure within the above-ground piping because pressure increased during injection as the limestone filters plugged. The injection rate generally started 0.2 L/s higher and ended 0.2 L/s lower than the average value reported in table 1 for each heat step in each injection cycle. The average injection temperature for water in each test cycle ranged from approximately 91°C in test cycle I to approximately 115°C in test cycle IV. The average rate of injection and withdrawal for all cycles was approximately 18.1 L/s.

Injection of heated water during test cycle I was shortened to approximately 5 days to evaluate the newly installed limestone precipitation filters and to repair a major pipe rupture in the heat exchanger. Repair of the above-ground piping necessitated the longer-than-scheduled (13 days instead of 5 days) storage period during test cycle I. Injection during test cycle II totaled 8 days. Problems with bearings in the turbine shaft pump in production well A and subsequent repair caused the storage period to extend to approximately 90 days. Withdrawal during test cycle II was 8 days. Test cycles III and IV were done as scheduled with approximately 8 days of injection and withdrawal and approximately 10 days of storage.

The time lag shown in figure 9 is the time needed for the water temperature in the aquifers and confining units to equilibrate. This is discussed in the Time-Lag Effect section.

Analysis of Thermal Data for Short-Term Test Cycles

The following sections of the report summarize thermal data from the test cycles and describe the movement of heat and the changes in temperature in relation to the hydraulic and thermal properties of the aquifer and confining units. Several possible explanations are given for observed trends at individual observation wells and measurement points. Temperature data for the individual observation wells at site A for the four test cycles are presented graphically as plots of temperature as a function of time (figs. 10-14) and as vertical-profile plots of temperature (figs. 17-20).

Temperature Graphs

Temperature graphs were used to determine the transient effects of temperature change at specific points within the aquifer, especially points at which aquifer properties changed. Included are plots of temperatures at production well A and observation wells AM1, AS1, AM2, and AM3. The temperatures shown for production well A were for the injected water measured at the wellhead. Relatively small temperature fluctuations of between 1 and 5°C, which represent intermittent failure of some thermocouples due to insulation wear at kinks in the wires, are evident in some of the graphs for the observation wells and should be ignored.

The highest temperatures measured in all cycles in every observation well were at altitudes of 45, 52, and 58 m. These altitudes represent the Ironton and Galesville Sandstones, which are the most permeable parts of the Franconia-Ironton-Galesville aquifer (Miller and Delin, 1993). The Ironton part of the aquifer (from 52 to 63 m in altitude) is approximately four times as permeable as the Galesville part of the aquifer (from 42 to 52 m in altitude). Examples of relative arrival times for temperature fronts at the observation wells can be seen in data from observation well AS1 (fig. 12 and table 2). For this study, arrival time was defined as the time at which the temperature first began to rise at a given monitoring point.

For the Ironton and Galesville Sandstones, the earliest arrival times for temperature fronts at every observation well for all cycles were at the 58 m altitude, the upper part of the Ironton Sandstone. The next arrival times for temperature fronts were at the 45 m altitude, and the latest arrival times were at the 52 m altitude. Although temperature fronts arrived last at the altitude of 52 m, the highest temperatures were recorded at this altitude for all observation wells except AM3. Although observation wells AM1 and AS1 are both 7 m from production well A at land surface, arrival times for well AM1 were earlier. This probably is because the bottom of well AM1 was about 6 m from production well A, whereas the bottom of well AS1 was about 13 m from production well A (fig. 5).

The movement of heat in the upper part of the Franconia Formation was considerably slower than in the Ironton and Galesville Sandstones. Temperature fronts reached observation well AS1 about 2.85 days into the first test cycle, or about at the start of heat 3, in the upper part of the Franconia Formation (fig. 12). The first temperature fronts to reach observation well AS1 in the upper part of the Franconia Formation were at altitudes of 93 m, then 88 m, and finally 99 m, as illustrated by the maximum temperatures in figure 12. Temperature fronts were not observed in the upper part of the Franconia

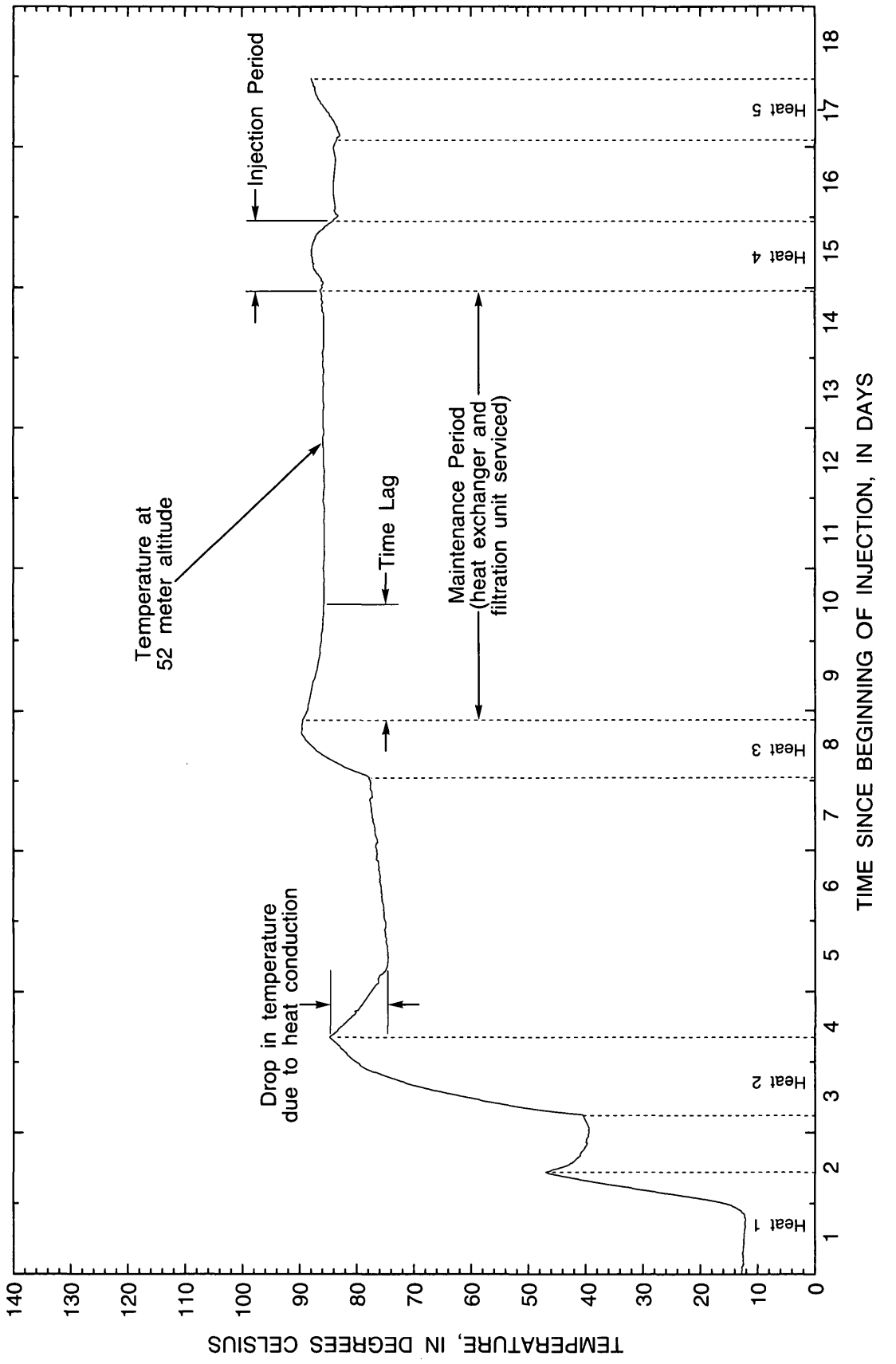

Figure 9.--Aquifer temperature, heat-conduction, and time-lag effects during injection and maintenance periods of test cycle I in observation well AM1.

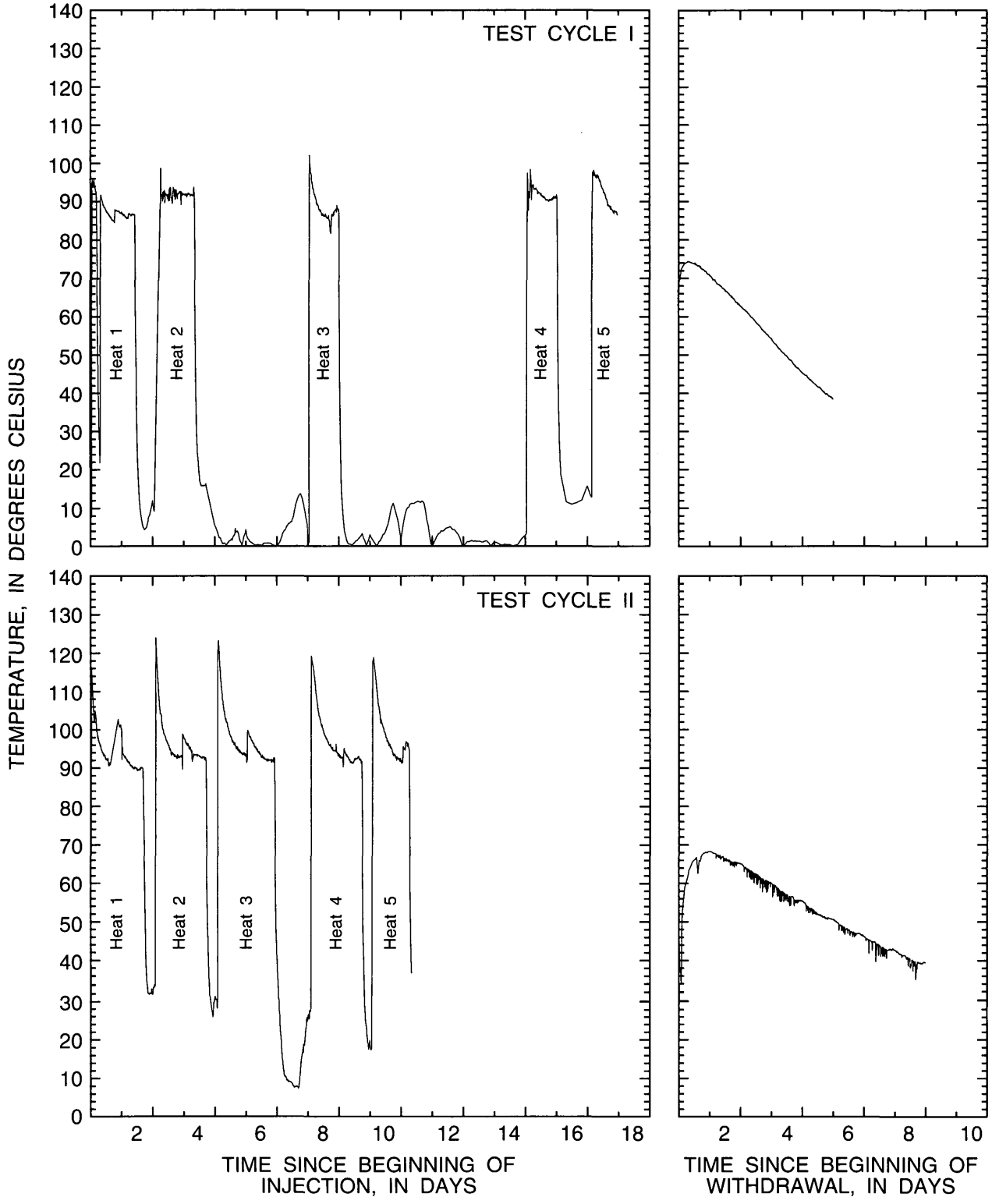

Figure 10.--Temperatures at the wellhead in production well A for the

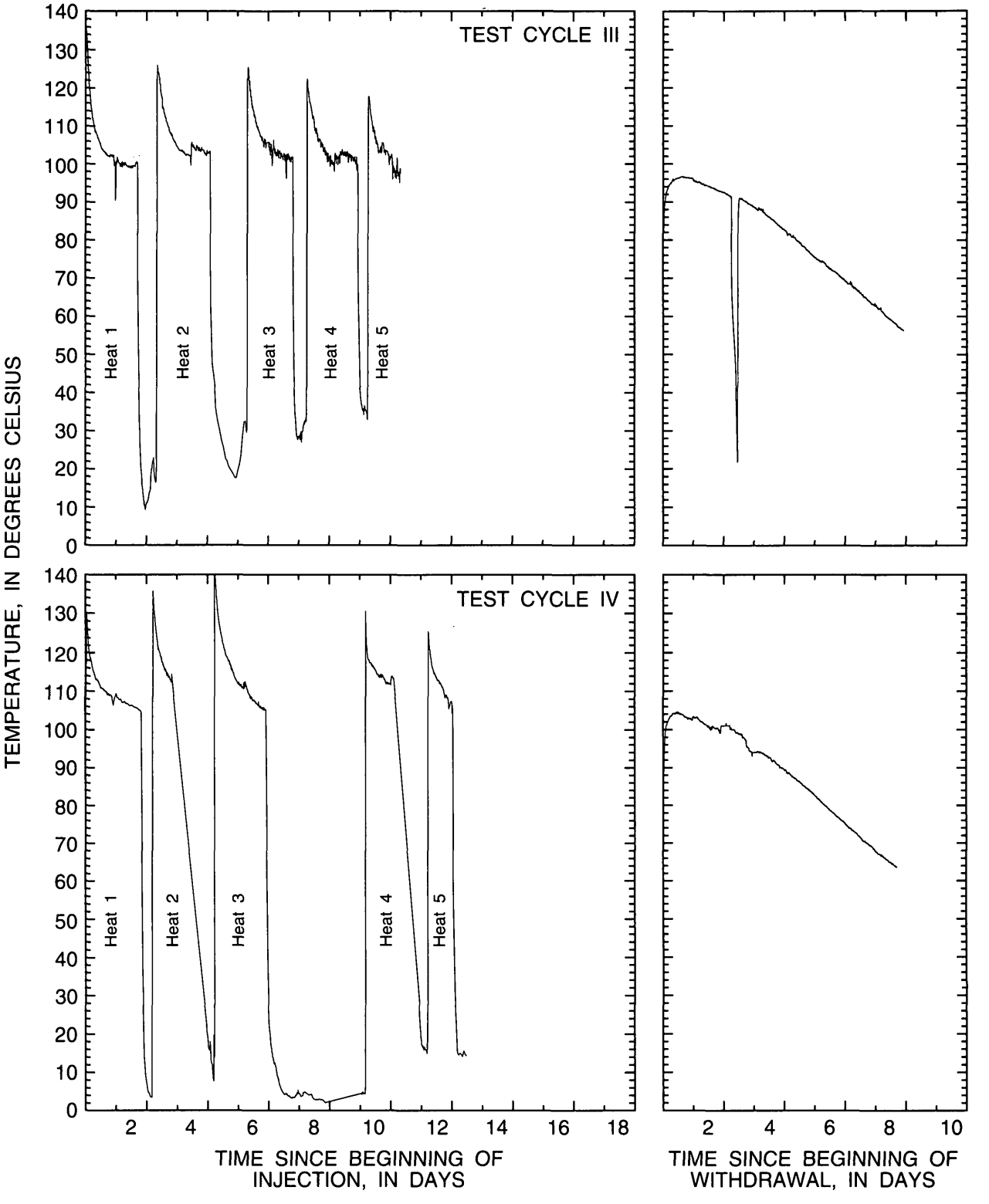

four short-term test cycles during periods of injection and withdrawal.

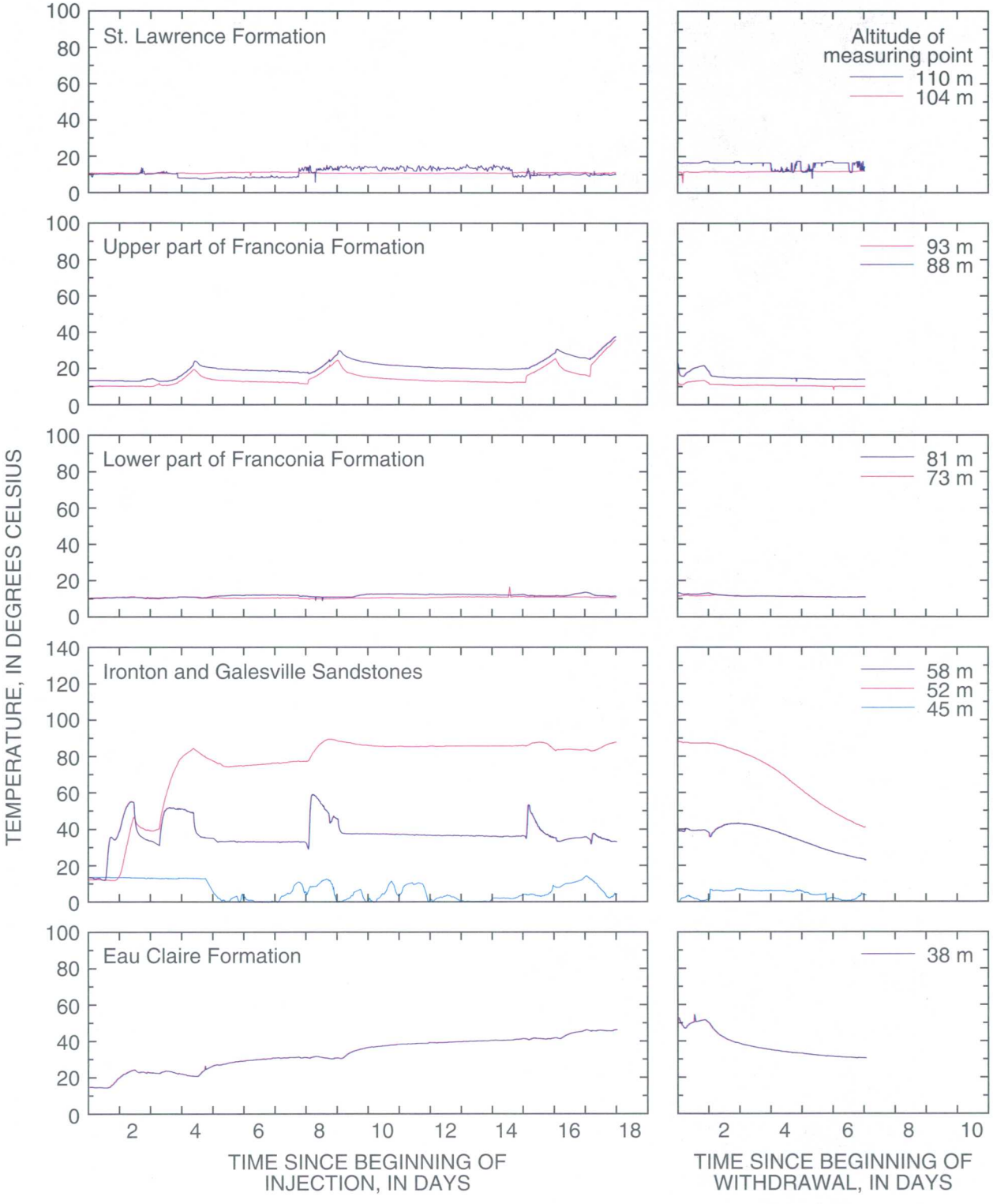

A. Test Cycle I

Figure 11.--Temperatures in observation well AM1 during periods of (C) test cycle III,

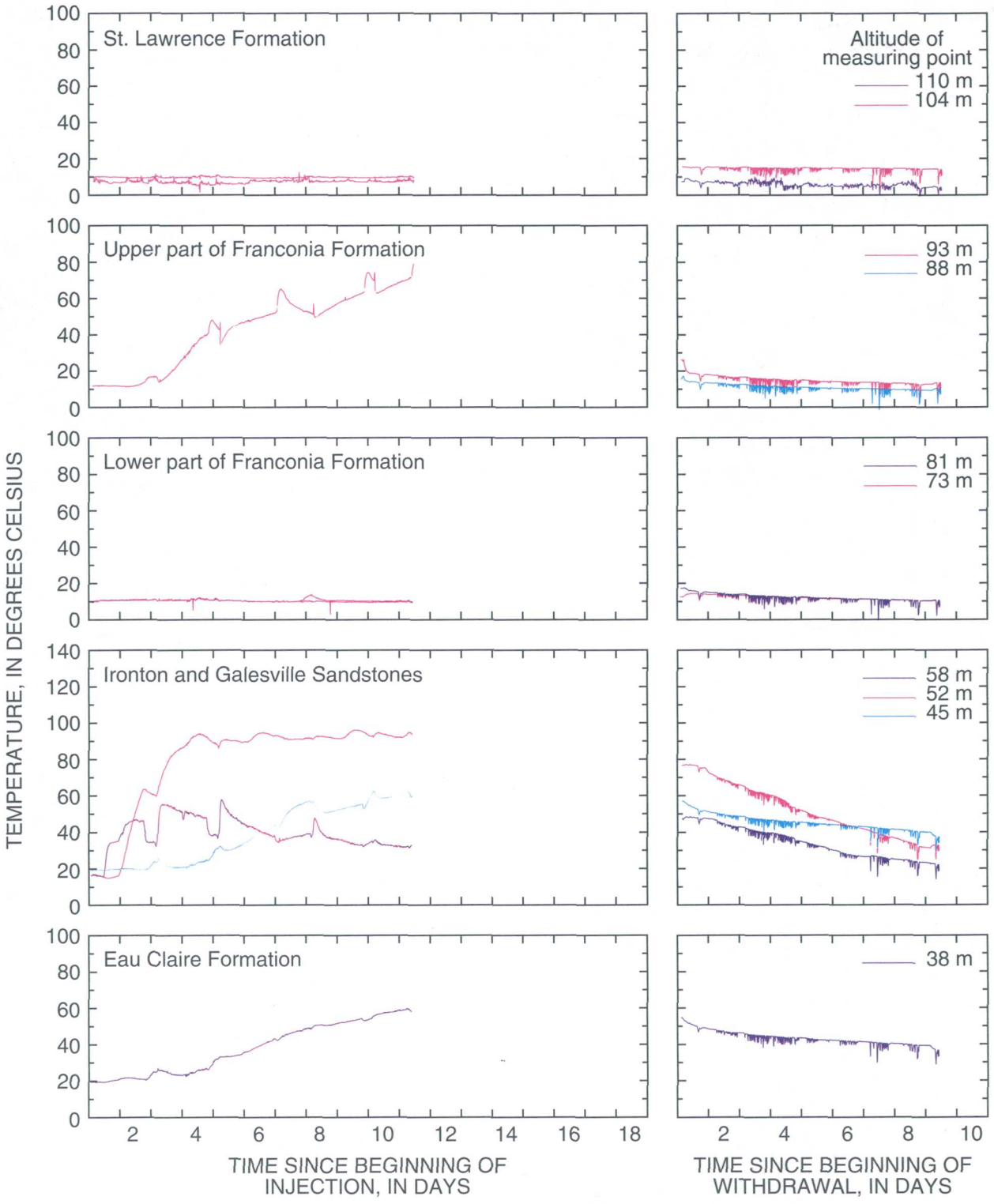

B. Test Cycle II

injection and withdrawal for (A) test cycle I, (B) test cycle II, and (D) test cycle IV.

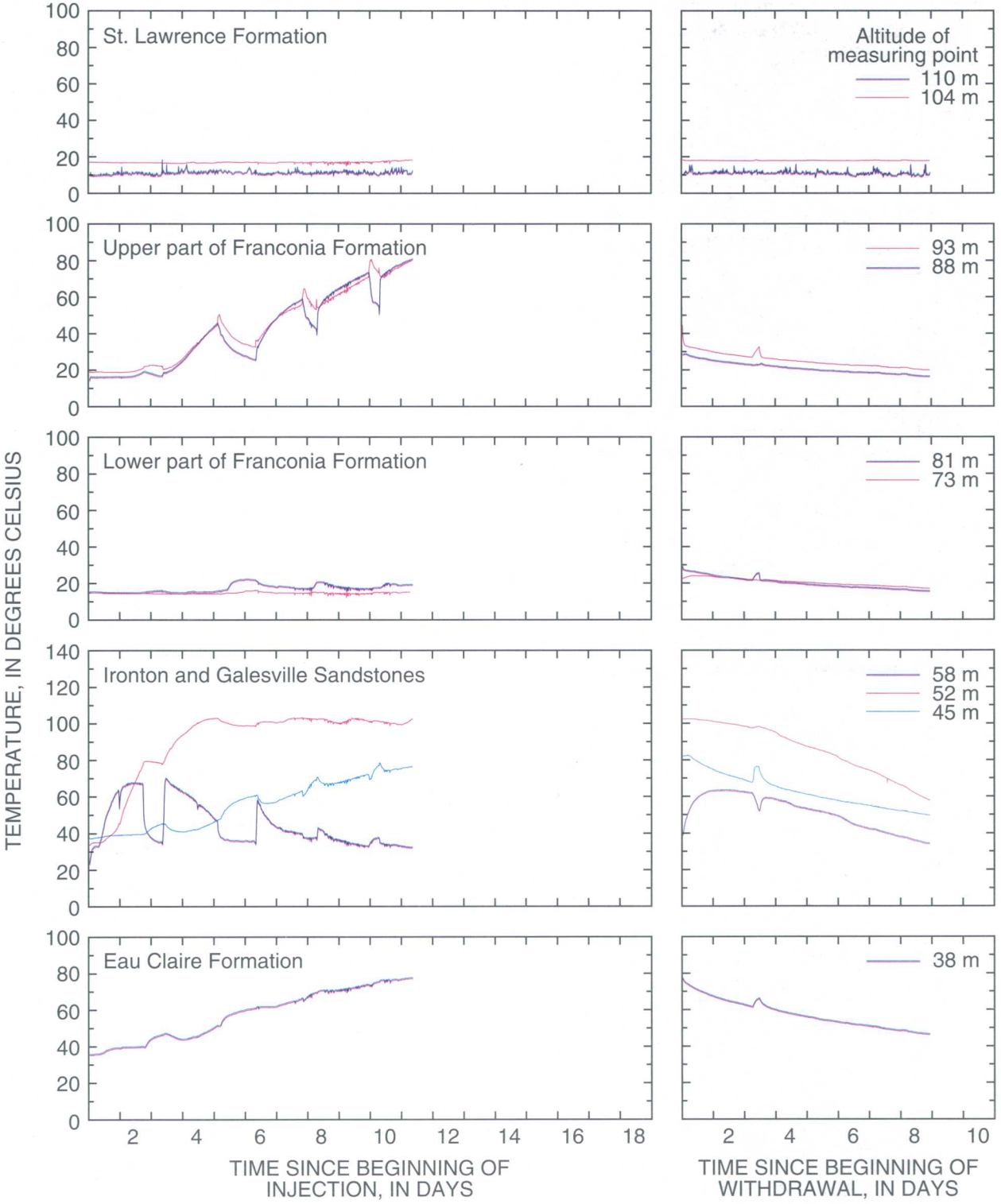

C. Test Cycle III

Figure 11.--Temperatures in observation well AM1 during periods of (C) test cycle III, and (D)

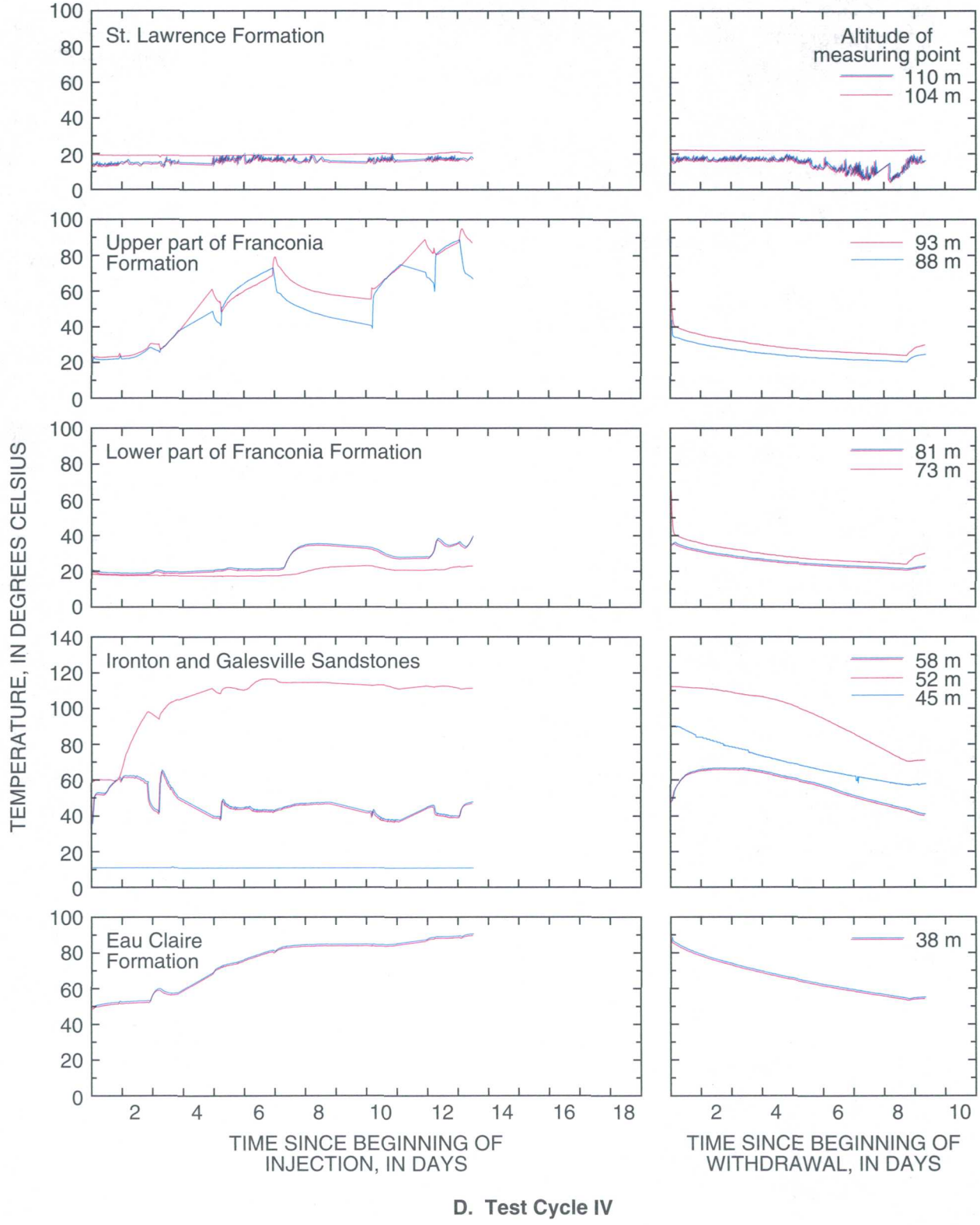

D. Test Cycle IV

injection and withdrawal for (A) test cycle I, (B) test cycle II, test cycle IV. -- Continued

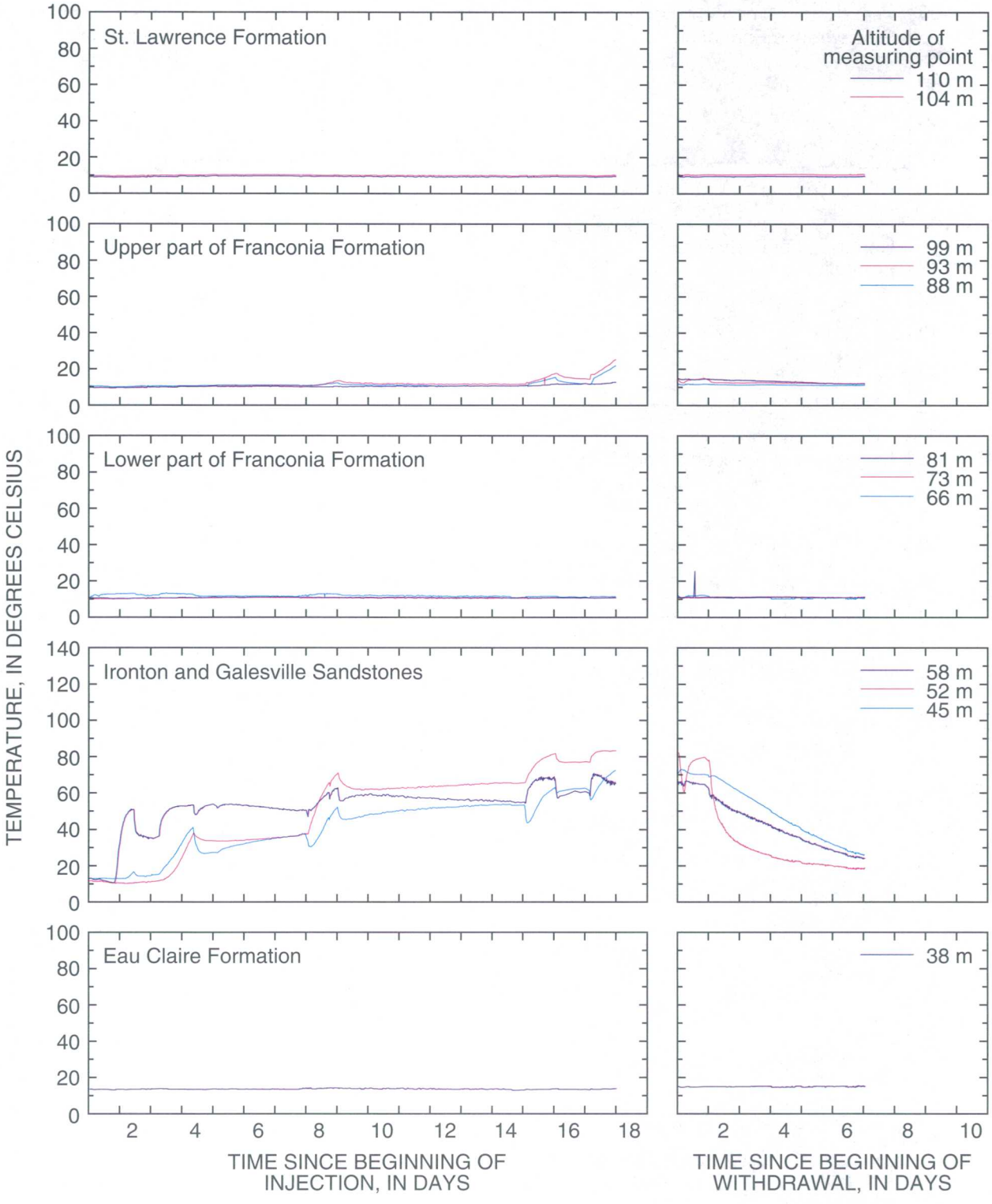

A. Test Cycle I

Figure 12.--Temperatures in observation well AS1 during periods of (C) test cycle III,

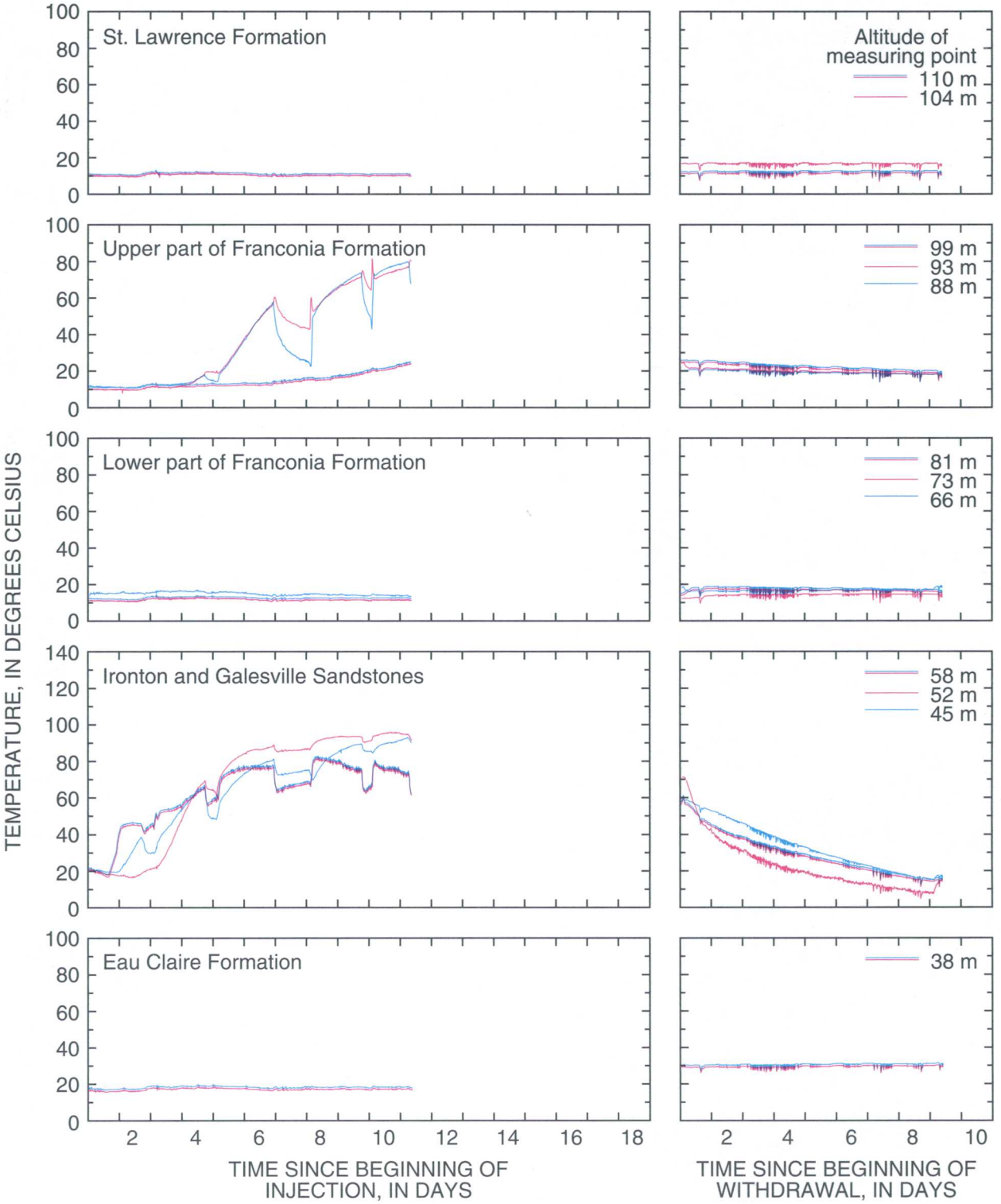

B. Test Cycle II

injection and withdrawal for (A) test cycle I, (B) test cycle II, and (D) test cycle IV.

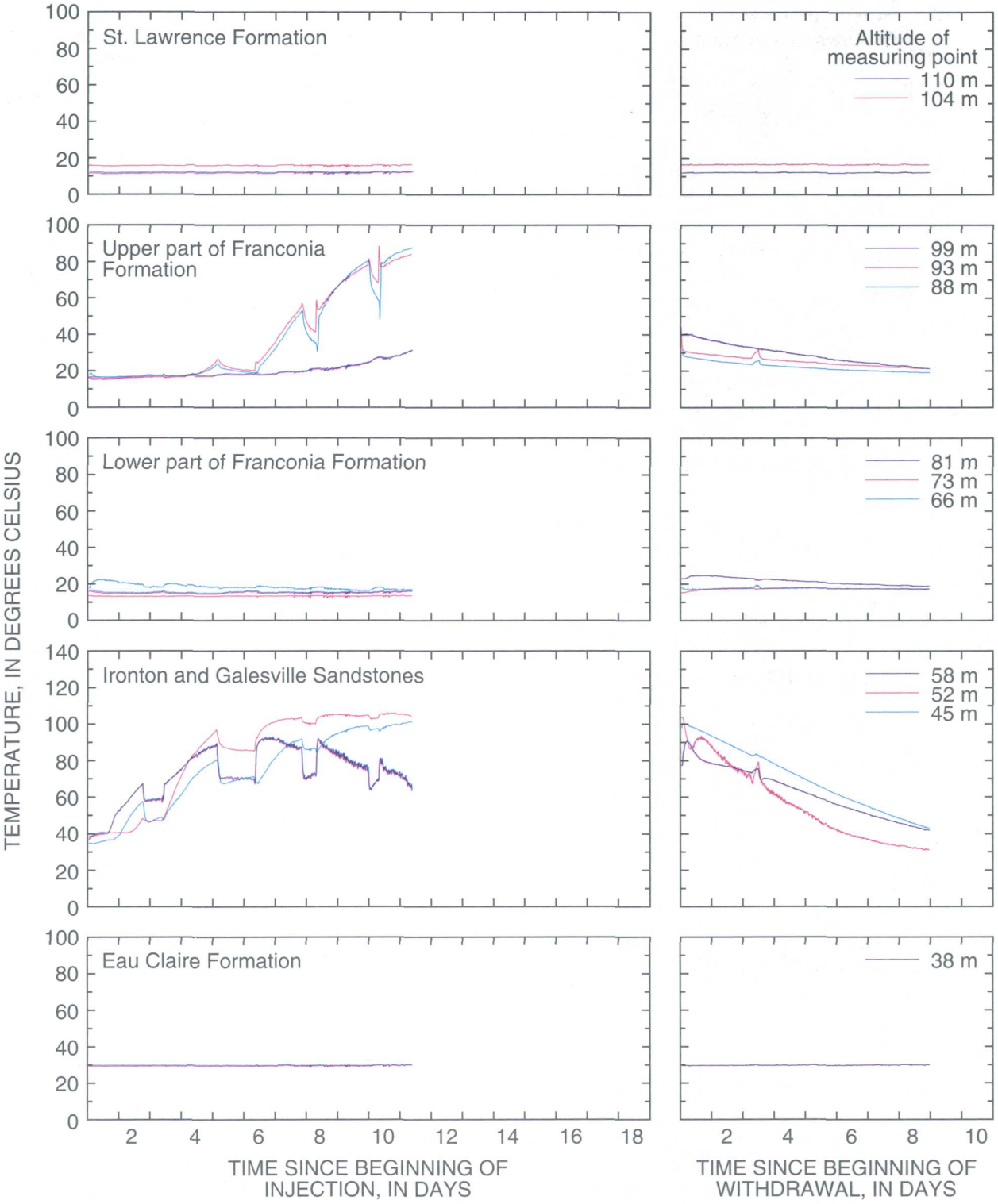

C. Test Cycle III

Figure 12.--Temperatures in observation well AS1 during periods of (C) test cycle III, and (D)

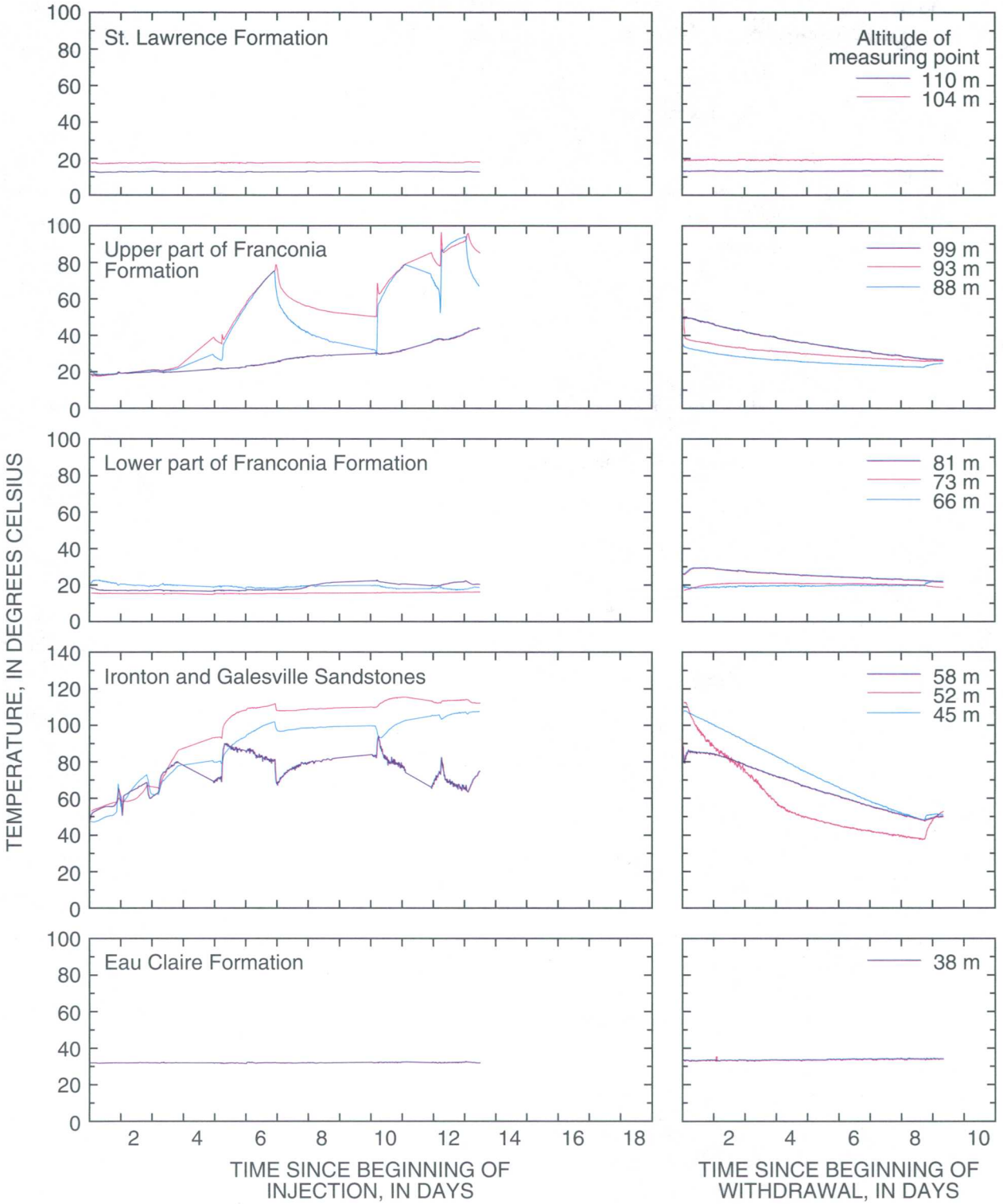

D. Test Cycle IV

injection and withdrawal for (A) test cycle I, (B) test cycle II, test cycle IV. -- Continued

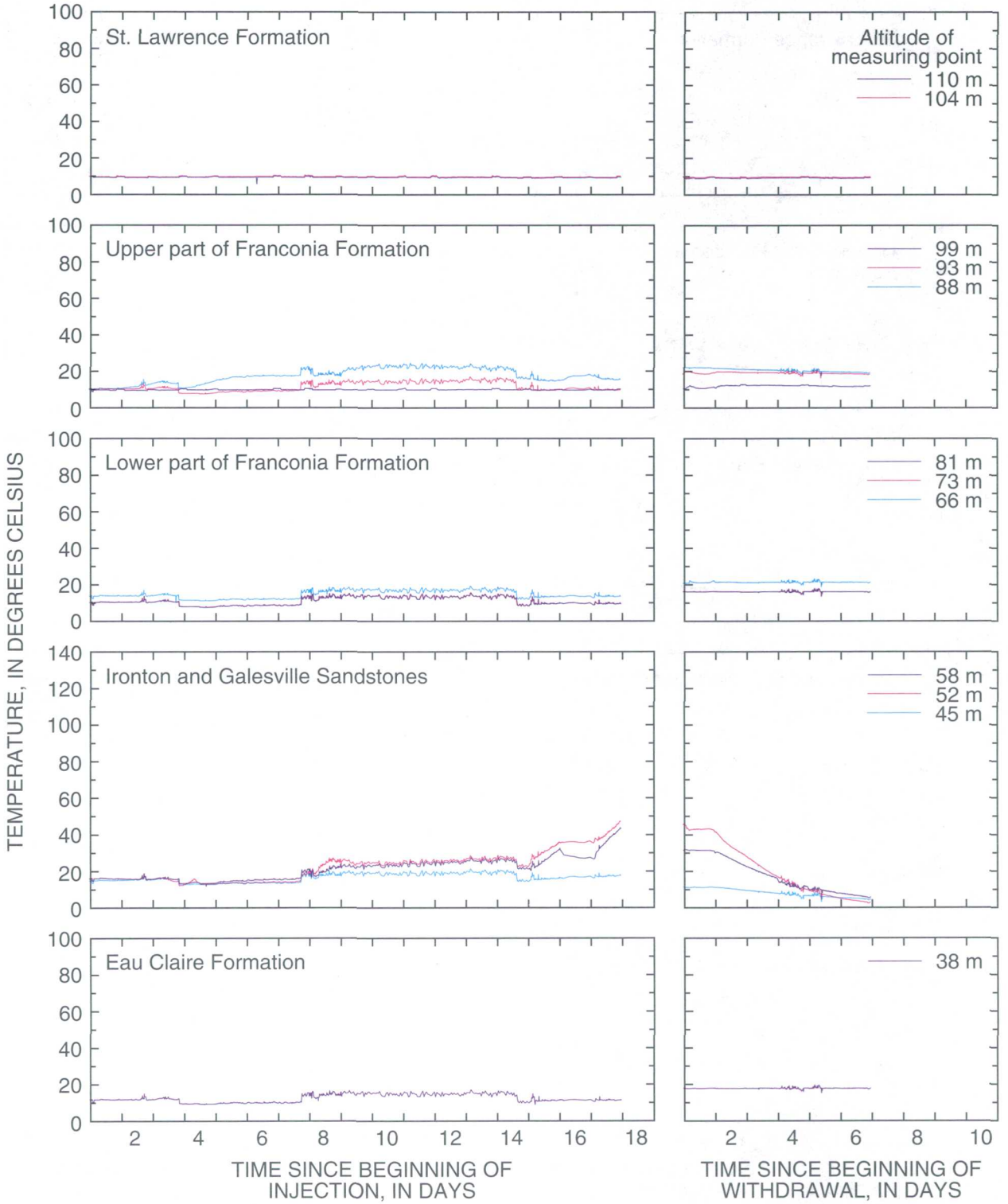

A. Test Cycle I

Figure 13.--Temperatures in observation well AM2 during periods of (C) test cycle III,

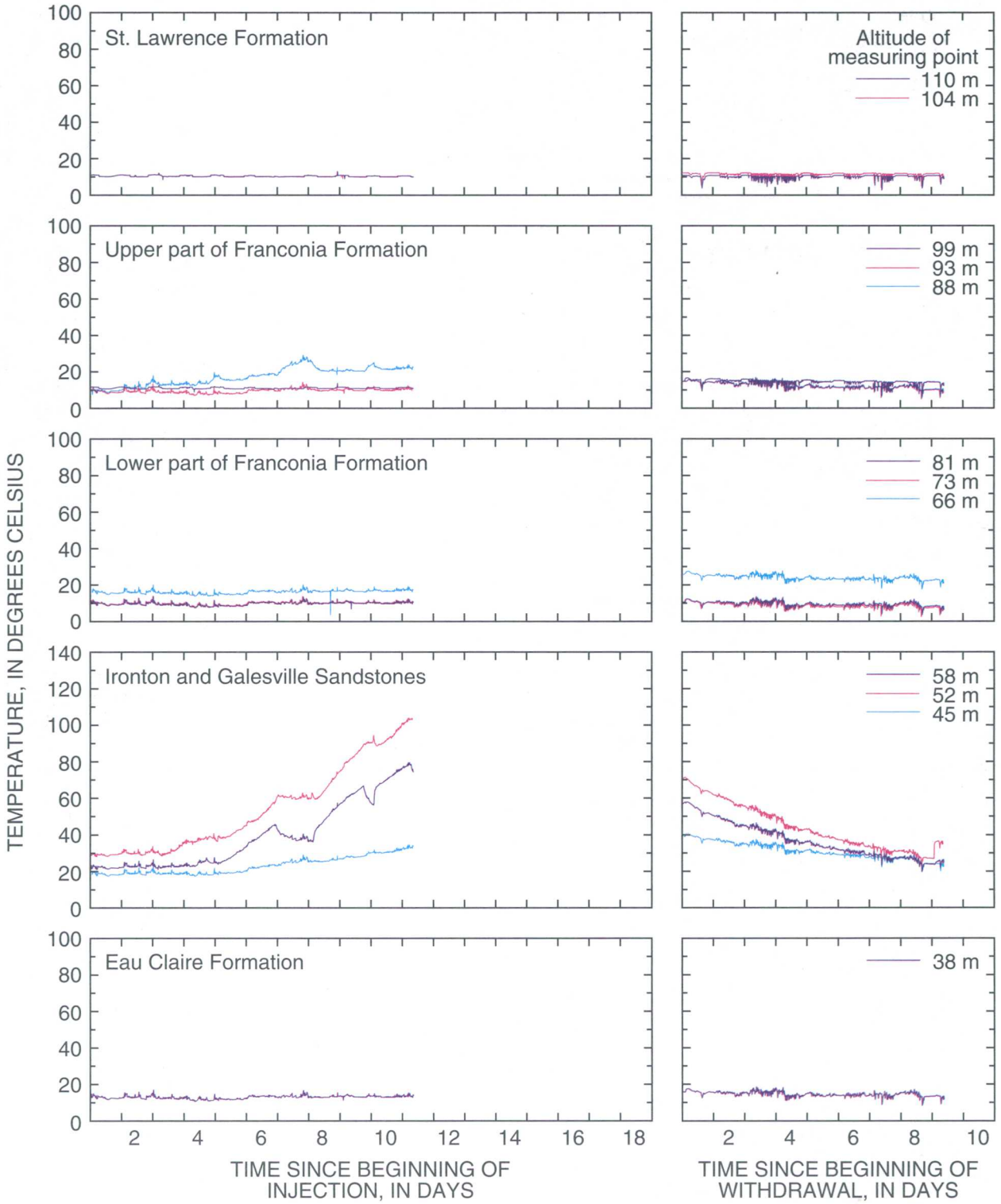

B. Test Cycle II

injection and withdrawal for (A) test cycle I, (B) test cycle II, and (D) test cycle IV.

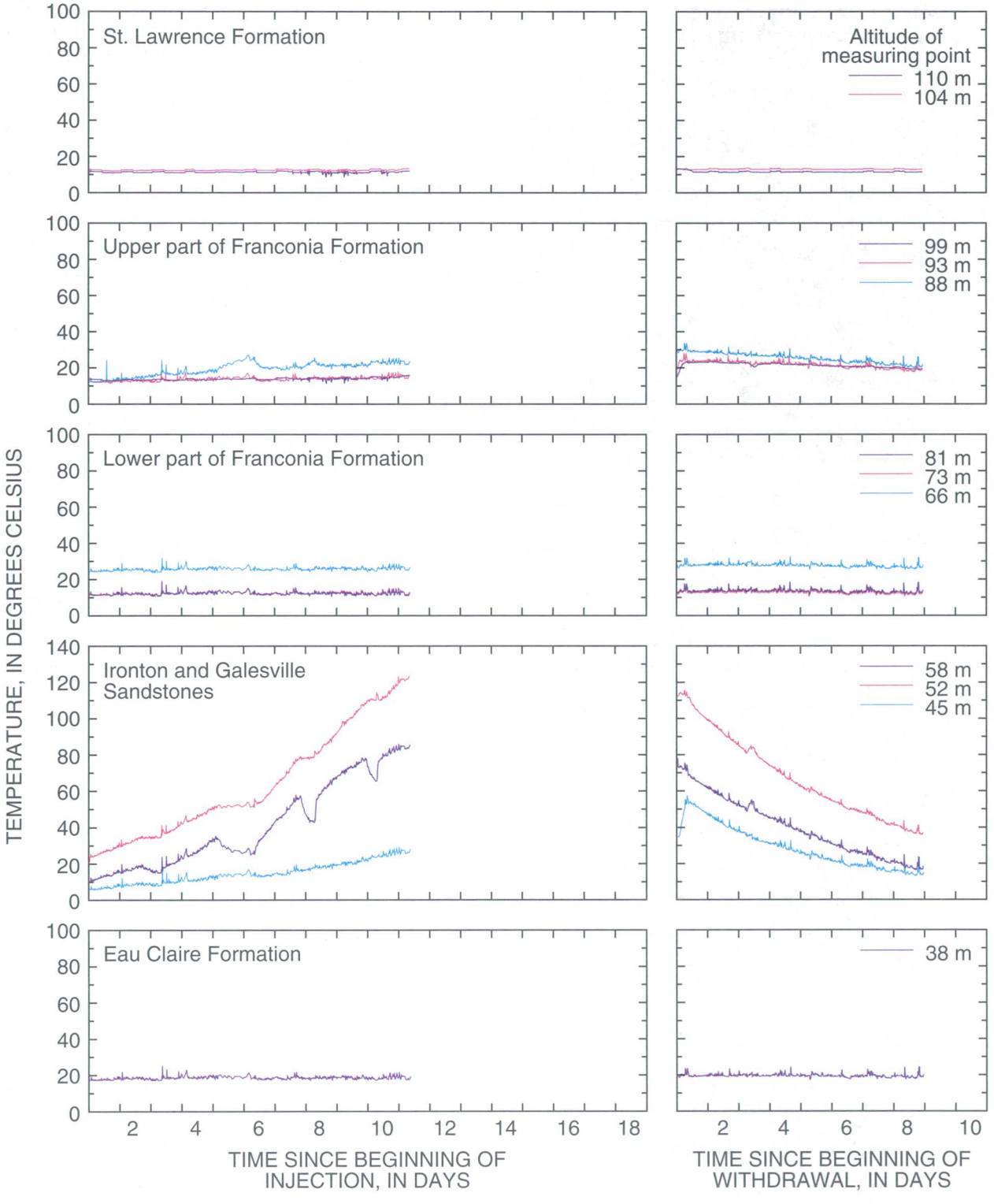

C. Test Cycle III

Figure 13.--Temperatures in observation well AM2 during periods of (C) test cycle III, and (D)

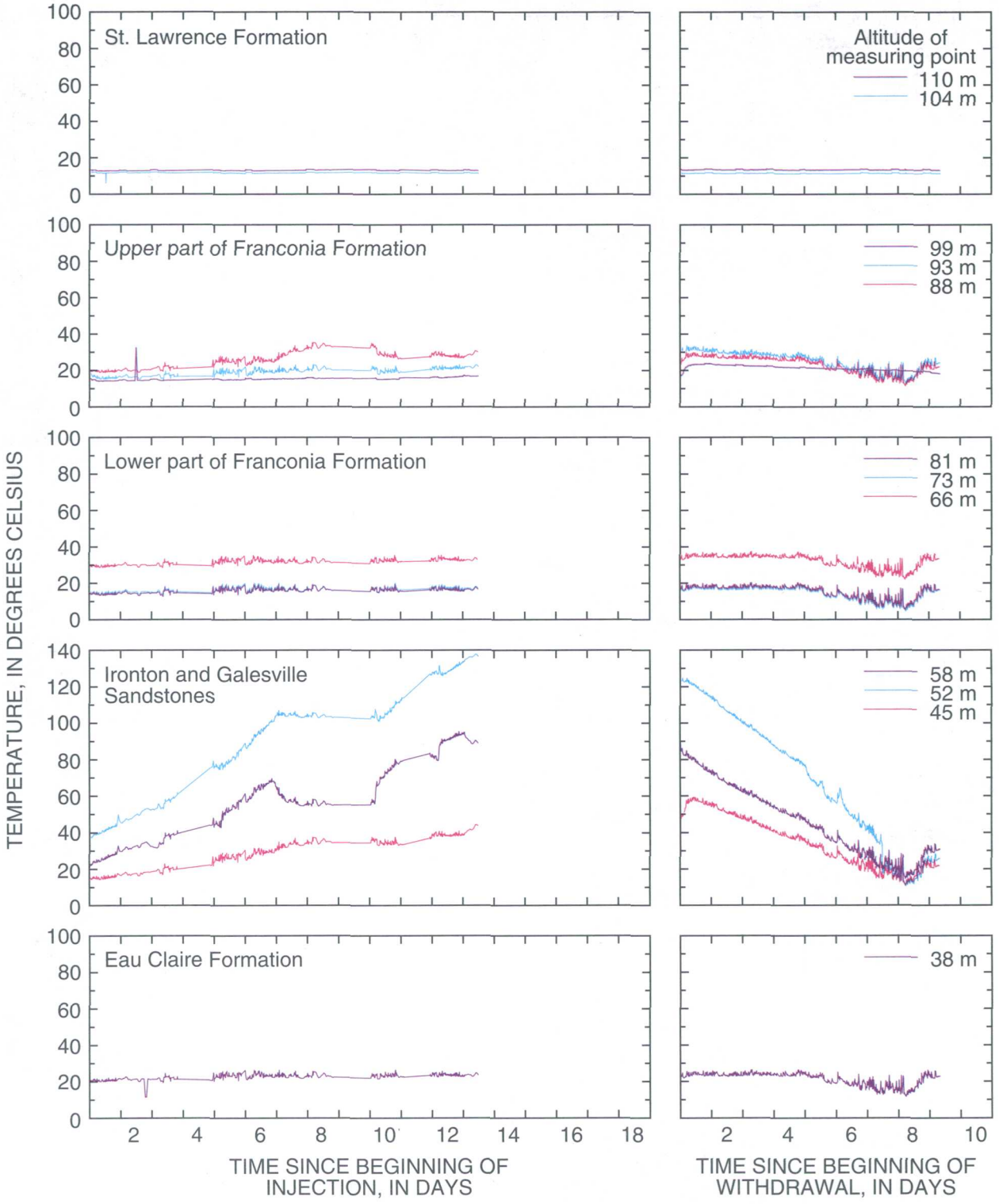

D. Test Cycle IV

injection and withdrawal for (A) test cycle I, (B) test cycle II, test cycle IV. -- Continued

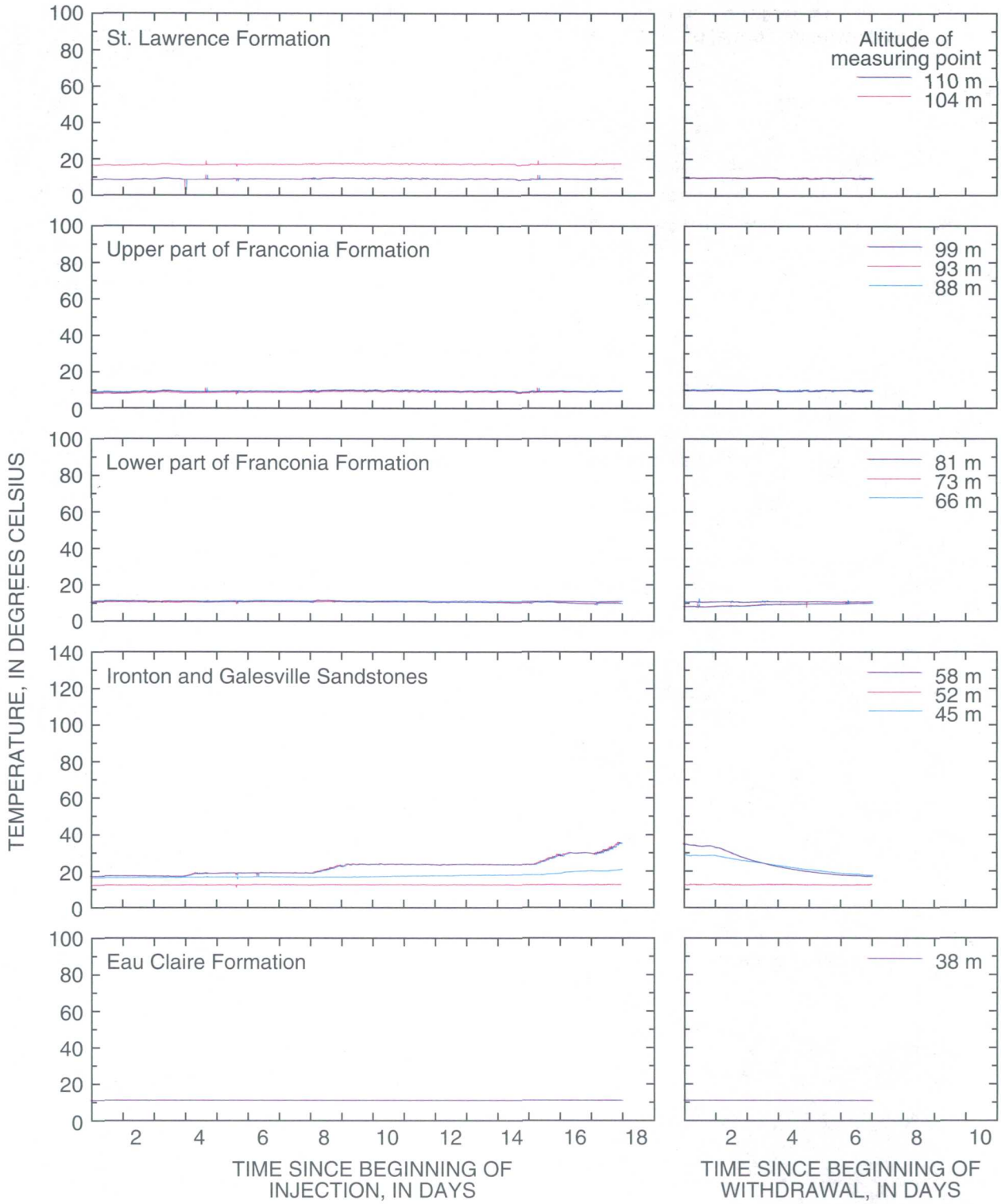

A. Test Cycle I

Figure 14.--Temperatures in observation well AM3 during periods of (C) test cycle III,

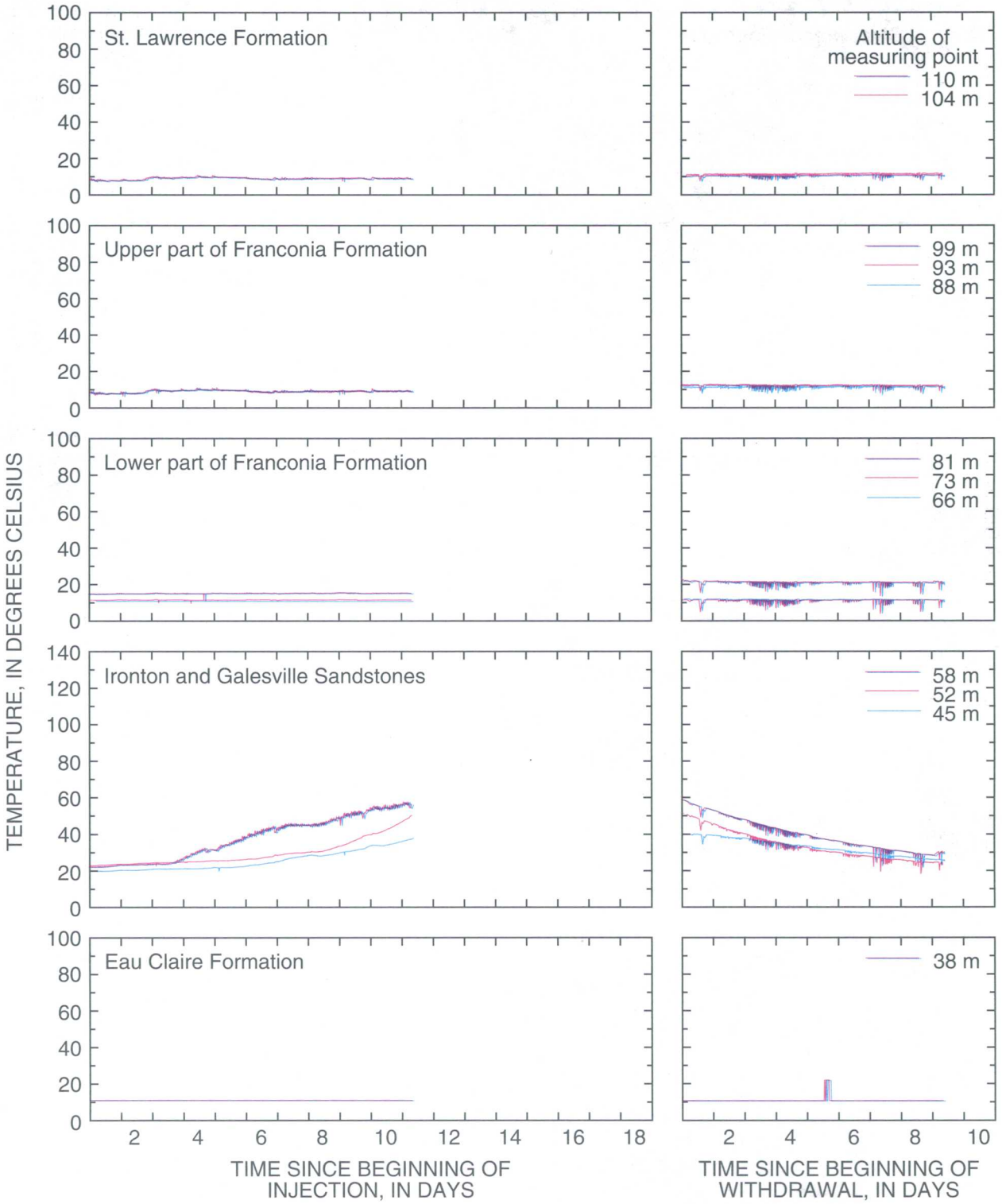

B. Test Cycle II

injection and withdrawal for (A) test cycle I, (B) test cycle II, and (D) test cycle IV.

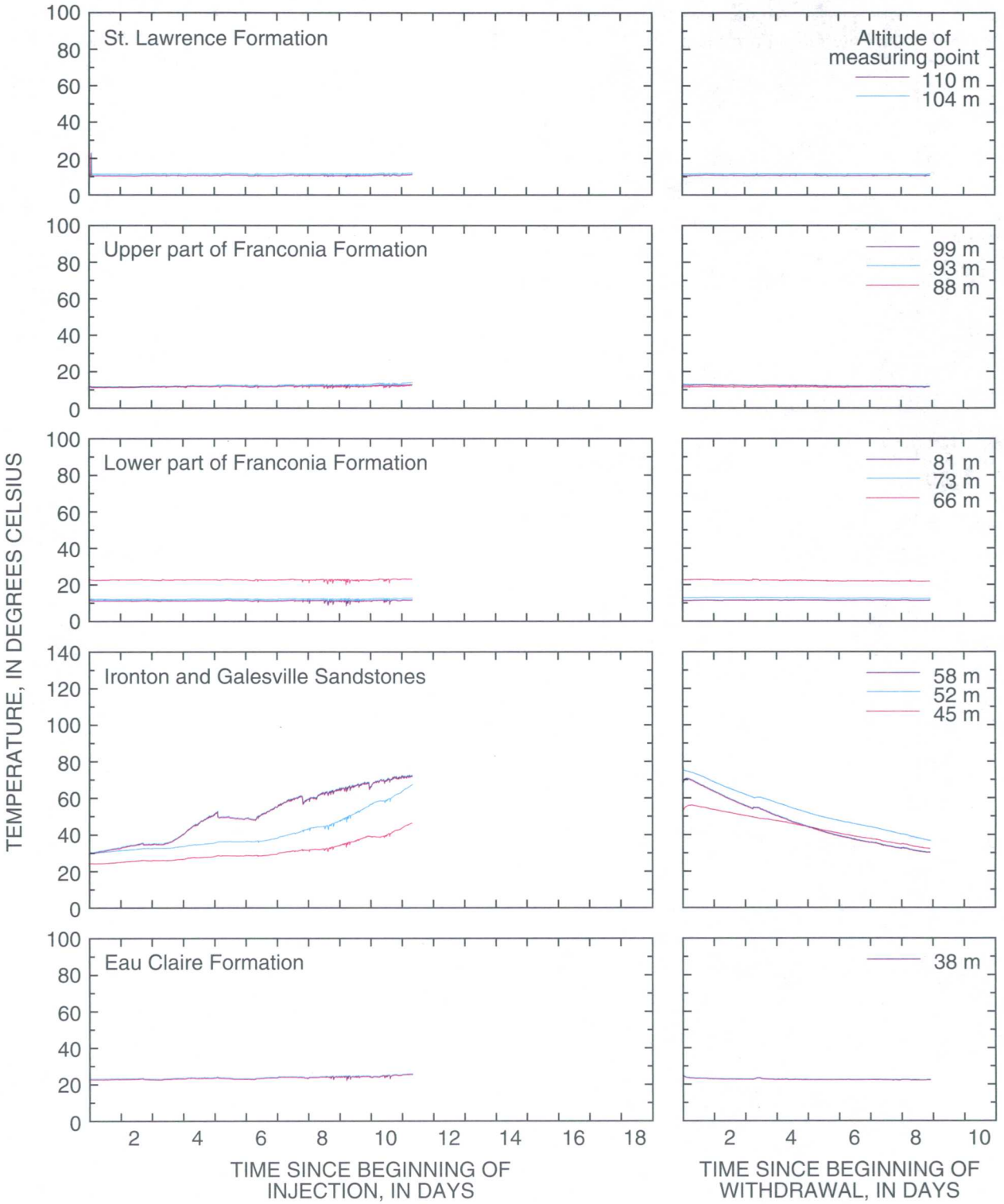

C. Test Cycle III

Figure 14.--Temperatures in observation well AM3 during periods of (C) test cycle III, and (D)

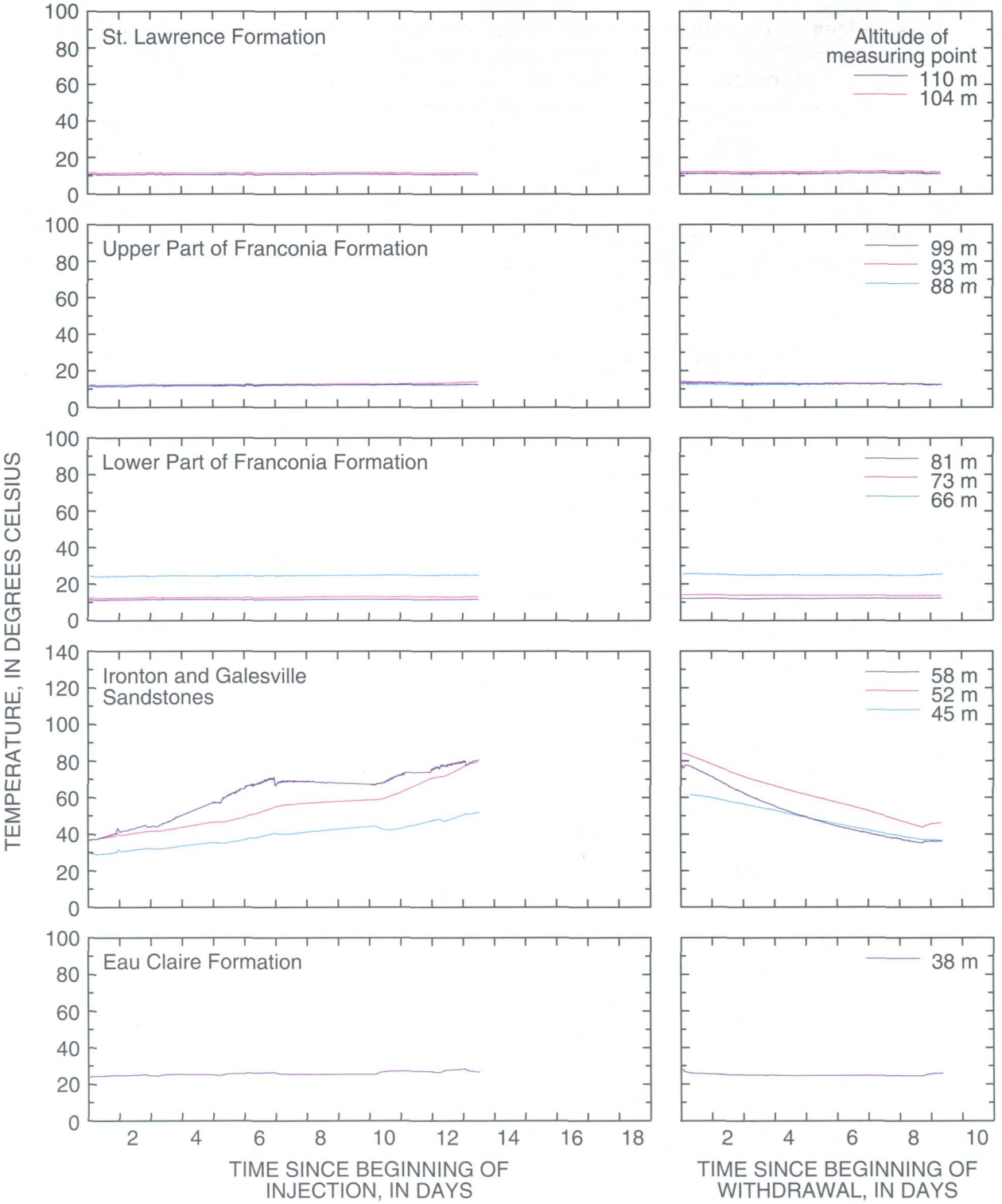

D. Test Cycle IV

injection and withdrawal for (A) test cycle I, (B) test cycle II, test cycle IV. -- Continued

Table 2.--Temperature front arrival time at measurement points in the upper part of the Franconia Formation and in the Ironton and Galesville Sandstones for short term test cycle I
[m, meters; nd, temperature front not detected; --, no data; do., ditto]

Well number and distance from injection well	Geologic unit	Altitude of measurement point, in meters above sea level	Time of temperature front arrival, in days since start of injection
AM1	Upper part of the Franconia Formation	99	2.80
7 m	do.	93	2.80
	do.	88	2.85
	Ironton and Galesville Sandstones	58	.52
	do.	52	.87
	do.	45	--
AS1	Upper part of the Franconia Formation	99	2.85
7 m	do.	93	2.85
	do.	88	2.85
	Ironton and Galesville Sandstones	58	.82
	do.	52	1.35
	do.	45	1.19
AM2	Upper part of the Franconia Formation	99	2.86
14 m	do.	93	1.61
	do.	88	1.66
	Ironton and Galesville Sandstones	58	1.62
	do.	52	1.66
	do.	45	1.66
AM3	Upper part of the Franconia Formation	99	nd
14 m	do.	93	nd
	do.	88	nd
	Ironton and Galesville Sandstones	58	3.00
	do.	52	nd
	do.	45	8.88

Formation at observation well AM3 (fig. 14), the farthest observation well from production well A, for test cycles I and II. This is because the relative permeability of the upper part of the Franconia Formation is about one-half that of the most permeable part of the Ironton and Galesville Sandstones.

Interpretation of the temperature graphs indicates little heat-conduction loss to the overlying St. Lawrence confining unit, altitude 110 m, the underlying Eau Claire confining unit, altitude 38 m, and the unscreened lower part of the Franconia Formation, altitudes 66 to 81 m. Between these three formations, however, heat-conduction losses were greatest in the Eau Claire confining unit. Some of the temperature increase in well AM1 may be due to horizontal heat convection, because the screened interval of production well A extended into

the top 1.5 m of the Eau Claire Formation (Miller and Delin, 1993). Although observation wells AM1 and AS1 were both 7 m from production well A at land surface, heat-conduction losses were greater for well AM1. This probably results because temperatures were greater at well AM1 than at AS1; the bottom of well AM1 was closer to the bottom of production well A than was the bottom of well AS1 (fig. 5). Because the water temperatures were greater near well AM1 than near well AS1, greater heat-conduction losses to the Eau Claire confining unit occurred.

Temperatures measured during the withdrawal periods indicate that the transport of heat within the aquifers is probably a function of permeability. The aquifer temperature cooled more rapidly in the Ironton and Galesville Sandstones than in the upper part of the Franconia Formation.

Temperatures at the beginning of the withdrawal period indicate there was convective heat loss down the well bore of production well A from the upper part of the Franconia Formation to the Ironton and Galesville Sandstones. Temperatures measured in the Ironton and Galesville Sandstones at the beginning of withdrawal were very similar to those at the end of injection for most of the observation wells (figs. 11-14) indicating that heat-conduction losses were minimal in the Sandstones during storage. But the temperatures measured in the upper part of the Franconia Formation (altitudes 88 and 93 m) in wells AM1 and AS1 at the beginning of withdrawal were significantly less than the temperatures measured at the end of the storage period. This heat loss likely was due to convective losses of heat from the upper part of the Franconia Formation down the well bore of production well A to the Ironton and Galesville Sandstones. Because the well was open to both formations and because hydraulic heads decrease with depth in the well, ground-water flow was down the well bore during periods of storage. Thus, a net loss of heat occurred because of the convective flow of heated water between the formations. In addition, the withdrawal plots illustrate that not all of the injected heat was recovered.

Although observation wells AM2 and AM3 were approximately the same radial distance away from production well A at land surface (fig. 5), the temperatures at well AM2 were noticeably higher than those at well AM3 (figs. 13 and 14). The graphs should be similar if the hydraulic and thermal properties are similar in both directions. The most likely explanation for the measured differences is the fact that the bottom of well AM2 was about 16 meters from production well A, whereas the bottom of AM3 was about 19 meters from production well A.

Potential Aquifer Clogging

Upon initial examination, the temperatures registered by the thermocouples at the 58 m altitude in observation wells AM1 and AS1 (figs. 11 and 12) appear unrepresentative of aquifer temperatures. The temperatures increased rapidly during the start of each heat phase and then either remained steady or decreased slowly through the remainder of that heat phase. These data differ considerably from temperatures measured in observation wells AM2 and AM3 (figs. 13 and 14) and seem to be contrary to expectations.

One possible explanation for the different trends at the 58 m altitude for AM1 and AS1 is that the aquifer rather than the well bore was gradually becoming clogged during injection; the permeability and porosity of the aquifer, and thus its ability to transmit heat, were reduced. Examination of aquifer materials indicates that mechanical and chemical processes of clogging probably were responsible. M.C. Hoyer (Minnesota Geological Survey, 1985, written commun.) described the sandstone core taken from observation well AC1 (fig. 3) at the 58 m altitude as being a coarse- to fine-grained, friable sandstone with little carbonate cement. Hoyer also noted that the Franconia-Ironton-Galesville aquifer is most friable at this location. Because of the lack of carbonate cement, it is possible that fine sand may have physically moved near production well A where ground-water velocities were highest during periods of injection and withdrawal. This sand could have moved away from production well A during injection, have repacked within pore spaces at some radial distance from the well bore, and effectively reduced the local permeability and porosity.

Muecke (1978) studied the movement of fine sandstone particles, termed formation fines, in relation to oil- and gas-well development. Muecke determined that mechanical bridging at pore restrictions occurs if certain conditions are met with respect to particle size and the rate of fluid moving through the pores. Although Muecke was unable to make quantitative measurements, he indicates that the percentage of fines that bridge pore spaces depends greatly on the concentration of the fines. When bridges form at pore exits, they act as effective traps for the particles that follow (fig. 15). Bridges can be broken by pressure surges or by reversing fluid-flow direction. Bridge stability, however, depends on the flow velocity where the bridges form. Bridges that form at high flow velocities are tightly packed and are stable during flow reversals. Bridges that form at low flow velocities are unstable, and even slight reversals in flow can unseat them; these fines are then free to move in the reverse direction until bridging occurs in that direction.

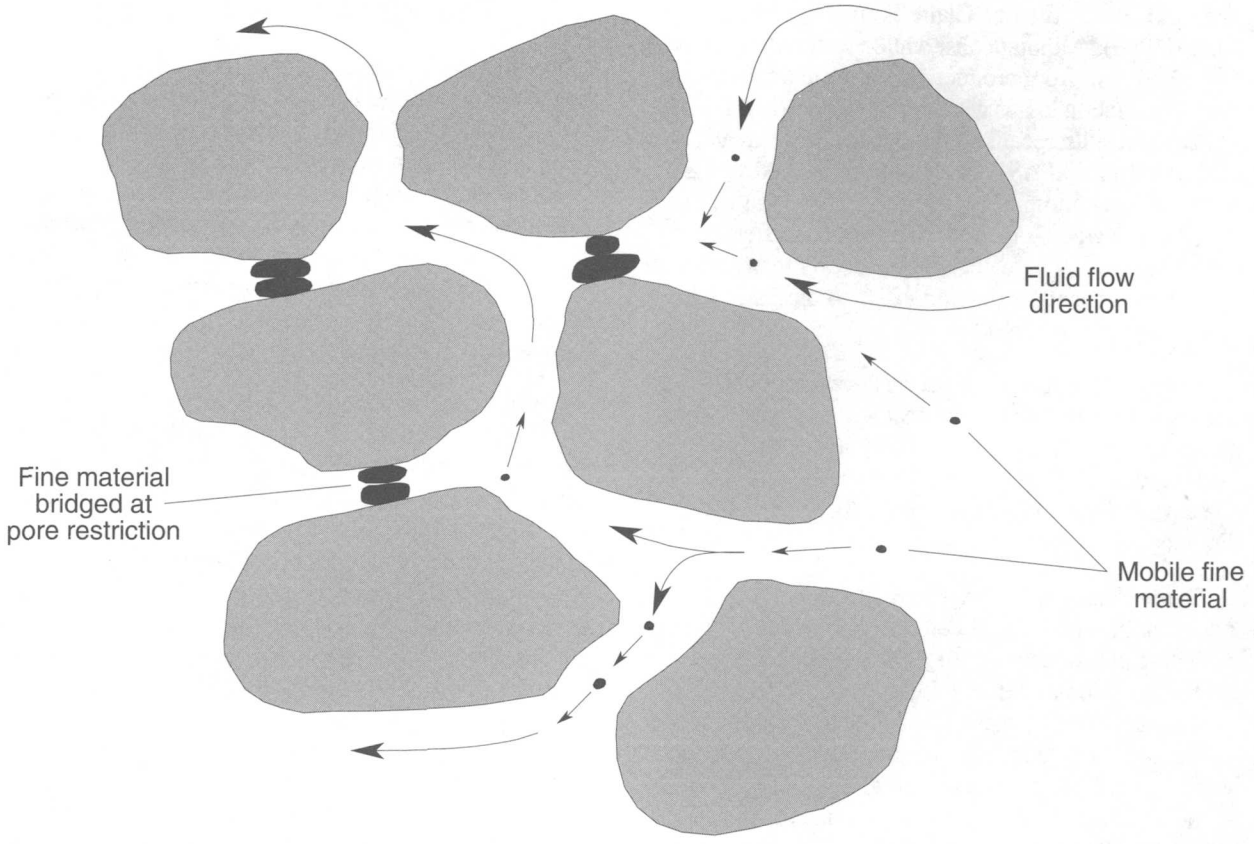

Figure 15.--Bridging of fine material at a pore restriction. (Modified from Muecke, 1978).

An additional observation made by Muecke during his single-phase flow experiments is that continued injection of a solids-free liquid into a matrix containing liquid and mobile fines results in rapid establishment of an equilibrium bridged condition. When this condition is established, continued injection of a solids-free liquid at a constant rate results in virtually no further movement of fine particles.

Mechanical clogging may have been compounded by precipitation of calcium carbonate that was not totally removed by the above-ground filter system. During the withdrawal of water, some carbonate could have re-entered solution, and some pores in the fine-grained sandstone could have unclogged. Some pores, however, could have remained bridged and generally decreased the permeability. Because the aquifer never returned to its initial ambient temperature, some carbonate-cemented grains would have also remained. As a result of this process, the permeability and porosity near the well bore would have decreased. Consequently, the temperature would actually have decreased as injection continued because of a lessening of advective heat transport and an increase in conductive heat transport. A lowering of permeability, and corresponding temperature, was not detected at the 58 m temperature-measurement altitude in observation wells AM2 and AM3 because fluid velocities probably were not high enough to induce migration of fine particles at these radial distances from production well A.

Time-Lag Effect

The concept of time-lag, as defined by Jaeger (1950) and described by Carslaw and Jaeger (1959), states that temperatures in a transport medium increase by advection during periods of heated water injection until they reach maximum values. Rates of heat transport are a function of the heat capacity and thermal conductivity of the aquifers and confining units. The transport of heat within an aquifer is primarily by advection (that is, by flow of the

injected water) and is secondarily by conduction through the aquifer materials. During periods of injection, temperatures at the same radial distance from the injection well are lower in confining units than in aquifers because heat transport in confining units is primarily by the slower process of conduction (fig. 16). When heat injection stops and conduction becomes the main heat-transport mechanism, temperatures in aquifers and confining units approach equilibrium. During periods of storage, temperatures increase in the confining units and decrease in the aquifers; the line of equal temperature approaches the vertical (fig. 16). The period from immediately after injection stops until an equilibrium temperature is achieved is defined as the time lag (fig. 9).

The duration of the time lag depends on the number of low-permeability zones within an aquifer and on the thickness, heat capacity, and thermal conductivity of the aquifers and confining units. Also of importance is the location of the temperature-measurement point, both vertically relative to confining units and horizontally relative to the injection well.

Time-lag heat conduction was detected at most temperature-measurement altitudes in the Ironton and Galesville Sandstone and in the upper part of the Franconia Formation in observation wells AM1 and AS1 (figs. 11 and 12), the wells closest to production well A. A time lag was also detected, but generally less pronounced, at some of the temperature-measurement altitudes in these formations in observation wells AM2 and AM3 (figs. 13 and 14), the most distant wells from production well A. A time lag was detected in observation well AM3 only at the 58 m altitude, which corresponds to the most permeable part of the injection zone.

Temperature Profiles

Temperature profiles at individual observation wells (figs. 17-20) are useful in (1) determining the effects of buoyancy flow (Miller and Delin, 1993), (2) examining temperature variations in relation to hydraulic and thermal properties of the aquifer, and (3) determining possible long-term trends of vertical heat loss from the aquifer. Temperature profiles are presented for the end of each heat phase during the injection period (heats 1 through 5), each storage period, and each withdrawal period. The temperature-measurement altitudes for each of the observation wells are shown in figure 4.

The temperature profiles were constructed by connecting the successive temperature-measurement altitudes with straight lines. This linear interpolation may not be totally representative of the temperature between the temperature-measurement points, especially where the temperature was interpolated across a major hydraulic or thermal boundary such as near confining layers and the unscreened lower part of the Franconia Formation. Contrasts in temperature across these boundaries were large (20 to 40°C), especially at observation wells AM1 and AS1, which were closest to production well A. The contrast in the advective heat-transport rate in the most permeable part of the aquifer and the conductive heat-transport rate in the least permeable parts of the aquifer and in the confining layers was most noticeable near production well A. Although detail is lacking for temperature variation at the hydraulic and thermal boundaries, the linear-interpolation method did not seriously hinder use of the temperature profiles in describing the energy-transfer processes within the aquifer and confining units.

The shape of the temperature profiles shown in figures 17 through 20 generally reflects the distribution of permeability described by Miller and Delin (1993) for the Franconia-Ironton-Galesville aquifer. Highest temperatures were in the Ironton and Galesville Sandstones, and lowest temperatures were in the lower part of the Franconia Formation. Temperatures in the Ironton and Galesville Sandstones and in the upper part of the Franconia Formation at each observation well generally reached a maximum during heat 5, as expected (figs. 17-20). The maximum temperature did not occur, or was not detected, during heat 5 in some of the test cycles because of one or more of the following factors: (1) an insufficient number of vertical monitoring points at each well; (2) the variation in injection temperature during each heat phase (table 1), which resulted in maximum temperatures that were not comparable; and (3) the relatively small changes in temperature (less than 5°C) that occurred over relatively short time periods of several hours that cannot be accounted for because of the complexity of the test cycles.

The convection of ground water created by the difference in density between the ambient-temperature aquifer water and the warmer injected water is termed buoyancy flow, (Hellstrom and others, 1979). Buoyancy flow causes thermal stratification and tilting of the thermal front (Miller and Delin, 1993). The effects of buoyancy flow are most readily observed near the top of an aquifer at the end of storage periods.

The effects of buoyancy flow were not readily noticeable in the temperature profiles at the test facility (figs. 17-20). The effects of buoyancy flow were most noticeable in the Ironton and Galesville Sandstones at observation well AM2 at the end of storage for test cycle II (fig. 19) and in the Ironton and Galesville Sandstones at observation well AM3 at the end of storage for test cycles

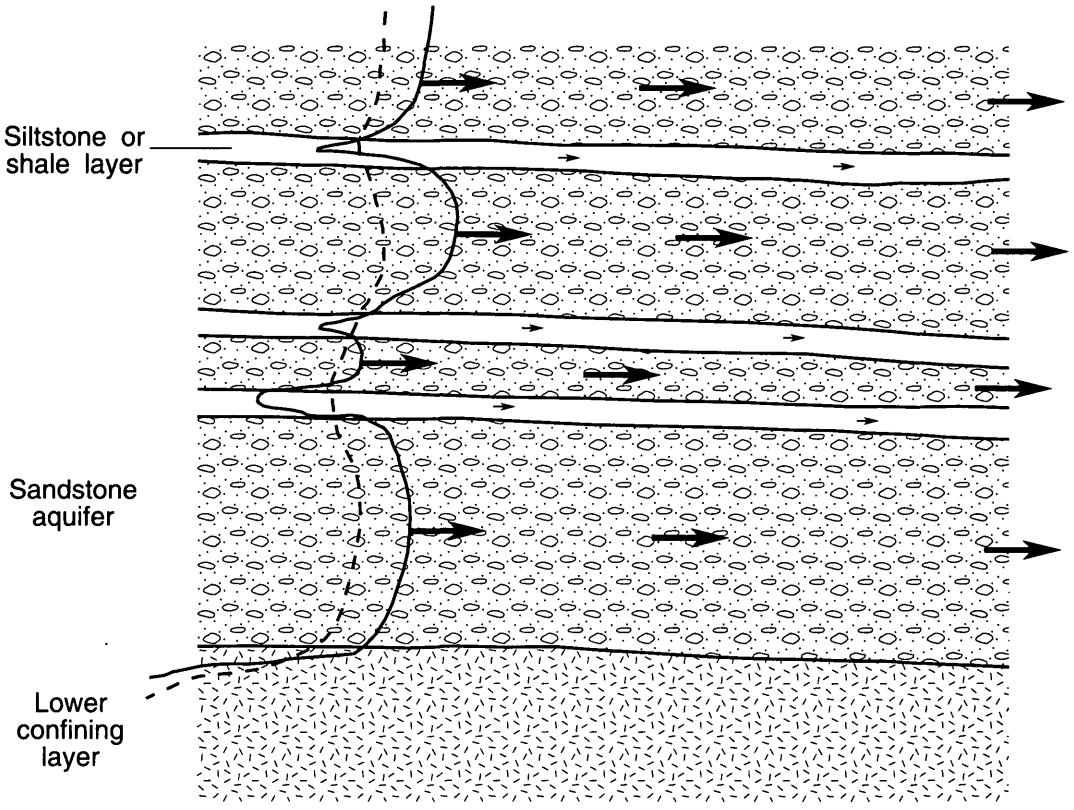

EXPLANATION

Line of equal temperature after periods of injection

Line of equal temperature after periods of storage

Direction of energy transport by condition

Direction of energy transport by advection

Figure 16.--Generalized temperature profiles after periods of injection and storage in a cross-section of sandstone and shale with different permeabilities. (Modified from Carslaw and Jaeger, 1959).

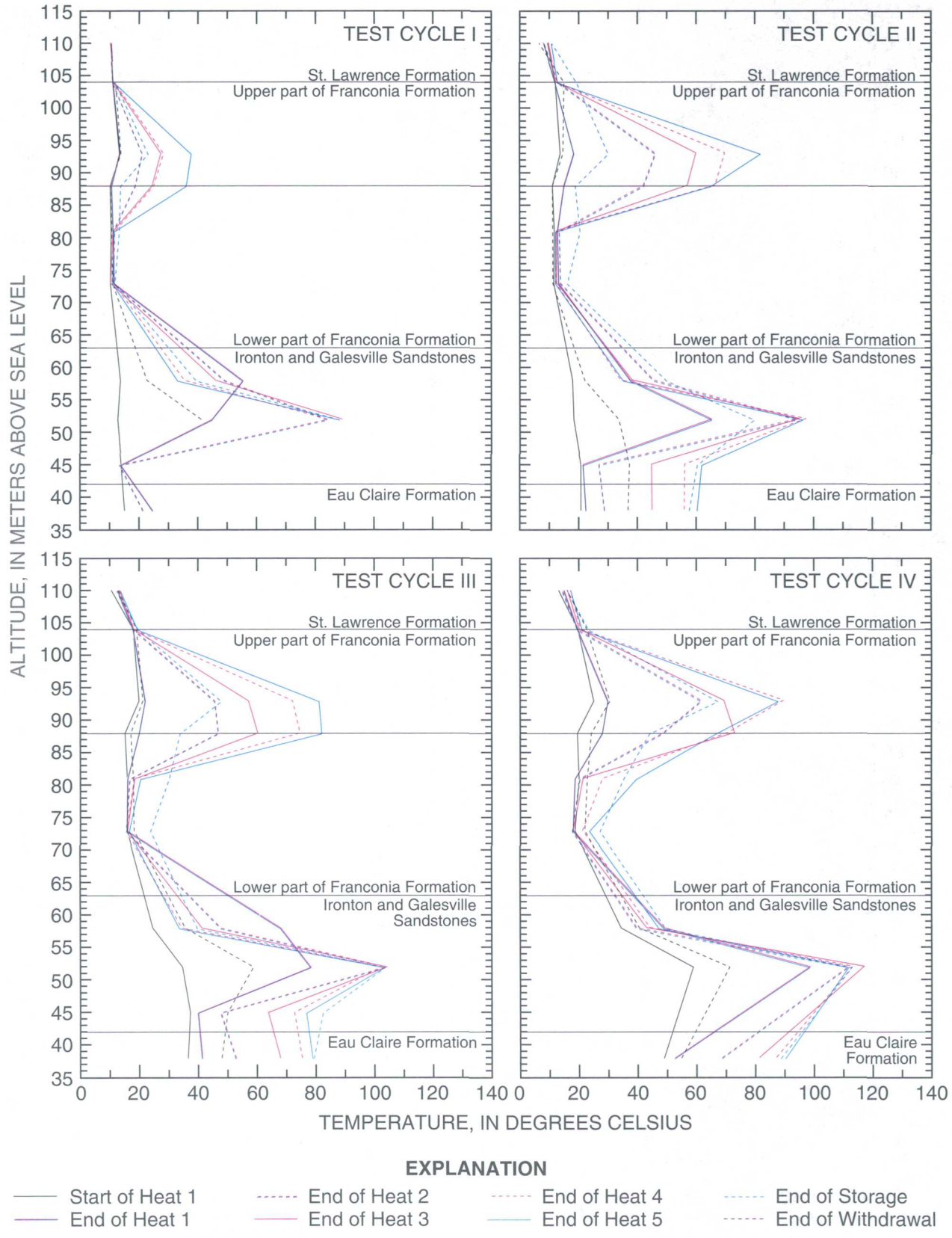

Figure 17.--Vertical profile of temperature for measurement points in observation well AM1, 7 meters from production well A.

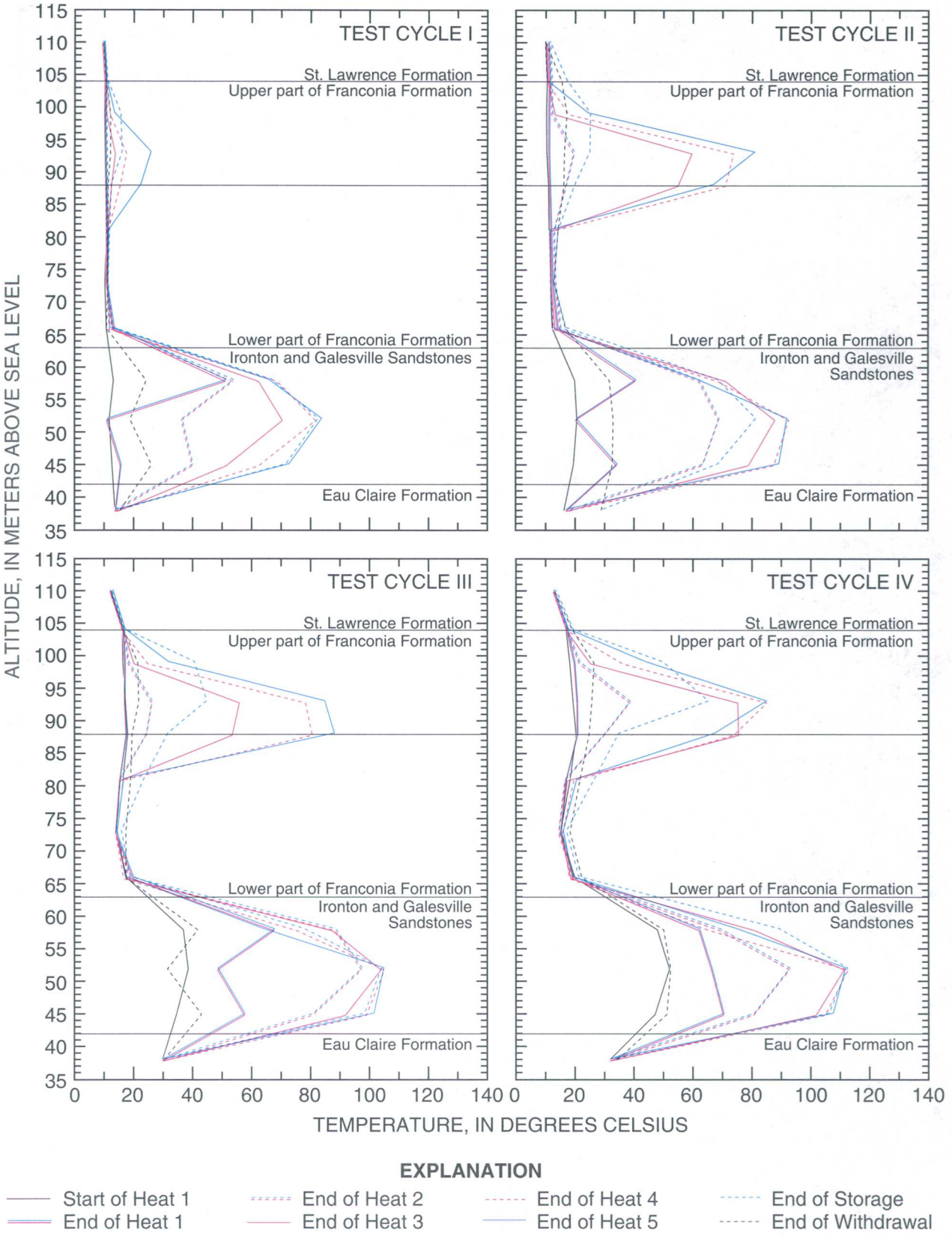

Figure 18.--Vertical profile of temperature for measurement points in observation well AS1, 7 meters from production well A.

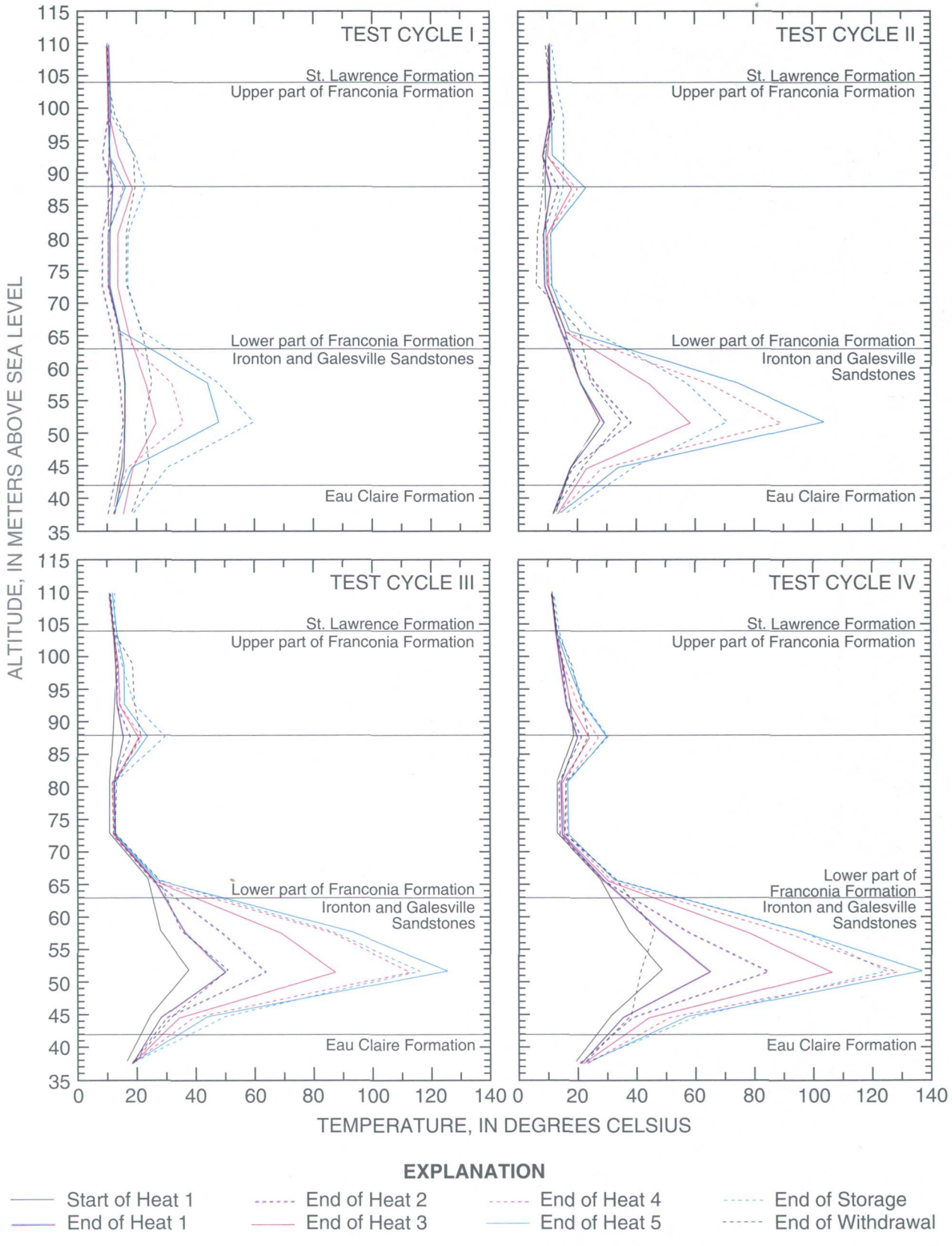

Figure 19.--Vertical profile of temperature for measurement points in observation well AM2, 14 meters from production well A.

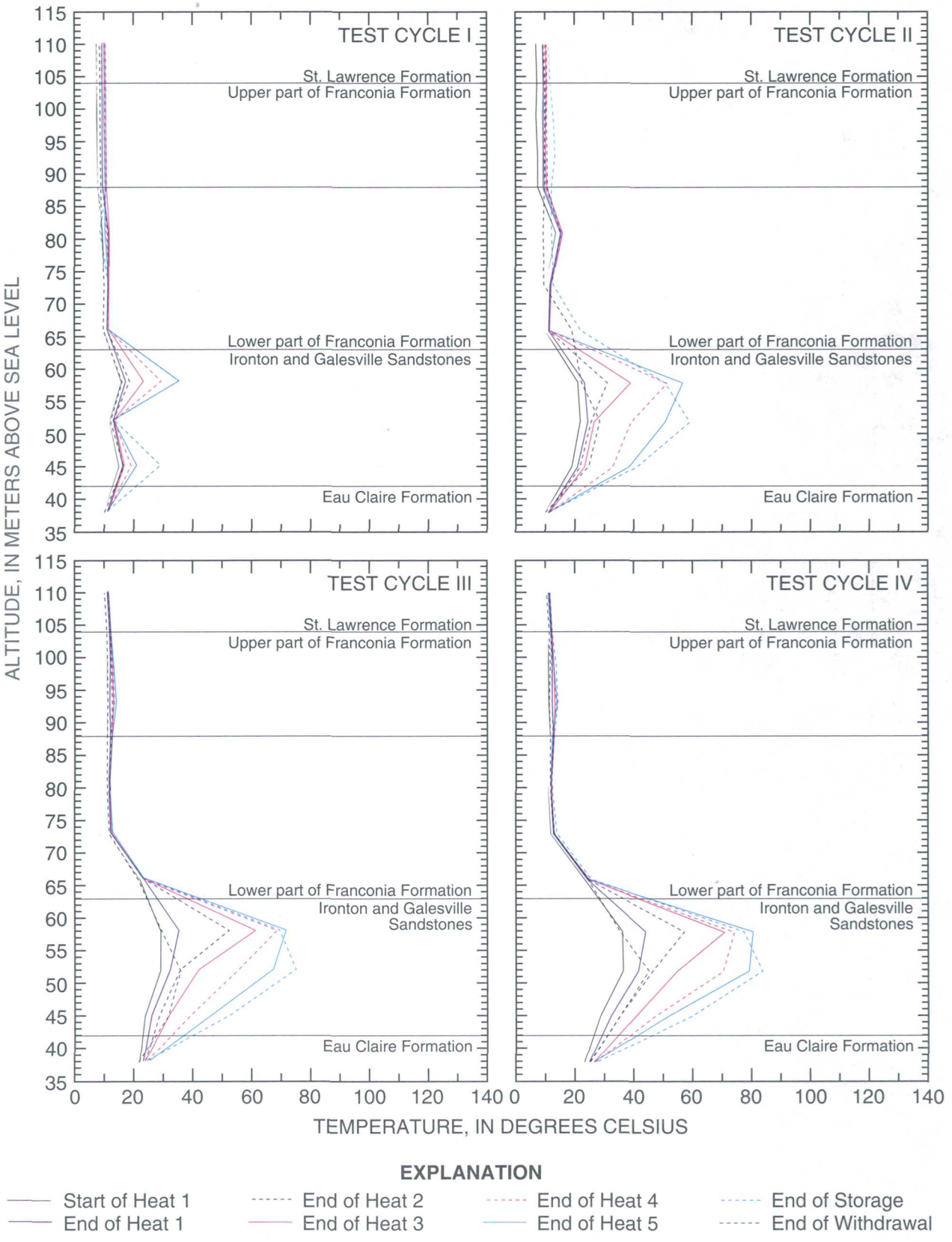

Figure 20.--Vertical profile of temperature for measurement points in observation well AM3, 14 meters from production well A.

II, III, and IV (fig. 20). The effects of buoyancy flow were most noticeable at the end of the storage period for test cycle II because the storage period lasted approximately 90 days instead of the planned 8 days, because of above-ground mechanical problems. This 90-day length of storage probably is more realistic than 8 days for an operational thermal-energy storage system and, perhaps, more accurately represents the potential long-term effects of buoyancy flow for the Franconia-Ironton-Galesville aquifer. Regardless of the length of storage, the actual buoyancy flow was small in comparison to the buoyancy flow as described by the sensitivity analysis for the Franconia-Ironton-Galesville aquifer (Miller and Delin, 1993).

The lack of consistent buoyancy flow in the test results probably was due to: (1) the relatively short duration of the storage periods; (2) an insufficient density of temperature-measurement locations; and (3) the presence of generally continuous, thin, horizontally bedded silt, shale, and clay stringers within the Franconia-Ironton-Galesville aquifer (Miller and Delin, 1993). These stringers could have reduced the effects of buoyancy flow by acting as barriers to convective flow induced by density differences in the water.

Another effect of the 90-day storage period for test cycle II was that temperatures in the upper part of the Franconia Formation decreased more at observation wells AM1 and AS1 than at observation well AM2, which was farther from production well A (figs. 17-20). Temperatures actually increased slightly at observation well AM3 in the upper part of the Franconia Formation, the observation well that was farthest from production well A.

Earlier model-sensitivity analyses (Miller and Delin, 1993) indicated that the decreases in temperature within the upper part of the Franconia Formation near production well A could be due to interformation flow within the well bore of production well A. The interformation flow, which was confirmed by use of a flow meter, resulted from a natural downward vertical gradient between the upper part of the Franconia Formation and the Ironton and Galesville Sandstones during periods of storage. This interformation flow caused advective flow of water in the upper part of the Franconia Formation past the observation wells toward production well A. Water from the upper part of the Franconia Formation was cooled as it traveled down production well A past the cooler, unscreened lower part of the Franconia Formation. This cooled water mixed with warmer water in the Ironton and Galesville Sandstones and maintained a positive advective flow outward into the sandstones. This flow of water into the Ironton and Galesville Sandstones tended to increase, or maintain, the temperatures measured at the observation wells.

During periods of storage, temperatures in the upper part of the Franconia Formation decreased at wells AM1 and AS1 (figs. 17 and 18), remained relatively constant at well AM3 (fig. 20), and increased slightly at well AM2 (fig. 19). Temperatures in the Ironton and Galesville Sandstones during periods of storage remained relatively constant at wells AM1 and AS1, increased at well AM3, and decreased at well AM2. The decrease in temperature in the upper part of the Franconia Formation at wells AM1 and AS1 likely resulted from interformation flow through production well A. The increase in temperature measured at well AM2 could be related to the areal anisotropy of the aquifer (Miller, 1984). Because well AM2 is on the minor axis of permeability relative to production well A, it could be less affected by advective heat flows than were wells AM1 and AS1; therefore, the temperature increase measured in the upper part of the Franconia Formation at well AM2 likely was due to vertical heat conduction rather than to horizontal advective flow. Similarly, the temperature decrease measured in the Ironton and Galesville Sandstones at well AM2 likely resulted from vertical heat-conduction losses.

The temperature increases measured in production well A at the beginning of each withdrawal period (fig. 10) likely were caused primarily by the effects of the well being completed in two different units. Interformation flow during periods of storage, described earlier, resulted in a slight cooling of water that flowed into the Ironton and Galesville Sandstones near the well bore. At the beginning of withdrawal periods, the water withdrawn from the Ironton and Galesville Sandstones was cooled as it traveled up the well bore past the unscreened lower part of the Franconia Formation. The water also lost heat through conduction to the well bore and casing at the beginning of each withdrawal period. Consequently, thermal equilibrium at the wellhead was not reached until from 12 to 24 hours into each withdrawal period (fig. 10).

Nonisothermal Modeling of Short-Term Test Cycles

A three-dimensional, anisotropic, nonisothermal, ground-water-flow, and thermal-energy-transport model was used to simulate the four short-term test cycles. The model has the same discretization as the preliminary three-dimensional, isothermal ground-water-flow model described by Miller and Delin (1993). Miller and Voss (1986) describe discretization of the model and the sensitivity of the lateral boundary conditions for various rates of heated-water injection.

The finite-difference, ground-water-flow, and thermal-energy-transport model used in this study was developed for waste-injection problems (Intercomp Resources Development and Engineering, 1976) and will be referred to in this report as the Survey Waste Injection Program (SWIP) code. The SWIP code can be used to simulate ground-water flow and heat and solute transport in a liquid-saturated porous medium; it contains both reservoir and well-bore modeling capabilities.

The major model assumptions are as follows:

1. Ground-water flow is laminar (Darcy), three dimensional, and transient.
2. Fluid density is a function of pressure, temperature, and concentration.
3. Fluid viscosity is a function of temperature and concentration.
4. The injected fluid is miscible with the in-place fluids.
5. Aquifer properties vary with location.
6. Hydrodynamic dispersion is a function of fluid velocity.
7. The energy equation can be described as: enthalpy in minus enthalpy out equals the change in internal energy of the system.
8. Boundary conditions allow natural water movement in the aquifer and heat losses to adjacent formations.
9. Thermal equilibrium exists within the simulated area.

The basic equation describing single-phase flow in a porous medium is derived by combining the continuity equation and Darcy equation for three-dimensional flow (Intercomp Resources Development and Engineering, 1976, p. 3.4):

$$\nabla \bullet \left[\frac{\rho k}{\mu}(\nabla p - \rho g \nabla z)\right] - q' = \frac{\partial}{\partial t}(\phi\rho) \ , \quad (1)$$

where

ρ = fluid density [M/L^3] (kg/m^3),
μ = fluid viscosity [M/L-T] (kPa-d),
k = intrinsic permeability [L^2] (m^2),
g = gravitational acceleration [L/T^2] (m/d^2),
z = spatial dimension in direction of gravity [L] (m),
p = pressure [M/L-T^2] (kPa),
q′ = mass rate of flow per unit volume from sources or sinks [M/T-L^3] (kg/d-m^3),
t = time [T] (d),
ϕ = porosity [dimensionless], and
∇ = gradient (for an axially symmetric cylindrical coordinate system ∇ is

$$(\frac{1}{r})(\frac{\partial}{\partial r}) + (\frac{\partial}{\partial z}),$$

where r is the radial dimension).

The energy-balance equation describing the transport of thermal energy in a ground-water system (Intercomp Resources Development and Engineering, 1976, p. 3.4) is:

$$\nabla \bullet \left[\frac{\rho k}{\mu} H (\nabla p - \rho g \nabla z)\right] + \nabla \bullet K \bullet \nabla T - q_L - q'H = \frac{\partial}{\partial t}[\phi\rho U + (1-\phi)(\rho C_p)_R T] , \quad (2)$$

where

H = enthalpy per unit mass of fluid [E/M] (J/kg),
K = hydrodynamic thermal dispersion plus convection [E/T-L-t] (W/m-°C),
T = temperature [t] (°C),
q_L = heat loss across boundaries [E/T-L^3] (W/m^3)
U = internal energy per unit mass of fluid [E/M] (J/kg),

$(\rho C_p)_R$ = heat of aquifer matrix [E/L^3-t] [J/m^3-°C], and

C_p = specific heat of aquifer matrix [E/M-t] (J/kg-°C) (All other terms are previously defined.)

Equations 1 and 2 are a nonlinear system of coupled partial-differential equations that is solved numerically by discretizing the aquifer into three dimensions (or two dimensions for radial flow) and developing finite-difference approximations.

Finite-difference equations (Intercomp Resources Development and Engineering, 1976, p. 3.5) whose solutions closely approximate the solutions of equations 1 and 2 are, for the basic flow equation:

$$\Delta[T_w(\Delta p - \rho g \Delta z)] - q = \frac{V}{\Delta t}\delta(\phi\rho) \ , \quad (3)$$

and for the energy equation:

$$\Delta[T_w H(\Delta p - \rho g \Delta z)] + \Delta(T_c \Delta T) - q_L - qH = \frac{V}{\Delta t}\delta[\phi\rho U + (1-\phi)(\rho C_p)_R T] \ , \quad (4)$$

where

q = mass rate of production or injection of liquid for a grid block

V = volume of the grid block

$$T_w = \frac{kA\rho}{\mu l} \quad (5)$$

$$T_c = \frac{KA}{l} \quad (6)$$

A = the area perpendicular to flow (that is, $\Delta x\Delta y$, $\Delta x\Delta z$, or $\Delta y\Delta z$), and

l = the distance between grid block centers.
(All other terms are previously defined.)

The finite-difference operators are defined as:

$$\Delta(T_w\Delta p) = \Delta_x(T_w\Delta_x p) + \Delta_y(T_w\Delta_y p) + \Delta_z(T_w\Delta_z p), \quad (7)$$

with the terms:

$$\Delta_x(T_w\Delta_x p) = T_{w,i+0.5,j,k}[p^{n+1}_{i+1,j,k} - p^{n+1}_{i,j,k}] - T_{w,i-0.5,j,k}[p^{n+1}_{i,j,k} - p^{n+1}_{i-1,j,k}], \quad (8)$$

and

$$\delta\kappa = \kappa^{n+1} - \kappa^n, \quad (9)$$

where
x, y, z= cartesian-space coordinates,
i, j, k = grid-block indices,
n = time level, t_n,
(All other terms are previously defined.)

Finally, the thermal-conductance term, K, in equation 6 may be further defined as (Intercomp Resources Development and Engineering, 1976, p. 3.7):

$$K = \phi\frac{\alpha u}{\phi}(\rho C_p)_w + K_m, \quad (10)$$

where
α = thermal dispersivity [L] (m),
ϕ = porosity [dimensionless],
u = volumetric flux (Darcy velocity) [L/T] (m/d),
$(\rho C_p)_w$ = heat capacity of water [E/L^3-t] (J/m^3-°C), and
K_m = molecular heat conductivity of porous media [E/T-L-t] (W/m-°C).

Model Design

Analysis of aquifer-test data (Miller and Delin, 1993; Miller, 1984) indicates that the Ironton and Galesville Sandstones and the upper part of the Franconia Formation are areally anisotropic and that the angle between the major axis of transmissivity and the axis between production wells A and B is approximately 30 degrees. Although the anisotropy may be considered small (less than 3:1), its effect on the movement and direction of heat flow for the hydrologic conditions at the ATES site is not known. Use of a radial-flow equation would neglect the effect of anisotropy. The potential errors introduced in the radial-flow assumptions are discussed by Miller and Delin (1993) in the section of that report describing the radial-flow model. On the basis of Miller and Delin's discussion, a three-dimensional model was constructed to represent anisotropic conditions and to simulate the ATES short-term test cycles.

Discretization of aquifer system

The area that can be modeled around the ATES doublet-well system is limited by (1) the constraint on the finite-difference grid spacings required by the model-solution techniques, (2) the lack of alignment of the axis of aquifer anisotropy and the axis on which the doublet wells are located, and (3) the prohibitive cost of running the model for large three-dimensional problems. Miller and Voss (1986) describe the construction of the finite-difference grid for the doublet-well system at the ATES site. The grid was simplified and the simulated region was reduced in size by use of an analytical solution for flow in an isotropic, isothermal, doublet-well system. The solution was modified to account for the effects of aquifer anisotropy and nonalignment of the principal direction of hydraulic conductivity with the doublet-well axis. The procedure is summarized below and described in more detail by Miller and Voss (1986).

The analytical solution for flow in the Ironton and Galesville Sandstones and in the upper part of the Franconia Formation are shown by Miller and Delin (1993, p. 48 and 49). The equipotentials and streamlines illustrated by Miller and Delin are the steady-state solutions to two-dimensional, isothermal flow in a homogeneous, confined, infinite, anisotropic aquifer that has no regional hydraulic gradient. For practical purposes, the Franconia-Ironton-Galesville aquifer may be treated as infinite, because lateral boundaries are not present within several kilometers of the test facility (Kanivetsky, 1979). The regional head gradient was estimated as less than 1×10^{-3}, which is negligible.

The cells in a finite-difference grid for a ground-water-flow model are generally sized to minimize computer storage and computation time while maintaining adequate discretization in space. The maximum cell size is determined by the nature of the finite-difference approximation of the ground-water-flow or transport equations. For the solution of transport equations, cell dimensions more than 1.5 times larger than an adjacent cell may cause oscillations in the distribution of the transported quantity in space. In order to prevent such oscillations, Intercomp Resources Development and Engineering (1976) suggests that cell size should be

restricted to less than twice the value of hydrodynamic dispersivity. For example, the hydrodynamic dispersivity of about 3 m used in this study restricts the maximum cell size to 6 m.

Although it is possible to construct a finite-difference grid that would encompass the entire area illustrated by Miller and Delin (1993, p. 48 and 49), the number of resulting cells and corresponding calculations would be impractical to model with the SWIP code. If cells were 6 m on a side, for example, 10,000 cells would be required to simulate the two-dimensional area shown by Miller and Delin. The flow-net analysis (Miller and Voss, 1986), makes it possible to reduce the modeled area and to simulate flow only in the area around production well A, the flow region where energy transport is of greatest concern (figs. 21-22). Flow outside this modeled region is represented by a specified flux at model boundaries, as determined by flow-net analysis.

The finite-difference grid for the ATES-site model was oriented such that the axis of maximum transmissivity was aligned with the horizontal-coordinate direction (Miller and Delin, 1993, p. 48 and 49). The origin of the field-coordinate system shown in figures 21 and 22 was arbitrarily chosen to be halfway between production wells A and B. A variably-spaced grid was designed because of restrictions on grid size for solution accuracy and stability inherent to the difference approximation used in the SWIP code (Intercomp Resources Development and Engineering, 1976). Cell sizes range from 0.3 m on a side at production well A to a maximum of 4.6 m on a side at the periphery of the model; cell sizes increase in all directions equally by a factor of 1.5 or less. The grid has 6 layers with 594 cells per layer (fig. 23). Vertical grid spacings were selected to correspond with aquifers and confining units (table 3). The lateral boundaries of the model correspond to the 10 m equipotential for the Ironton and Galesville Sandstones (fig. 21) and to the 2.9 m equipotential for the upper part of the Franconia Formation (fig. 22).

Flux calculation at model boundaries

Appropriate flux rates must be specified at the model boundaries such that the boundaries accurately represent ground-water flow and heat transport between the modeled area and the area outside the simulated region. The correct boundary fluxes can be determined by analysis of the flow net for steady-state conditions. The total flow crossing an equipotential (figs. 21 and 22) is equal to the injection rate and is thus known. In addition, an equal amount of flow is represented by each streamtube. Therefore, if quasi-steady-state flow is assumed, the distribution of fluxes along an equipotential is known for any injection rate.

Table 3.--Layer number, thickness, and corresponding hydrogeologic unit for the three-dimensional model of heat transport

Layer	Thickness (meters)	Hydrogeologic unit
1	8	St. Lawrence Formation (confining unit)
2	14	Upper part of the Franconia Formation (aquifer)
3	24	Lower part of the Franconia Formation (confining unit)
4	15	Ironton Sandstone (aquifer)
5	6	Galesville Sandstone (aquifer)
6	30	Eau Claire Formation (confining unit)

One form of boundary-flux specification simulated by use of the SWIP code (Intercomp Resources Development and Engineering, 1976, p. B.11) is:

$$e_{w_{ij}} \Delta t = \alpha_{ij} V (P_I - P_{ij}^{n+1}), \qquad (11)$$

where

$e_{w_{ij}}$ = the fluid-influx rate at boundary cell i,j [L/T] (m^3/d),

α_{ij} = a constant factor that gives the fraction of the entire grid boundary that cell i,j represents [dimensionless],

V = an aquifer-flux coefficient [L^3/(M/L-T^2)] (m^3/kPa),

P_I = a fixed pressure at some distance outside the model boundary [M/L-T^2] (kPa), and

P_{ij}^{n+1} = the pressure in boundary cell i,j at time of the (n+1)th time step [M/L-T^2] (kPa), and

Δt = time [T] (d).

For an infinite aquifer, the pressure outside the model boundary (P_I) is maintained at the initial system pressure (P_{ij}^0) before pumping. For simulation of the doublet-well system, the initial pressure (P_{ij}^0) is held constant along a locus somewhere between the wells. In a homogeneous, isotropic aquifer, this locus would be the perpendicular bisector of the well axis; however, in the anisotropic Franconia-Ironton-Galesville aquifer, the locus is along a line at an oblique angle to the well axis (Miller and Delin, 1993, p. 48 and 49).

The aquifer-flux coefficient (V), is calculated by use of equation 11 for an equipotential by letting P_I equal the initial pressure (P^0_{ij}), α_{ij} equal 1 (representing the entire boundary), e_w equal the steady-state injection rate for each formation, and P_{ij}^{n+1} equal the steady-state pressure at the equipotential. Values of V were calculated for the 10-m equipotential (fig. 21) for the Ironton and Galesville Sandstones and the 2.9 m equipotential (fig. 22) for the upper part of the Franconia Formation, as 12.6 and 3.8 m^3/d-kPa (cubic meters per day-kilopascal), respectively. Because the 32 streamtubes illustrated in figures 21 and 22 represent equal rates of flow, values for the constant α_{ij} were determined for the model boundary in each layer from the percentages of streamtubes that intersect each boundary cell. The location of lateral-flux boundaries in the model that represent these equipotentials are illustrated in figure 24.

Miller and Delin (1993) describe calibration of the model to isothermal conditions to define the hydraulic properties and boundary conditions that best characterize the doublet-well system. From results of these model analyses, the boundary fluxes computed by flow-net analysis accurately represented the doublet-well flow field in the anisotropic aquifer. Therefore, the hydraulic representation of the ground-water-flow system by the model was considered to be satisfactory.

Representation of Thermal Properties

This section of the report provides a brief description of the thermal properties of the aquifer used as variables in the nonisothermal model. The relation of these variables to hydraulic properties of the aquifer is described, and possible effects of these variables on the transport of energy in the modeled aquifer system is discussed.

Heat capacity is the amount of heat required to raise the temperature of a material a specified amount. It is the product of density and specific heat and is a measure of the ability of a material to store heat. Values of 1.81×10^6 and 3.89×10^6 J/m^3/°C were used for heat capacity of rock and water, respectively (table 4). These values were based on data from Sommerton and others (1965), Clark (1966), Helgeson and others (1978), and Robie and others (1978). The values were calculated by use of methods described by Martin and Dew (1965). The value of rock heat capacity represents sandstones similar to those in the Franconia-Ironton-Galesville aquifer.

The constant of proportionality between the heat flux and the temperature gradient is termed thermal conductivity. It is the quantity of heat transmitted in unit time through a unit cross-sectional area under a unit temperature gradient. For purposes of data analysis, thermal conductivity was assumed to be isotropic in the aquifer system. For a parallel-conduction model (Bear, 1972), where heat conduction occurs simultaneously through the fluid and the aquifer matrix (rock), thermal conductivity is defined as

$$\Upsilon = \theta\Upsilon_f + (1-\theta)\Upsilon_r, \qquad (12)$$

where

Υ = thermal conductivity of the aquifer [E/L - T - t] J/m - s - °C,
Υ_f = thermal conductivity of the fluid [E/L - T - t] J/m - s - °C,
Υ_r = thermal conductivity of the rock [E/L - T - t] J/m - s - °C, and
θ = aquifer porosity [dimensionless].

Thermal conductivity tends to decrease with increasing temperature (Blair and others, 1985). This should not be a problem in data analysis or in application of model results at the ATES site because the temperatures required to seriously affect the value of thermal conductivity were well above those measured during short-term testing. Values of thermal conductivity (table 4) were obtained from Clark (1966).

Thermal diffusivity is defined as the transport of energy by conduction due to the exchange of kinetic energy between molecules. Thermal diffusion is independent of fluid velocities and is usually constant in saturated porous media. Thermal diffusivity for an isotropic system may be defined as:

$$K = \frac{\Upsilon}{[\rho_f C_f + (1-\theta)\rho_r C_r]}, \qquad (13)$$

where

K = thermal diffusivity [L^2/T] (m^2/s),
Υ = thermal conductivity of the aquifer [E/L - T - t] (J/m - s - °C),
ρ_f = the density of fluid [M/L^3](kg/m^3),
ρ_r = the density of rock [M/L^3] (kg/m^3),

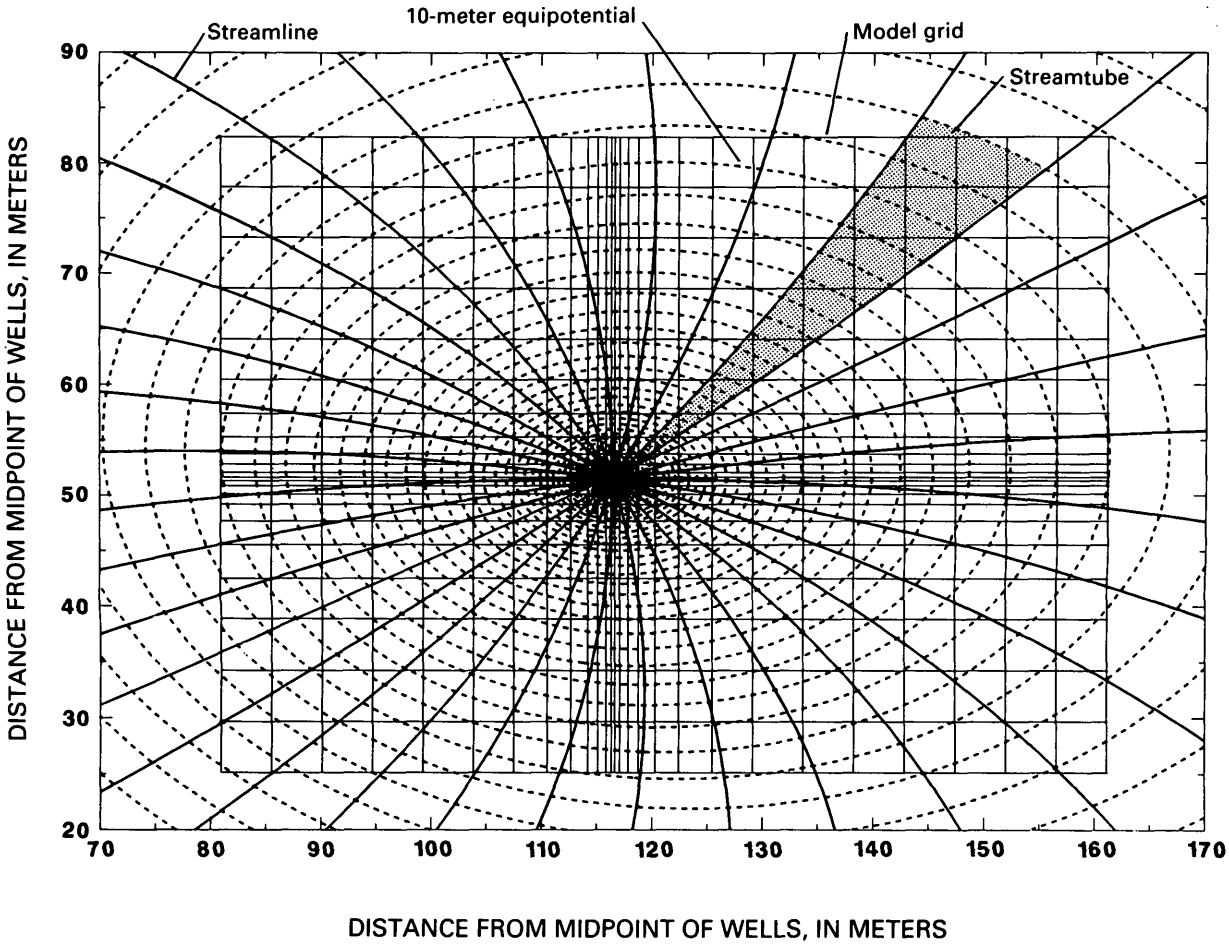

Figure 21.–Model grid and flow net for the Ironton and Galesville Sandstones near production well A.

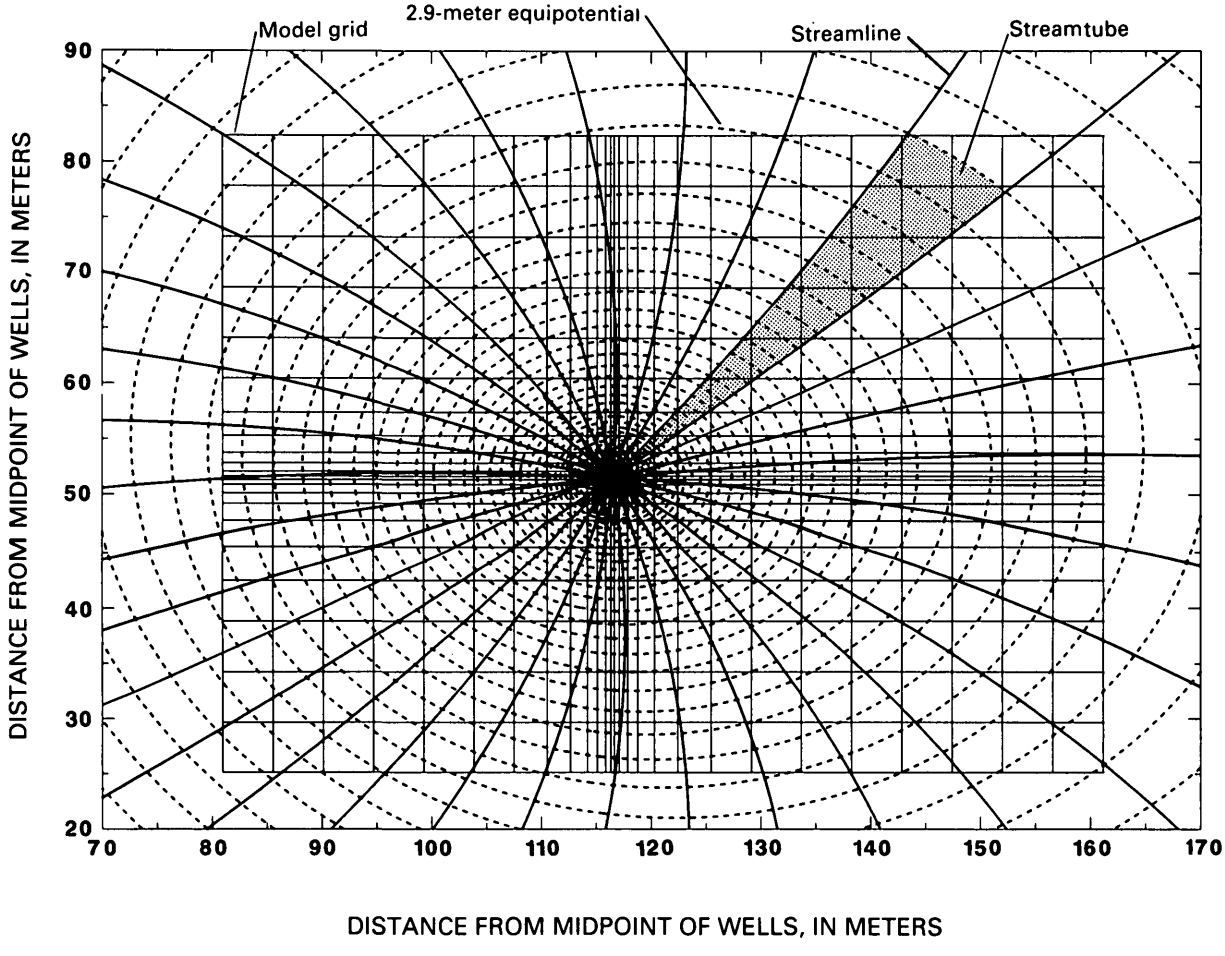

Figure 22.--Model grid and flow net for the upper part of the Franconia Formation near production well A.

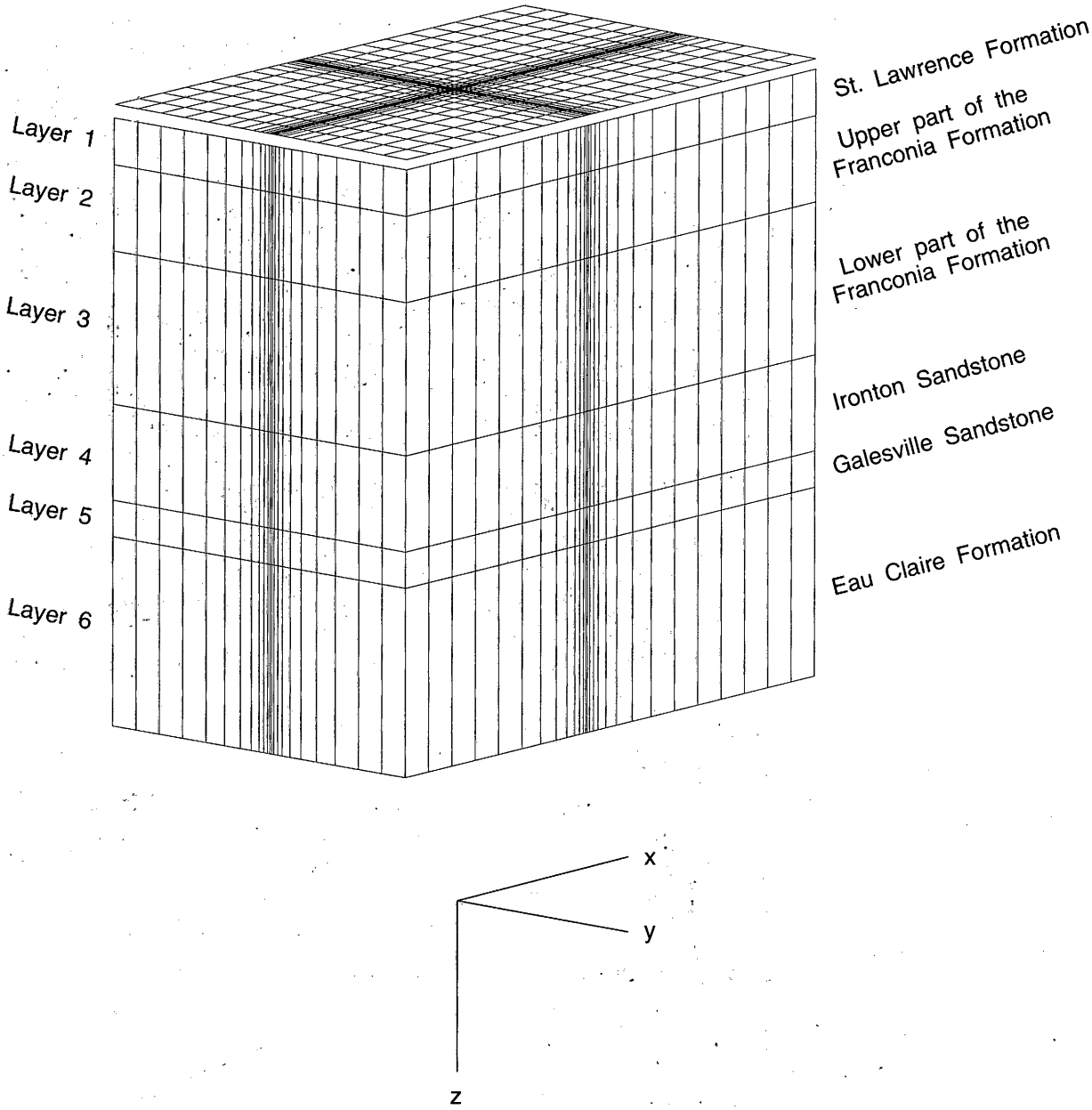

Figure 23.--Finite-difference grid, in three dimensions, for the Aquifer Thermal-Energy Storage (ATES) site model.

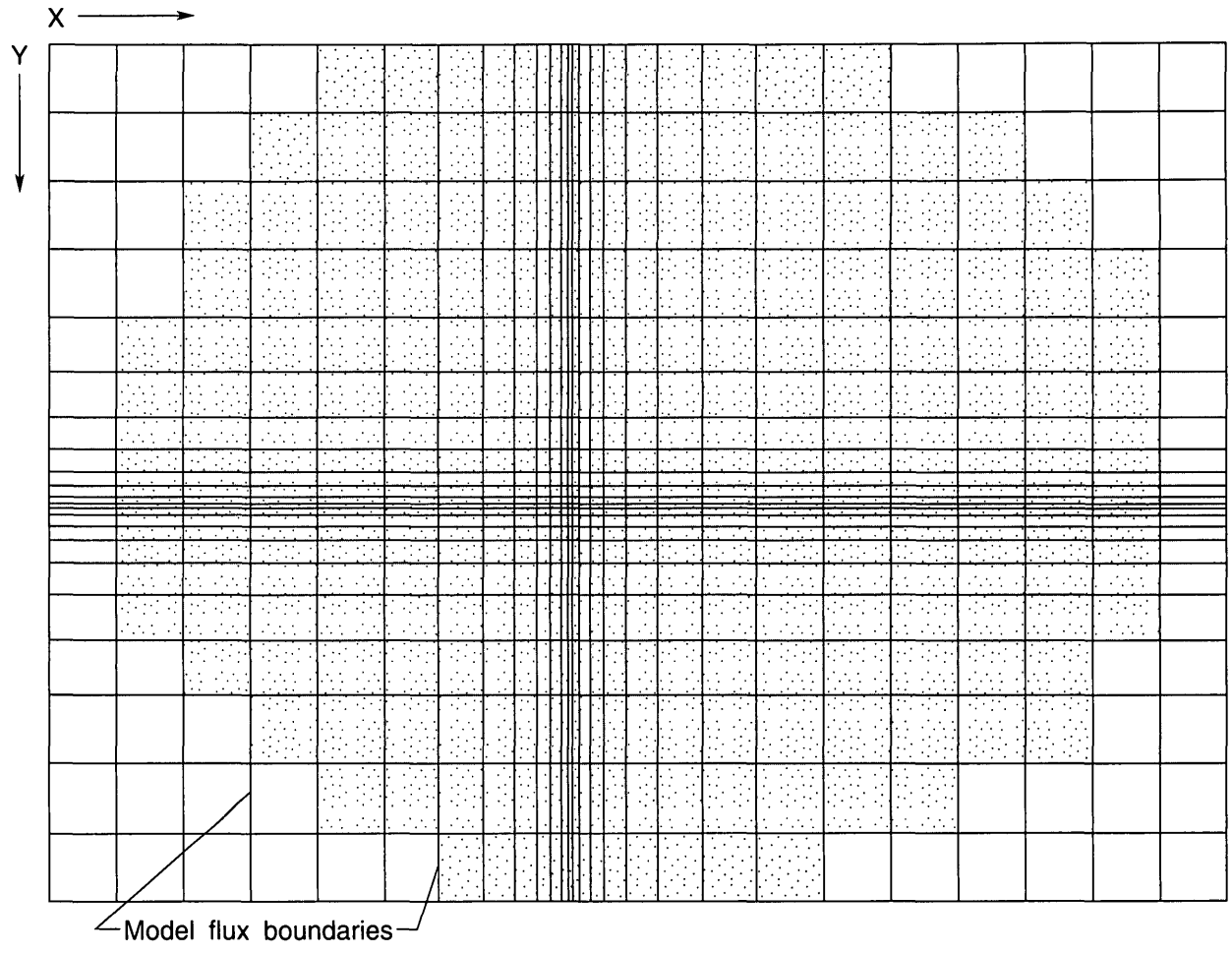

EXPLANATION

Cell in which heat transport was simulated:

Layers 1-3 - St. Lawrence and Franconia Formations

Layers 4-6 - Ironton and Galesville Sandstones and the Eau Claire Formations

Figure 24.--Model cells near production well A in which heat transport was simulated.

Table 4.--Thermal properties used for simulation of the short-term test cycles

Thermal property	Amount and unit of measure
Thermal conductivity, rock	= 2.20 watts per meter-degree Celsius*
Thermal conductivity, aquifer water at 20 degrees Celsius	= 0.60 watts per meter-degree Celsius*
Thermal diffusivity	= 1.56×10^6 square meter second
Heat capacity, rock	= 1.81×10^6 joules per cubic meter-degree Celsius
Heat capacity, aquifer water	= 3.89×10^6 joules per cubic meter-degree Celsius
Longitudinal dispersivity	= 3.33 meters
Transverse dispersivity	= 0.33 meters

* From Clark, 1966

C_f = specific heat of fluid [E/M - t] (J/kg - °C),
C_r = specific heat of rock [E/M - t] (J/kg - °C), and
θ = aquifer porosity [dimensionless].

The value of 1.56×10^6 m^2/s (square meter per second) (table 4) used for thermal diffusivity is representative of sandstones in the Franconia-Ironton-Galesville aquifer (Kappelmeyer and Haenel, 1974).

Thermal dispersion (D_{ij}), resulting from fluctuations of velocity and temperature in the pore space, is similar to the more common term of mechanical hydrodynamic dispersion used in solute mass-transport problems. The coefficient of thermal dispersion term consists of two parts: (1) energy transport due to changes in the local velocity vector; and (2) energy transport due to the exchange of kinetic energy between molecules, or to thermal diffusivity. Bear (1972) notes that the coefficient of thermal dispersion is a second-order tensor that depends on a fourth-order tensor (dispersivity).

For the case of a local-coordinate system where one of the axes coincides with the velocity vector, the X and Y axes also coincide with the principal axes of dispersion. For an isotropic medium, the dispersion tensor may be written in matrix notation as:

$$D_{ij} = \begin{bmatrix} (\lambda_{11} + K) & 0 & 0 \\ 0 & (\lambda_{22} + K) & 0 \\ 0 & 0 & (\lambda_{22} + K) \end{bmatrix}, \quad (14)$$

where
D_{ij} = the coefficient of thermal dispersion [L](m),
λ_{11},λ_{22} are the longitudinal and transverse dispersivities respectively for an isotropic medium [L](m),
K = thermal diffusivity [L^2/T] (m^2/s).

Bear (1972) points out that diffusion is negligible and dispersion is dominant in flow systems with relatively large fluid velocity. Diffusion dominates dispersion for small fluid velocities.

The terms λ_{11}, λ_{22} in equation 14 are values of dispersivity for an isotropic medium where λ_{11} is considered longitudinal, or parallel to the direction of fluid flow, and λ_{22} is considered transversal, or perpendicular to fluid flow. Green (1963) and Bear (1972) suggest that dispersivity is of small importance in dispersion compared to thermal conduction. Sauty and others (1979) suggest that Bear may have considered only laboratory values of dispersivity, however, and not field or macrodispersivities in his determination of the importance of the dispersivity term.

Model Calibration

Model-computed temperatures were compared to measured data at each of the observation wells for each period of injection and withdrawal for the four short-term test cycles. Plots of measured and simulated temperatures (figs. 25-29) are arranged so that injection and withdrawal periods can be compared for the four test cycles at each observation well. The colored solid lines (figs. 25-29) represent averages of measured temperatures and the corresponding colored dashed lines represent the model-computed values. Actual temperature measurements were averaged for all measurement points within each hydrogeologic unit in an attempt to make measured and model-computed data comparable. Table 5 lists the measurement-point altitudes for which data were averaged to correspond with the model's vertical layering.

Table 5.--Altitudes of measurement points where temperatures were averaged to correspond with model layers

Model layer	Hydrogeologic unit	Altitude(s) of measurement points
1	St. Lawrence Formation	110, 104
2	Upper part of the Franconia Formation	99, 93, 88
3	Lower part of the Franconia Formation	81, 73, 66
4	Ironton Sandstone	58, 52
5	Galesville Sandstone	45
6	Eau Claire Formation	38

A detailed description of the differences between model-computed and average temperatures is beyond the scope of this report. Trends in the average temperatures will be discussed and related to model results to describe thermal processes that may explain the results. As described earlier, some thermocouples failed intermittently because of insulation wear at kinks in the wires. These failures appear as small temperature fluctuations in figures 25 through 29 and are not discussed further in the report.

A factor that should be considered when comparing model-computed temperatures with measured data is the radial distance of measurement points from production well A. Because of the limitations of finite-difference modeling, the actual location of measurement points may not be exactly simulated in the model at the correct radial distance (fig. 5). The smallest deviations within the model area are for production well A and observation well AM1, and the greatest deviation is for observation well AM3. Model-computed temperatures for each monitoring point at the site were correlated with measured values on the basis of results of the deviation survey.

Representation of variable pumping rates and injection temperatures must be considered when comparing model-computed and average temperatures. This is illustrated in figure 25, which shows injection temperatures recorded at the wellhead and injection temperatures simulated with the model. The filtration system for calcium carbonate removal caused an overall decrease in efficiency of the above-ground heat exchanger and resulted in a decrease of injection temperatures with time. Therefore, an average temperature was used for the period of heat injection and for the period when the filtration unit was serviced. Thus, the initial high and low temperature peaks measured at the wellhead were not simulated by the model.

The four short-term test cycles, including the inactive or rest periods between individual test cycles, were simulated. Therefore, the total length of the simulation, approximately 400 days, represented a period from the start of injection in test cycle I to the end of withdrawal for test cycle IV. A continuous model simulation of the four test cycles was necessary because of conductive flow of thermal energy away from the injection zones, particularly near production well A, during periods of storage between test cycles.

Temperature was redistributed within the aquifer and confining units because of thermal conduction between each test cycle. The rate of heat conduction depended on the length of time between periods of injection and on the amount of thermal energy in the aquifers and confining units. Knowledge of the initial distribution of energy within the aquifer at the start of a test cycle, therefore, was critical in determining the overall thermal efficiency of the aquifer for the cycle. Thermal efficiency of the aquifer was computed by dividing the total energy injected into the aquifer system by the total energy withdrawn from the system.

The initial thermal conditions for the simulation of test cycle I were approximated because of the aborted heated-water injection test in May 1982, before the installation of the calcium carbonate filtration units. Although an attempt was made to recover the heat injected during the aborted test and to return the aquifer to its ambient temperature of approximately 10°C, temperature measurements in observation wells AM1 and AS1 indicated that some residual heat remained within 7 m of production well A. Because there were not enough temperature-measurement points near production well A to determine the distribution of temperature, the residual heat from the aborted test was not precisely known. Therefore, a vertically-uniform temperature of 10°C was assumed as the initial condition for the simulation of test cycle I.

The model was calibrated to nonisothermal conditions to ensure that the hydraulic and thermal properties selected were reasonable for simulation of heat transport in the flow system. The relative importance of each property was evaluated during preliminary model analyses (Miller and Delin, 1993). Model sensitivity to changes in the hydraulic properties of hydraulic conductivity, porosity, and vertical anisotropy, plus

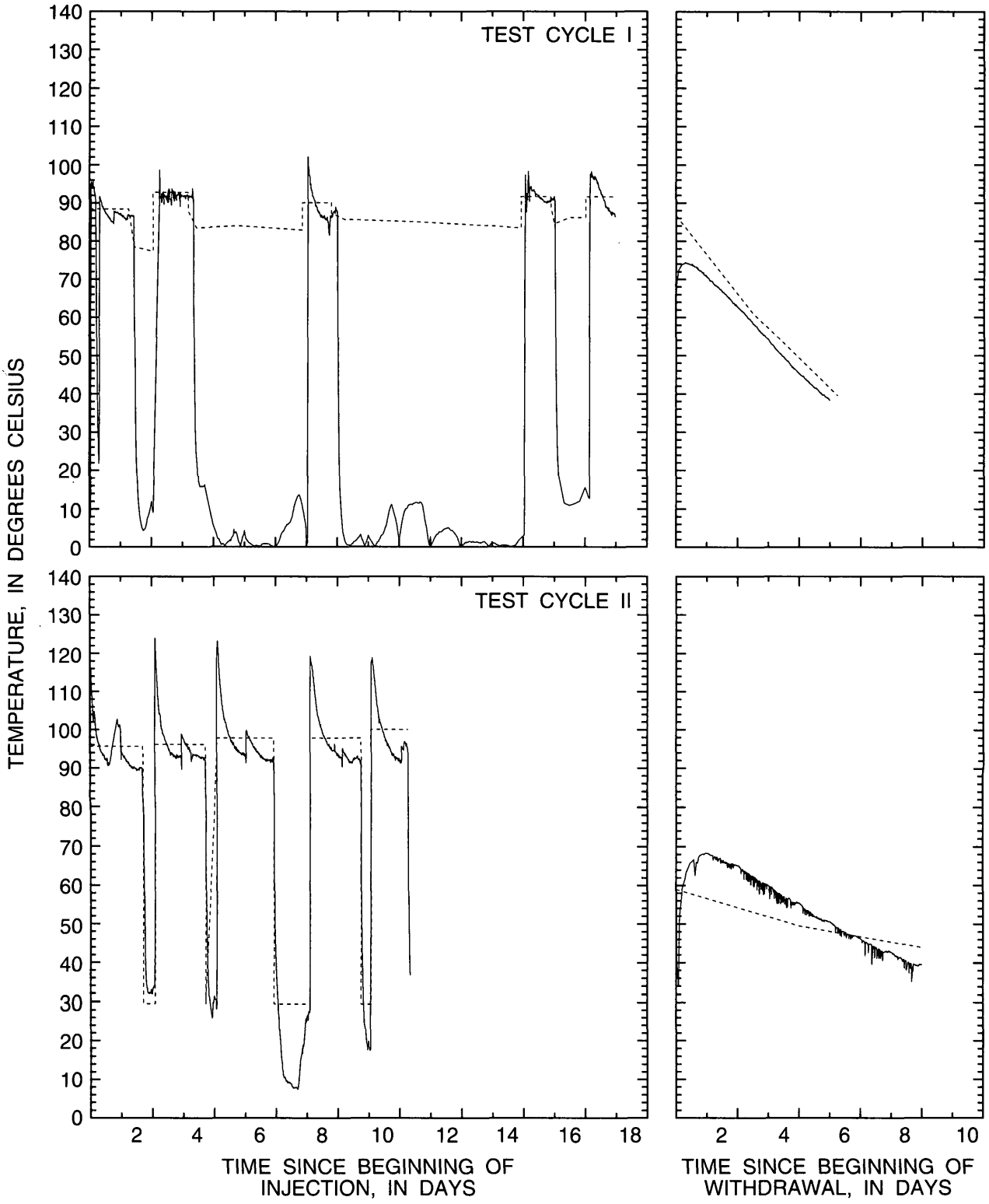

Figure 25.--Model-computed and measured injection temperatures during periods of

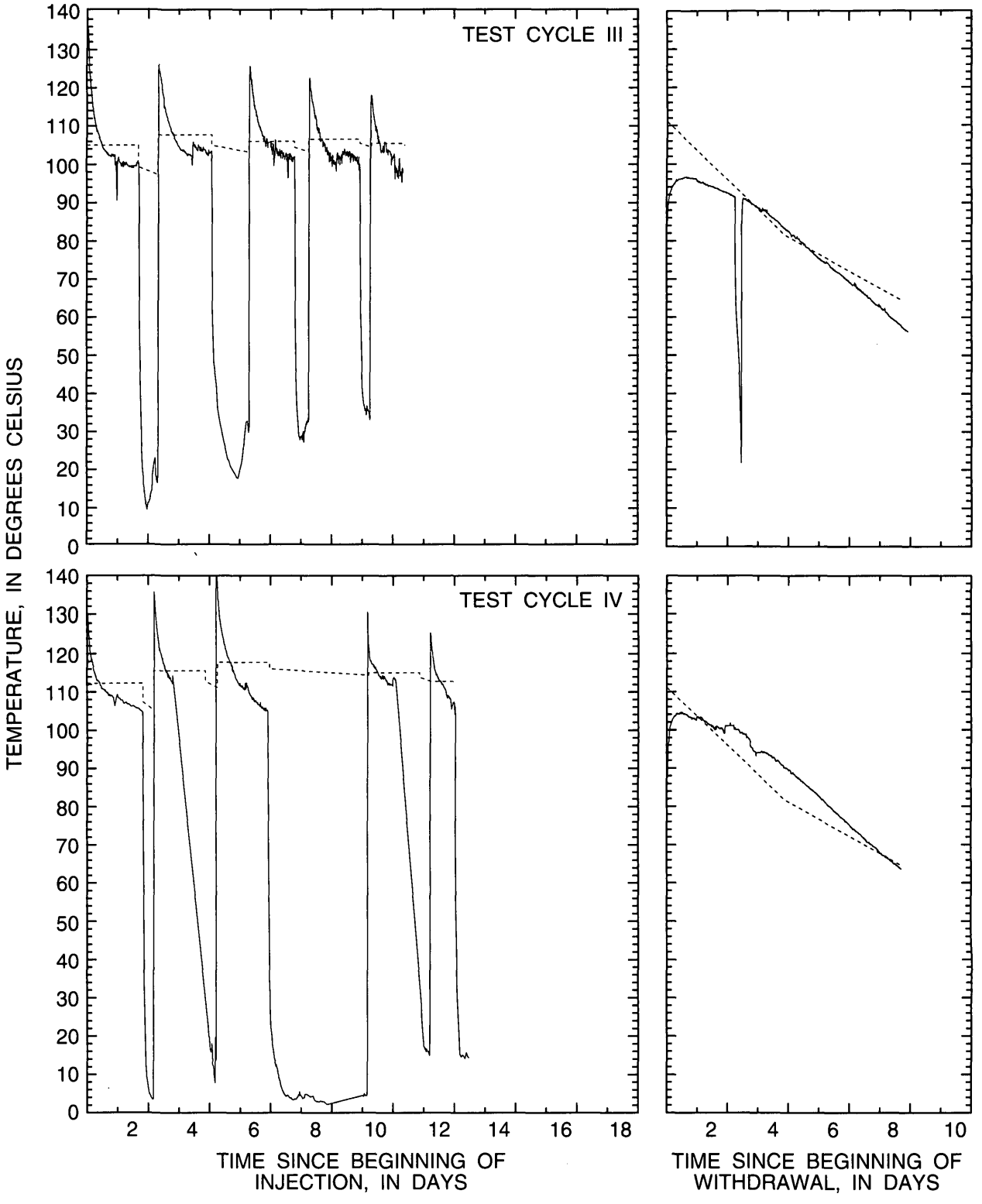

at production well A for the four short-term test cycles injection and withdrawal.

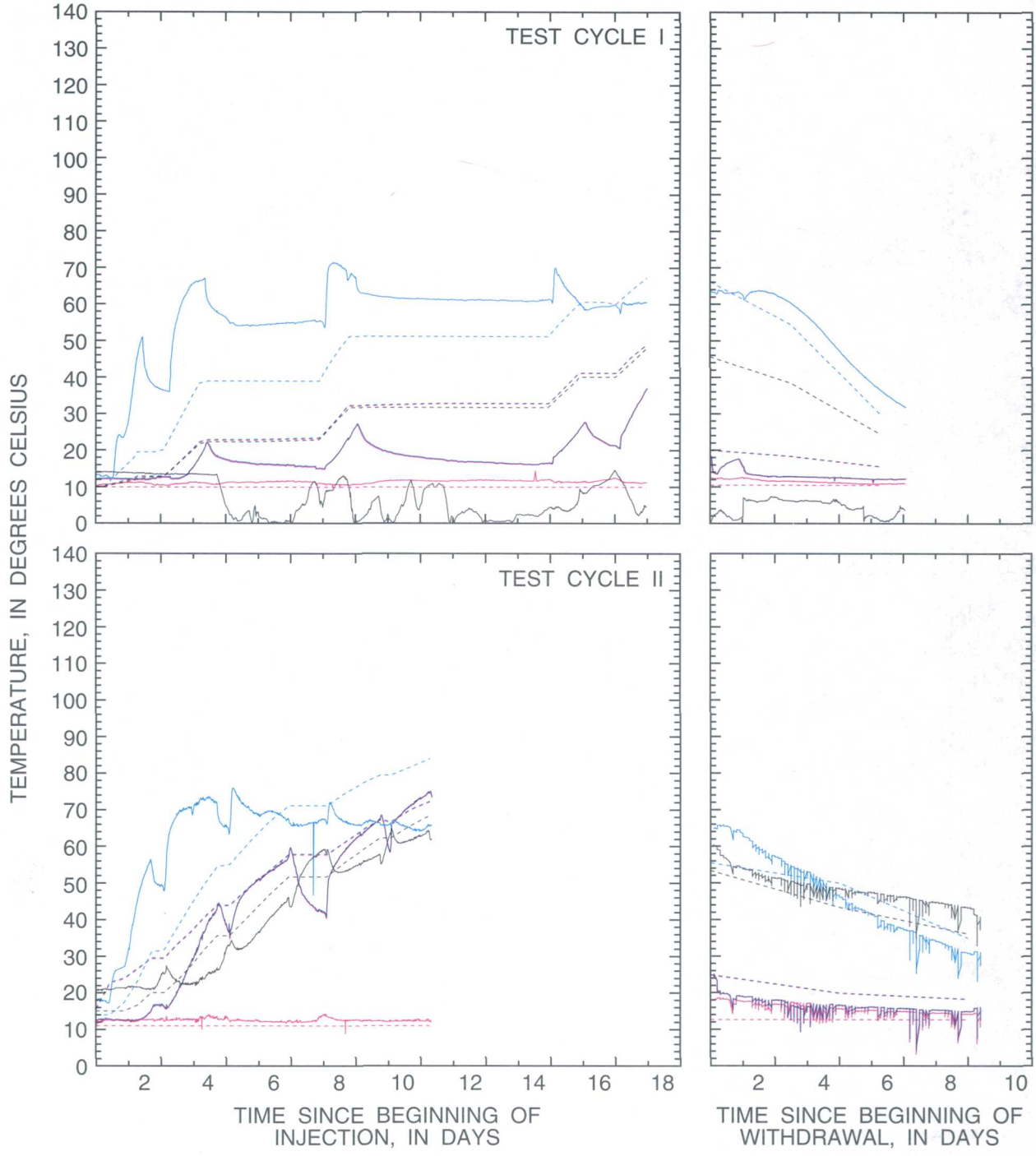

Figure 26.--Model-computed and average measured injection cycles during periods of

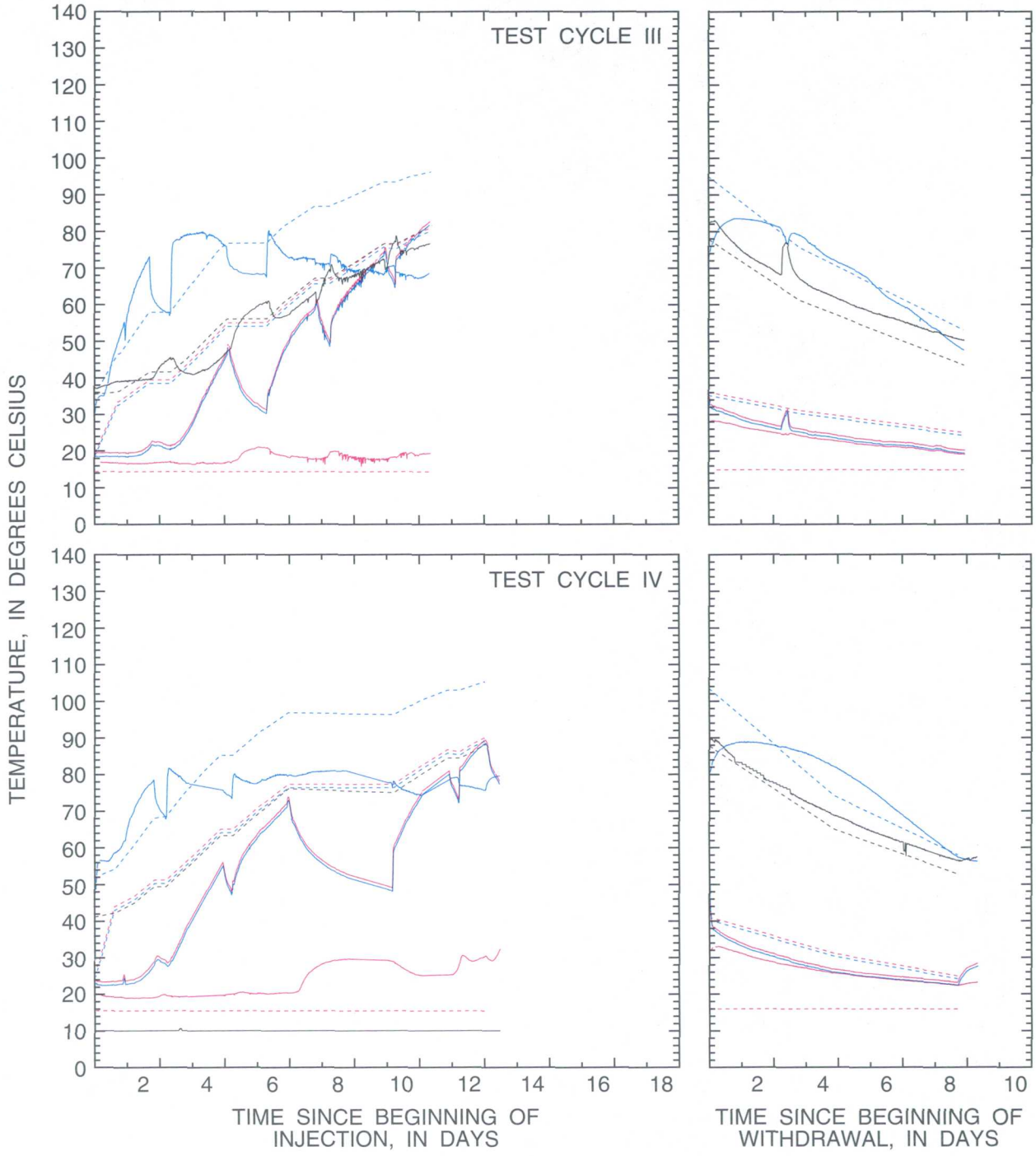

temperatures at observation well AM1 for the four short-term test injection and withdrawal.

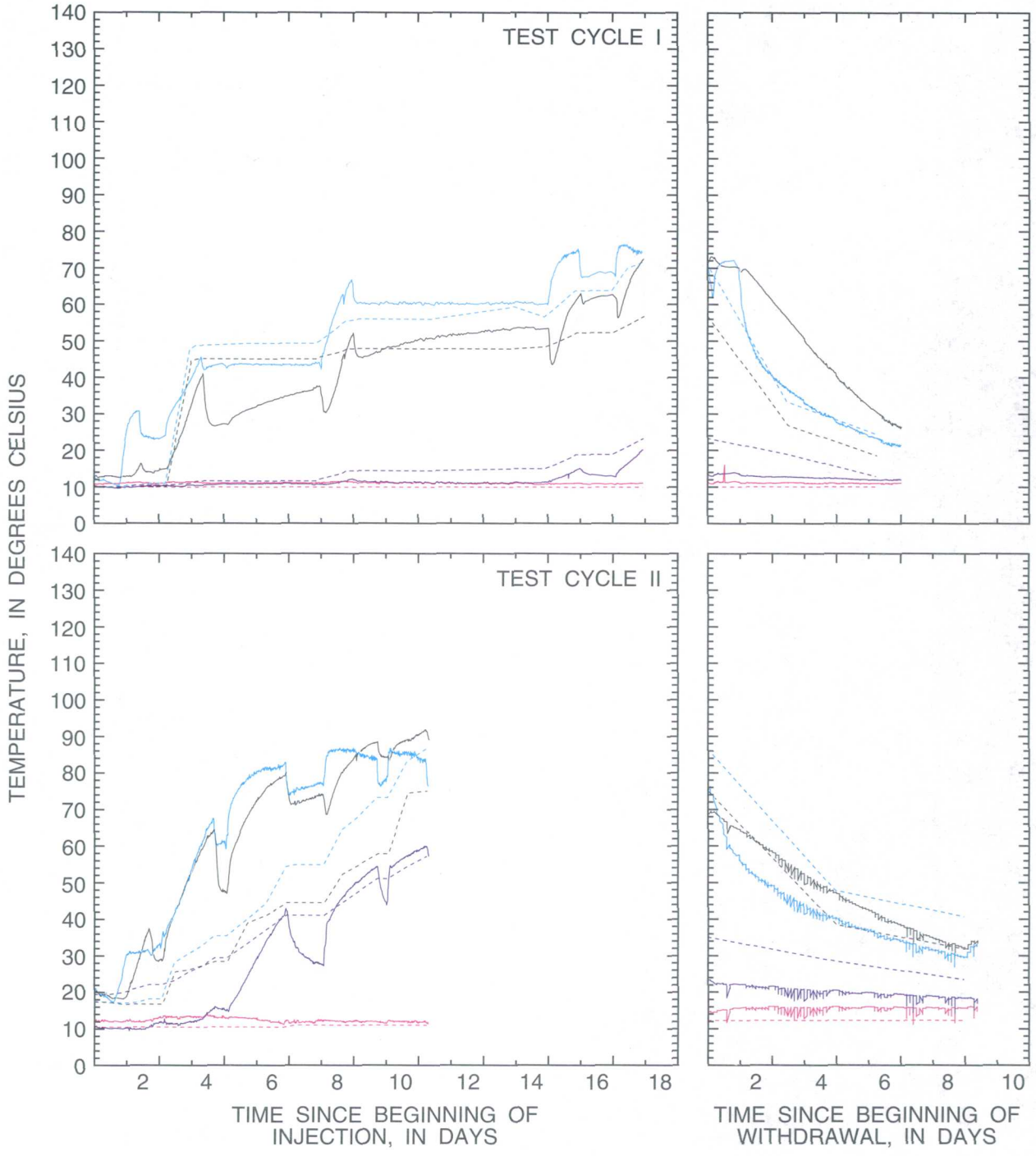

Figure 27.--Model-computed and average measured injection cycles during periods of

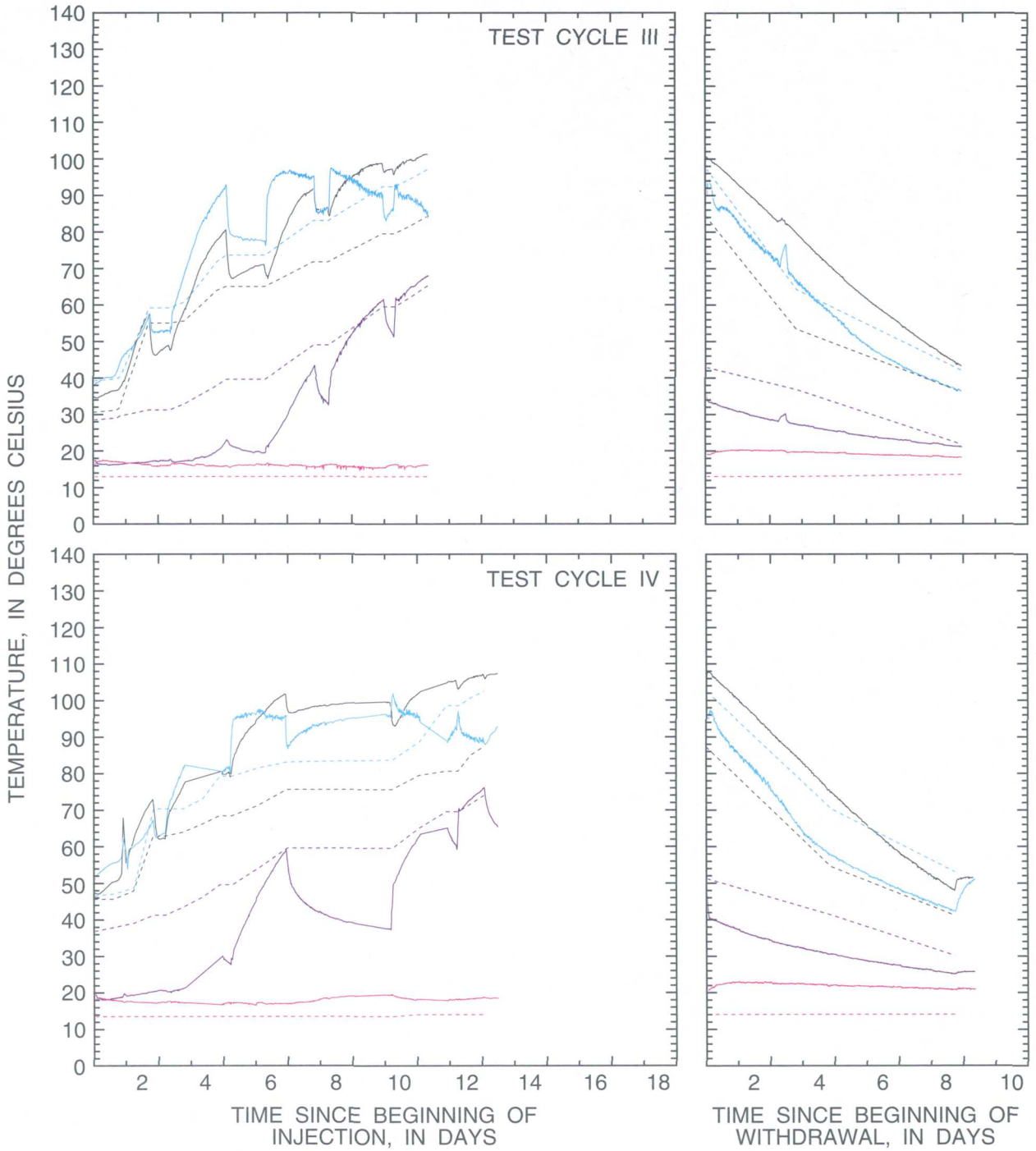

temperatures at observation well AS1 for the four short-term test injection and withdrawal.

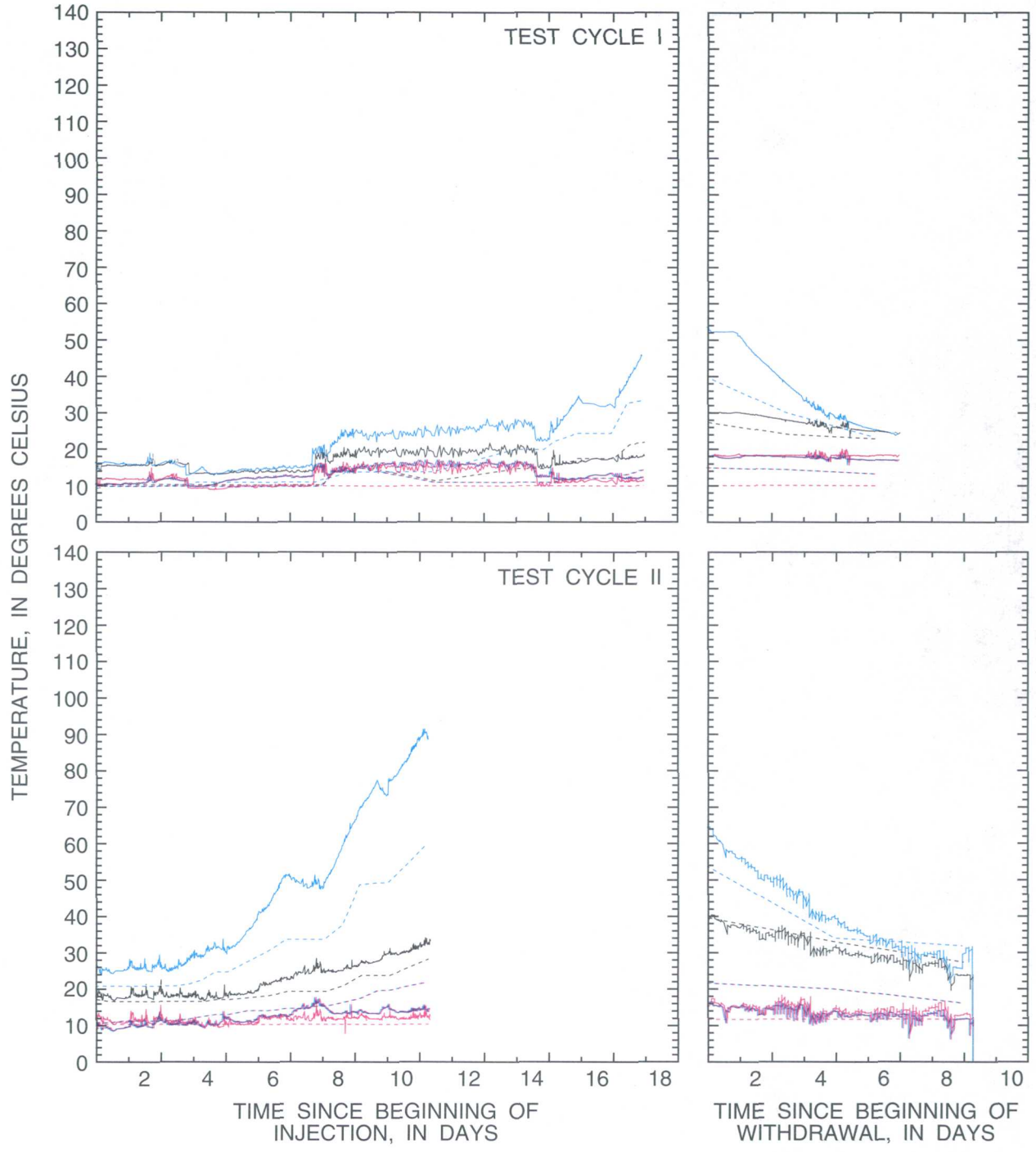

Figure 28.--Model-computed and average measured injection cycles during periods of

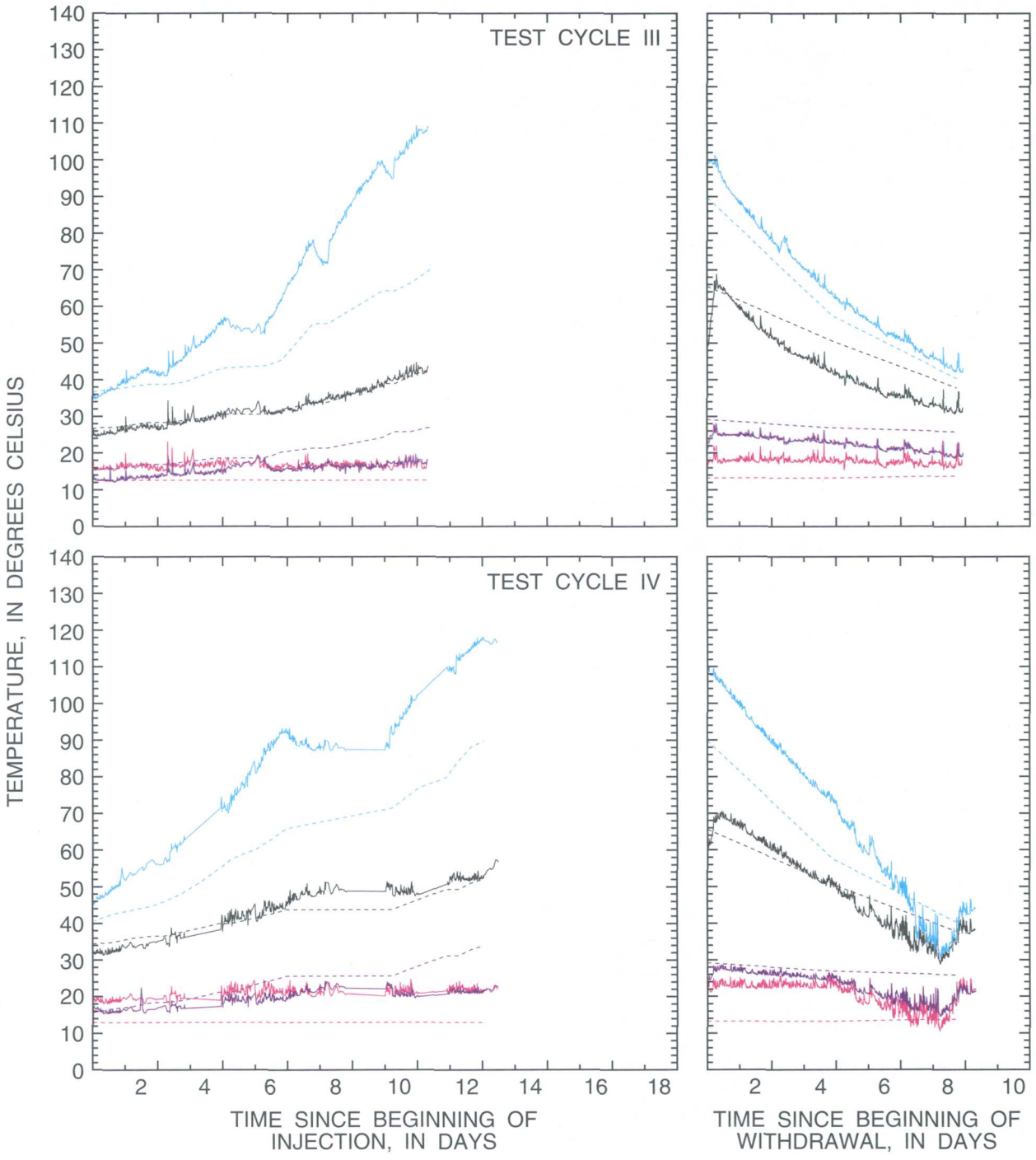

temperatures at observation well AM2 for the four short-term test injection and withdrawal.

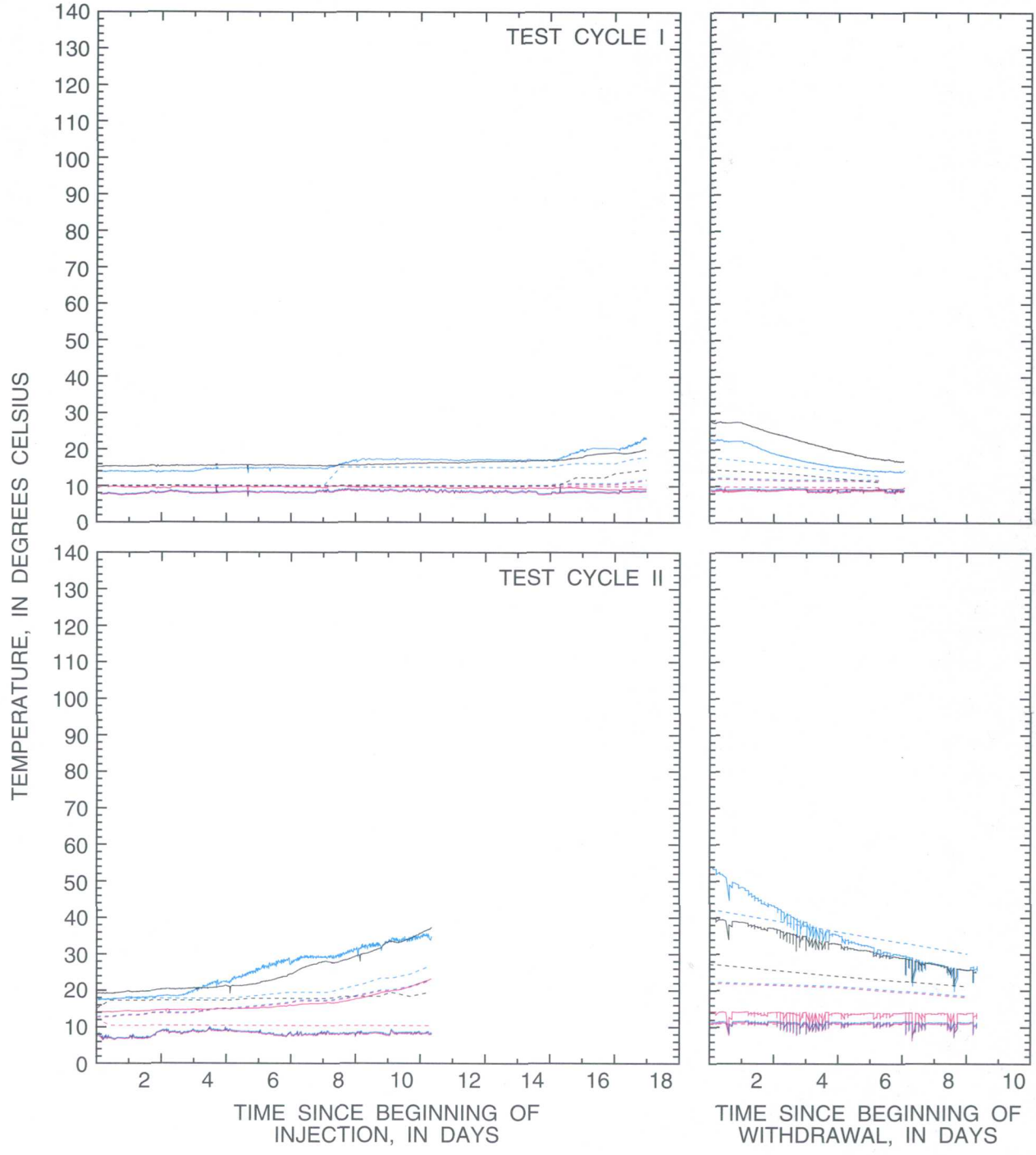

Figure 29.--Model-computed and average measured injection cycles during periods of

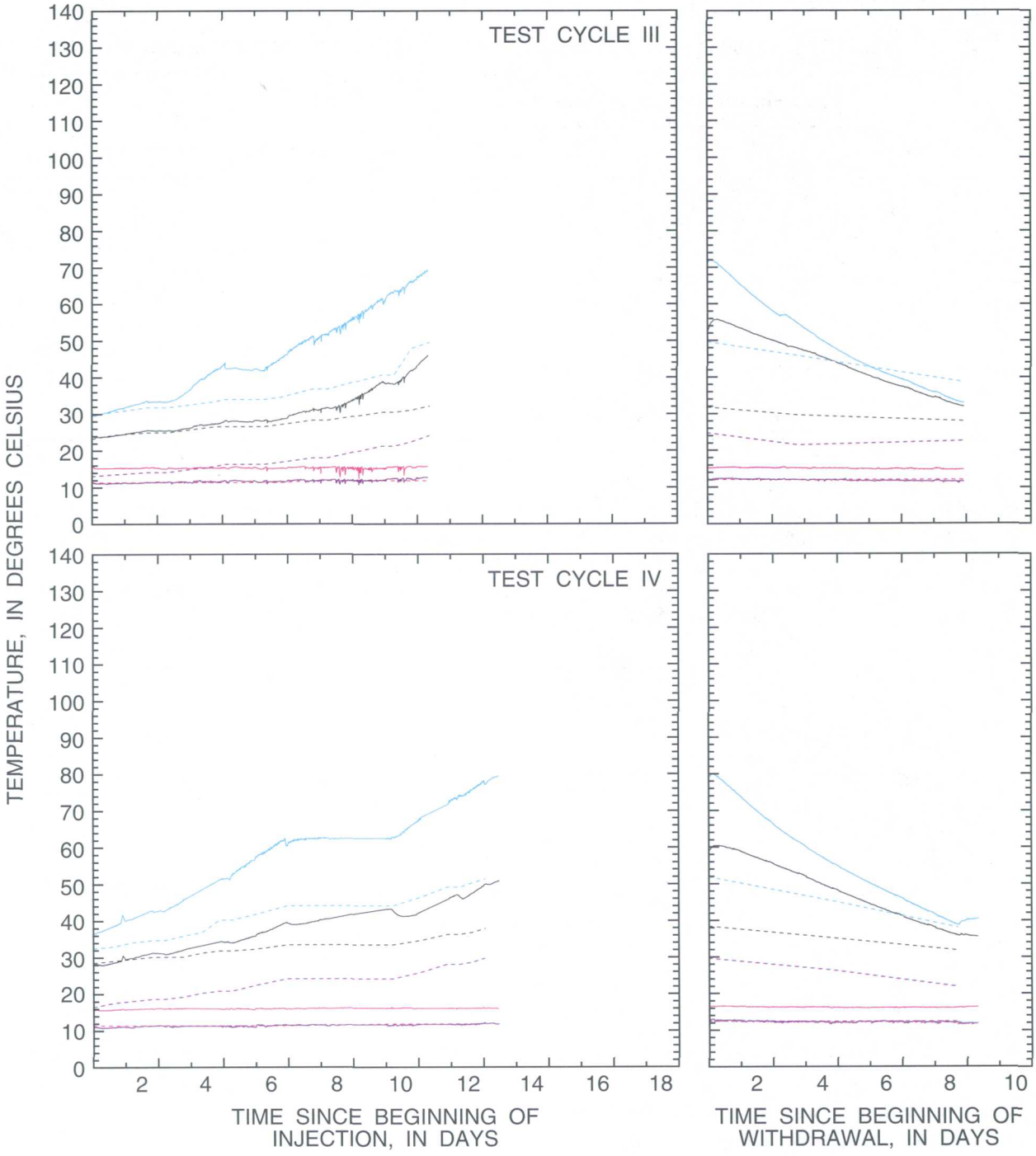

temperatures at observation well AM3 for the four short-term test injection and withdrawal.

Table 6.--Hydraulic properties used for simulation of the short-term test cycles

Model layer	Hydraulic conductivity, in meters per day			Anisotropy, K_x/K_y	Porosity (percent)
	K_x	K_y	K_z		
1	0.003	0.003	0.00003	1.00	26.8
2	2.89	1.71	.222	1.69	28.2
3	.03	.03	.0003	1.00	27.3
4	5.78	2.51	.380	2.30	25.2
5	1.45	.628	.095	2.30	25.6
6	.003	.003	.00003	1.00	31.6

Table 7.--Comparison of model-computed thermal efficiencies of the aquifer and final withdrawal-water temperatures at production well A with corresponding calculated and measured values for the four short-term test cycles

Short-term test-cycle number	Thermal efficiency of aquifer (in percent)		Final withdrawal-water temperature (in degrees Celsius)	
	Calculated	Model computed	Measured	Model computed
I	59.0	60.0	39.4	39.9
II	46.0	49.4	39.4	43.8
III	62.0	58.0	56.7	58.3
IV	59.0	62.0	63.9	64.4

model sensitivity to changes in the thermal properties of thermal conductivity of rock, heat capacity of rock, and thermal dispersivity were tested. The individual model properties were varied from assumed base values. The hydraulic and thermal properties simulated in the model are shown in tables 6 and 4, respectively. On the basis of results of this sensitivity analysis, the model was most sensitive to changes in thermal dispersivity. Therefore, only the longitudinal and transverse thermal dispersivities were varied during nonisothermal model calibration. The remaining hydraulic and thermal properties were estimated within the range of published values (Miller and Delin, 1993).

Calibration of the model to nonisothermal conditions consisted of comparing model-computed thermal efficiencies and withdrawal-water temperatures to calculated and measured values (table 7). Calibration of the model also was achieved by comparing model-computed and average temperatures at the observation wells during the test cycles (figs. 25-29). The longitudinal and transverse dispersivities were varied during nonisothermal model calibration on the basis of relative hydraulic conductivities of the aquifer in the longitudinal and transverse directions (Miller, 1984; Miller and Delin, 1993). The longitudinal dispersivity was varied from 1.0 to 30 m and the transverse dispersivity was varied from 0.1 to 3.0 m. Values of 3.3

and 0.33 m for longitudinal and transverse dispersivity, respectively, simulated aquifer thermal efficiencies, wellhead temperatures, and average temperatures close to measured values.

Analysis of Simulations

The model accurately calculated thermal efficiencies of the aquifer to within an average of about 5 percent of calculated values for the four short-term test cycles (table 7). The poor correspondence between model-computed and calculated efficiencies for test cycle II is likely related to the long storage period of 90 days compared to storage periods of 10 to 13 days for the other cycles (table 1). The model also accurately calculated withdrawal-water temperatures to within an average of about 3 percent of measured values for the four test cycles (table 7). The lack of correspondence between model-computed and averaged temperatures for test cycle II is once again likely due to the abnormally long storage period for this cycle.

Model-computed and averaged temperatures for production well A compare closely (fig. 25). The closest overall agreement between model-computed and average temperatures was for observation well AM2 (fig. 28). The trends of the model-computed temperature profiles and the model-computed temperatures at the end of each injection and withdrawal cycle acceptably match average temperatures for most model layers. The acceptable match between model-computed and average temperatures for observation well AM2 is likely related to lack of aquifer clogging in this direction. Observation well AM2 is on the axis of minimum transmissivity (Miller, 1984). The trends of the model-computed injection- and withdrawal-temperature profiles for observation wells AS1 (fig. 27) and AM3 (fig. 29) do not agree as well with average temperatures. The model-computed temperatures at the end of injection are generally about 5 to 10°C lower than average temperatures for these wells. In contrast, the model-computed temperatures at the end of injection for observation well AM1 (fig. 26) were generally 5 to 20°C higher than average temperatures. These differences might result from the fact that the model does not simulate the effects of aquifer clogging by mechanical or chemical processes. Consequently, duplication of the trends in measured temperatures at observation wells AM1 and AS1 related to aquifer clogging was not expected in the model-computed graphs. This lack of correspondence between model-computed and average temperatures at observation wells AM1 and AS1 lends some support to the hypothesis of aquifer clogging.

As described earlier, aquifer clogging within the Galesville Sandstone at observation well AM1 resulted in a general decrease in temperature measured at the well at the 58 m altitude. Results of the model indicate that an increase in temperature would be expected at this location if the aquifer were not clogged. Correspondence between model-computed and average temperatures at other levels in observation well AM1 is acceptable during periods of injection and withdrawal for all four test cycles. On the basis of model-computed results at observation well AM1, therefore, the model accurately represents field conditions.

Although observation wells AM2 and AM3 are at approximately the same radial distance from production well A (fig. 5), the model-computed temperatures more closely match the average temperatures for well AM2 than for well AM3 (figs. 28 and 29). The lack of correspondence for observation well AM3 may be related to hydrofracturing of the Ironton and Galesville Sandstones during installation of observation well AS1 (M.C. Hoyer, Minnesota Geological Survey, 1985, written commun.). Hydrofracturing may have caused an increase in permeability near well AS1. Because well AS1 is much closer to well AM3 than to AM2 (fig. 5), aquifer permeability near well AM3 may be higher than was indicated by hydraulic tests at the site (Miller, 1984). The resultant increase in flow towards well AM3 would have caused higher average temperatures for this well than for well AM2. Because the model did not simulate the effects of hydrofracturing, any increase in average temperatures at well AM3 caused by this mechanism could not be duplicated. Long-term test-cycle data would be helpful to describe the potential effects of hydrofracturing and to evaluate use of the model as a tool in predicting temperatures at the observation wells.

The calibrated nonisothermal model is a tool for evaluating aquifer thermal-energy storage. The model can be used to calculate the recovery temperature and thermal efficiency of the aquifer for selected rates of withdrawal and injection, injection temperature, and duration of injection, storage, and withdrawal periods. Results of model analyses indicate that the model is accurate in computing thermal efficiency of the aquifer and temperatures at production well A during periods of withdrawal. The model is less accurate in simulating temperatures at the observation wells because of the effects of aquifer anisotropy, aquifer clogging, and, possibly, hydrofracturing. The model necessarily is a simplification of the flow system, and accuracy of the model results is limited by the accuracy of the hydraulic and thermal input data on which the computations are based. In addition, different combinations of input data could conceivably yield the same results.

Summary

The University of Minnesota started a project in May 1980 to evaluate use of the Franconia-Ironton-Galesville aquifer for thermal-energy storage. High-temperature water (88.5 to 117.9°C) was injected through a well during four periods ranging in duration from 5.25 to 8.01 days. Periods of storage ranged in duration from 9.62 to 89.71 days, and periods of withdrawal ranged from 5.28 to 8.00 days. Approximately equal rates of injection and withdrawal, from 17.4 to 18.6 L/s, were maintained for each test cycle. Each period of injection was interrupted four times to service the heat exchanger and above-ground chemical-precipitation filters.

Temperature graphs indicate that the shortest arrival times for temperature fronts, and the hottest temperatures measured at all observation wells, were in the Ironton and Galesville Sandstones. The next shortest arrival times, and somewhat cooler temperatures, were in the less permeable upper part of the Franconia Formation. The latest arrival times for temperature fronts were measured in the lower part of the Franconia. Because the lower part of the Franconia was not screened, heat within this part of the aquifer was transported by conduction. Very little heat conduction was measured in the St. Lawrence Formation and in the Eau Claire Formation, confining layers to the aquifer.

Clogging within the aquifer by calcium carbonate precipitation and by movement of fine-grained material near the well bore could explain some anomalies of temperatures and pressures measured in the Ironton Sandstone. A decrease in temperature was measured at several of the temperature-measurement locations in the upper part of the Franconia Formation and in the Ironton and Galesville Sandstones immediately after heated-water injection was stopped. The exact mechanism for this temperature change is not fully understood, but it is probably related to the difference between conductive and advective rates of thermal-energy transport and to variations in permeability within the aquifer. Buoyancy flow within the aquifer was minimal, as evidenced by temperature profiles at individual observation wells during periods of injection, storage, and withdrawal.

A three-dimensional, anisotropic, nonisothermal, ground-water-flow, and thermal-energy-transport model was used to simulate the four short-term test cycles. The model simulated a 400-day period from the start of injection of test cycle I to the end of withdrawal for test cycle IV and included the storage periods between test cycles. Calibration of the model to nonisothermal conditions consisted of comparing model-computed thermal efficiencies and withdrawal-water temperatures to calculated and measured values. Calibration of the model also was achieved by comparing model-computed and average temperatures at the observation wells during the test cycles. Sensitivity of the model to adjustments of hydraulic conductivity, porosity of the aquifer, thermal conductivity and heat capacity of rock, vertical anisotropy, and thermal dispersivity was tested during preliminary model analyses. On the basis of these analyses, the only input properties varied during model calibration were the longitudinal and transverse thermal dispersivity, which were simulated at 3.3 and 0.33 m, respectively. The model accurately simulated aquifer thermal efficiencies to within an average of about 5 percent of calculated values for the four test cycles. The model accurately simulated withdrawal-water temperatures to within an average of about 3 percent of measured values for the four test cycles. Graphs of model-computed temperatures acceptably matched graphs of average temperatures.

The calibrated nonisothermal model is a tool for evaluating aquifer thermal-energy storage. The model can be used to calculate the recovery temperature and thermal efficiency of the aquifer for selected rates of injection and withdrawal, injection temperature and duration of injection, storage, and withdrawal periods. Results of model analyses indicate that the model is most accurate in simulating thermal efficiency of the aquifer and temperatures of production well A during periods of withdrawal. The model is less accurate in simulating temperatures at the observation wells because of the effects of aquifer anisotropy, aquifer clogging, and, possibly, hydrofracturing.

References Cited

Bear, Jacob, 1972, Dynamics of fluids in porous media: New York, Elsevier, 764 p.

Blair, S.C., Deutsch, W.J., and Mitchell, P.J., 1985, Permeability, geochemical, and water quality tests in support on an aquifer thermal energy storage site in Minnesota: Battelle Pacific Northwest Laboratory, PNL-5438, 510 p.

Carslaw, H.S., and Jaeger, J.C., 1959, Conduction of heat in solids: London, England, Oxford University Press, 510 p.

Clark, S.P., 1966, Book of physical constants: Geological Society of America Memoir 97, 587 p.

Czarnecki, J.B., 1983, Fortran computer programs to plot and process aquifer pressure and temperature data: U.S. Geological Survey Water-Resources Investigations Report 85-4051, 49 p.

Green, D.W., 1963, Heat transfer with flowing fluid through porous media: University of Oklahoma, unpublished, Ph.D. thesis.

Guyton, W.F., 1946, Artificial recharge of glacial sand and gravel with filtered river water at Louisville, Kentucky: Economic Geology, v. 41, no. 6, p. 644-658.

Hausz, Walter, 1974, Heat storage in wells, *in* Proceedings of Institute of Gas Technology Symposium, Chicago, Illinois, April 17, 1974, 8 p.

Helgeson, H.C., Delaney, J.M., Nesbitt, H.W., and Bird, D.K., 1978, Summary and critique of the thermodynamic properties of rock forming minerals: American Journal of Science, v. 278-A, 229 p.

Hellstrom, Göran, Tsang, Chin-Fu, and Claesson, Johan, 1979, Heat storage in aquifers—buoyancy flow and thermal stratification problems: Lund University, Sweden, 70 p.

Intercomp Resources Development and Engineering, Inc., 1976, A model of calculating effects of liquid waste disposal in deep saline aquifers: U.S. Geological Survey Water-Resources Investigations 76-61, 128 p.

Jaeger, J.C., 1950, Conduction of heat in composite slabs: Quarterly Journal of Applied Mathematics, v. 8, no. 2, p. 187-198.

Kanivetsky, Roman, 1979, Hydrogeologic map of Minnesota, bedrock hydrogeology: Minnesota Geological Survey State Map Series, Map S-2, 1 sheet, scale 1:500,000.

Kappelmeyer, O., and Haenel, R., 1974, Geothermics with special reference to application: Berlin-Stuttgart, Gebruder Borntraeger.

Kazmann, R.G., 1971, Exotic uses of aquifers: Proceedings of American Society of Civil Engineers, v. 97, no. IR3, p. 515-522.

Labadie, J.W., and Helweg, O.J., 1975, Step-drawdown test analysis by computer: Ground Water, v. 13, no. 5, p. 438-444.

Lawrence Berkeley Laboratory, 1978, Thermal energy storage in aquifers: Lawrence Berkeley Laboratory Publication LBL Report 8431.

Leggette, R.M., and Brashears, M.L., Jr., 1938, Groundwater for air conditioning on Long Island, New York: Transactions of the American Geophysical Union, p. 412-418.

Martin, W.L., and Dew, J.N., 1965, How to calculate air requirements for forward combustion: Petroleum Engineer, February 1965.

Mercer, J.W., Faust, C.R., and Miller, W.J., 1980, Review of simulation techniques for aquifer thermal energy storage (ATES): Battelle Pacific Northwest Labs., PNL-3769, 183 p.

Meyer, C.F., and Todd, D.K., 1973, Conserving energy with heat storage wells: Environmental Science and Technology, v. 7, no. 6, p. 512-516.

Meyer, C.F., Hausz, W., Ayres, B.L., and Ingram, H.M., 1976, Role of heat storage wells in future U.S. energy systems: General Electric TEMPO, GE76TMP-27A, 175 p.

Miller, R.T., 1984, Anisotropy of the Ironton-Galesville Sandstones near a thermal-energy-storage well—St. Paul, Minnesota: Ground Water, v. 22, no. 5, p. 532-537.

_____ 1985, Preliminary modeling of an aquifer thermal-energy storage system, *in* Subitzky, Seymour, eds., Selected Papers in the Hydrologic Sciences: U.S. Geological Survey Water Supply Paper 2270, p. 1-20.

Miller, R.T., and Delin, G.N., 1993, Cyclic injection, storage, and withdrawal of heated water in a sandstone aquifer at St. Paul, Minnesota—field observations, preliminary model analysis, and aquifer thermal efficiency: U.S. Geological Survey Professional Paper 1530-A, 55 p.

Miller, R.T., and Voss, C.I., 1986, Finite-difference grid for a doublet well in an anisotropic aquifer: Ground Water, v. 24, no. 4, p. 490-496.

Molz, F.J., Warman, J.C., and Jones, T.E., 1978, Aquifer storage of heated water, Part I—a field experiment: Ground Water, v. 16, no. 4, p. 234-241.

Muecke, T.W., 1978, Formation fines and factors controlling their movement in porous media: Journal of Petroleum Technology, February 1979, p. 144-150.

Norvitch, R.F., Ross, T.G. and Brietkrietz, Alex, 1973, Water resources outlook for the Minneapolis-St. Paul Metropolitan Area, Minnesota: Metropolitan Council of the Twin Cities, 219 p.

Norvitch, R.F. and Walton, M.S., eds., 1979, Geology and hydrologic aspects of tunneling in the Twin Cities area, Minnesota: U.S. Geological Survey Miscellaneous Map Series, Map 1157, 7 sheets.

Robie, R.A., Hemminway, B.S., and Fisher, J.R., 1978, Thermodynamic properties of minerals and substances at 298°K and 1 bar (105 pascals) pressure and at higher temperatures: U.S. Geological Survey Bulletin 1452, 456 p.

Rorabaugh, M.I., 1953, Graphical and theoretical analysis of step-drawdown test of artesian well: Proceedings of American Society of Civil Engineering, Separate no. 362, v. 79, 23 p.

Sauty, J.P., Gringarten, A.C., and Landel, P.A., 1979, The effects of thermal dispersion on injection of hot water in aquifers, *in* Proceedings of the Second Invitational Well Testing Symposium, Berkeley, California, 1978: Lawrence Berkely Laboratory, p. 122-131.

Sniegocki, R.T., 1963, Problems in artificial recharge through wells in the Grand Prairie Region, Arkansas: U.S. Geological Survey Water-Supply Paper 1615-F, 25 p.

Sommerton, W.H., Mehta, M.M., and Dean, G.W., 1965, Thermal alteration of sandstones: Journal of Petroleum Technology, May, p. 589-593.

Tsang, C. F., 1979, A review of current aquifer thermal energy storage projects: Lawrence Berkeley Laboratory, LBL-9834, 21 p.

Walton, Matt, Hoyer, M.C., Eisenreich, S.J., Holm, N.L., Holm, T.R., Kanivetsky, Roman, Jirsa, M.A., Lee, H.C., Lauer, J.L., Miller, R.T., Norton, J.L., and Runke, Hal, 1991, The University of Minnesota aquifer thermal energy storage (ATES) field test facility - system description, aquifer characterization, and results of short-term test cycles: Pacific Northwest Laboratories Report PNL-7220, UC-202, 318 p.

Wenzel, L.K., 1942, Methods of determining permeability of water-bearing materials: U.S. Geological Survey Water-Supply Paper 887, 192 p.

Werner, D., and Kley, W., 1977, Problems of heat storage in aquifers: Journal of Hydrology, v. 34, p. 35-43.

MILLER AND DELIN--

CYCLIC INJECTION, STORAGE, AND WITHDRAWAL OF HEATED WATER IN A SANDSTONE AQUIFER AT ST. PAUL, MINNESOTA: ANALYSIS OF THERMAL DATA AND NONISOTHERMAL MODELING OF SHORT-TERM TEST CYCLES

U.S. Geological Survey /OFR 93-435